

# BOOK OF ABSTRACTS



**ECMS 2019**

**9<sup>th</sup> European Conference  
on Mineralogy and Spectroscopy**

## 9<sup>th</sup> European Conference on Mineralogy and Spectroscopy, September 11-13, 2019, Prague, Czech Republic, Břevnov Monastery

One of the real advantages of scientific congresses and conferences is that people can share their ideas and visions, and may find a way to implement them. They serve as useful feedback as well as stimulation of future research. In the past, conferences have also served as a powerful weapon against all boundaries, primarily during the years of the "Iron Curtain" in Europe. We should be glad that no such a curtain exists today; boundaries prevail only in our minds (which is, fortunately, our own struggle only). Following the European Spectroscopic Conferences first held in Rome (1988), then in Berlin (1995), Kiev (1996), Paris (2001), Vienna (2004), Stockholm (2007), Potsdam (2011), Rome (2015), the 9<sup>th</sup> European Conference on Mineralogy and Spectroscopy (ECMS 2019) is hosted by Prague. Břevnov Monastery, which is now an archabbey, was the oldest male monastery in the Kingdom of Bohemia, founded in 993 and connected with the great personality of Saint Adalbert (956–997). The rule is of Saint Benedict, Ordo Sanctum Benedictum. Since their beginning, monasteries have been the centers of theology, philosophy, education and science. We are delighted that the conference venue combines both great history and great spirit.

The Bohemian countries (historic designation of countries that belonged to the Czech/Bohemian Crown, later on a part of the Austrian Empire) have great and long tradition of mineralogical research, which is primarily connected with the long history of mining ores since the early middle ages, such as Kutná Hora, Jihlava, later on Jáchymov (the origin place of tolar/thaler silver coins, predecessor of dolar) and Příbram. Many great and renowned scientists worked in Bohemian countries. As examples may serve Georg Bauer (known as Georgius Agricolas) (1494–1555), Tadeáš Hájek z Hájku (in Latin known as Hagecius) (1555–1600), Tycho Brahe (1546–1601), Johannes Kepler (1571–1630), Joseph Stepling (1716–1778), Joachim Barrande (1799–1883), Franz Xaver Maximillian Zippe (1791–1863), František Pošepný (1836–1895) and others, namely those who were active during the second half of the 19<sup>th</sup> century as professors of the Mining Academy in Příbram. The 20<sup>th</sup> century became providential for great personalities in Czech mineralogy, such as František Slavík (1876–1957), Ludmila Kaplanová-Slavíková (1890–1943), Vojtěch Rosický (1880–1942), František Ulrich (1899–1941), Radim Nováček (1905–1942) and later on Josef Sekanina

(1901–1986), Jiří Novák (1902–1971), Rudolf Rost (1912–1999), Jiří Krupička (1913–2014), Zdeněk Pouba (1922–2011), Karel Paděra (1923–2010), Lubor Žák (1925–2008), Jan Kutina (1924–2008), František Čech (1929–1996) and Petr Černý (1934–2018). While the first half of the century was tragically affected by the two world wars (many of the scientists died, others were imprisoned), the second half was marked by the totalitarian Communist regime (many scientists were persecuted or imprisoned, others were deprived of their jobs). Despite these dire circumstances, scientific activities continued to be stimulated due to an immeasurable effort and often personal credit of the above-mentioned personalities. In the difficult years under the Communist ruling, **Ing. Jiří Čejka, DrSc.** (born 1929 in Roudnice nad Labem) embarked on his scientific career and has had to overcome various obstacles throughout the years. Nowadays, he is a world-renowned expert in the field of vibration spectroscopy of uranium minerals and compounds, and still scientifically active! This year, Jiří Čejka celebrates his **90<sup>th</sup> birthday**, and, therefore, we decided to dedicate one of the scientific sessions focused on Uranium mineralogy to him and also symbolically dedicate the entire conference to his honor. We are convinced that Jiří is the best representative of an interdisciplinary approach in science as he is originally a chemist, who has

gradually fallen in love with uranium mineralogy and spectroscopy. This is more than characteristic for interdisciplinary nature of the ECMS conferences, as from their beginning. We hope you will enjoy the great hospitality of Prague with its sightseeing and history, as well as the stimulating atmosphere of the conference!

On behalf of the Scientific Committee  
*Jakub Plášil*

# ORGANIZING PARTNERS



Czech Geological Society



MASARYK UNIVERSITY  
Czech Republic



Palacký University  
Olomouc



CZECH  
GEOLOGICAL  
SURVEY



NATIONAL  
MUSEUM



Czech Academy  
of Sciences



CHARLES  
UNIVERSITY

EDUKOL

# ORGANIZING COMMITTEE



**Jan Cempírek** (Masaryk University, Brno, Czech Republic)

**Jan Filip** (Palacký University, Olomouc, Czech Republic)

**František Laufek** (Czech Geological Survey, Prague, Czech Republic)

**Ivo Macek** (National Museum, Prague, Czech Republic)

**Jakub Plášil** (Czech Academy of Sciences, Prague, Czech Republic)

**Radek Škoda** (Masaryk University, Brno, Czech Republic)

**Jakub Trubač** (Charles University, Prague, Czech Republic)

# KEYNOTE SPEAKERS

---



## Peter C. Burns

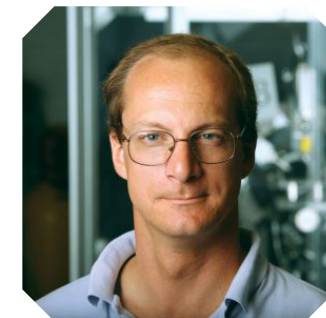
*University of Notre Dame, IN, USA*

### „New landscapes of uranium mineralogy“

Peter C. Burns is the Henry Massman Professor of Civil and Environmental Engineering and Earth Sciences and Concurrent Professor of Chemistry and Biochemistry at the University of Notre Dame, Director of the Center for Sustainable Energy at Notre Dame (ND Energy), and Director of the NNSA-funded Actinide Center of Excellence.

Following undergraduate and graduate studies in Canada and post-doctoral appointments at Cambridge University and the University of New Mexico, Burns joined the faculty of the University of Illinois-Urbana in 1996 and moved to the University of Notre Dame in 1997. Burns' research interests include aspects of actinide materials, including uranium mineralogy and geochemistry, actinide environmental chemistry, actinide solid state chemistry (especially uranium and neptunium), and nanoscale actinide clusters. Starting in 2005, Burns developed a family of more than 100 nanoscale uranium-oxygen cage clusters and has developed applications of these materials that take advantage of their unique properties, such as an inexpensive and environmentally sustainable approach to spent nuclear fuel recycling. Selected awards include the Donath Medal of

the Geological Society of America, the Mineralogical Society of America Award, the Young Scientist, Hawley, and Peacock medals of the Mineralogical Association of Canada, Life Fellow of the Mineralogical Society of America, Honorary Member of the Russian Mineralogical Society, and Life Member of Clair Hall College, University of Cambridge. Burns' research in mineralogy, solid-state chemistry, and nanoscience has produced more than 400 published archival journal contributions, as well as three books. He is Past President of the International Mineralogical Association.



## Janice Bishop

SETI Institute, CA, USA

### „Characterizing the surface of Mars through remote spectral identification of minerals“

Dr. Janice Bishop is a chemist and planetary scientist who explores the planet Mars using spectroscopy. She attended Stanford University for a BS in Chemistry and MS in Earth Science in 1988, followed in 1994 by a PhD in Chemistry with a joint thesis project in Planetary Geology sponsored by a NASA Graduate Student Researchers Program Fellowship. She was awarded an Alexander von Humboldt Fellowship for a postdoc in Berlin at the German Aerospace Center (DLR) and then a National Research Council Fellowship at NASA Ames in California. She has been a research scientist at the SETI Institute since 1999 and is currently Chair of Astrobiology and a member of the Science Council at the SETI Institute. Her investigations of CRISM spectral data from orbit at Mars are revealing clays and sulfates in the ancient rocks that provide information about the geochemical environment at the time the minerals formed. Dr. Bishop studies the spectral fingerprints of minerals and rocks in the lab for identification of these in the Martian data. Her research also involves collecting and studying Mars analog rocks and soils at a variety of locations including volcanic islands, cold

deserts, hydrothermal regions, acidic aqueous sites, and meteorites which are the only Martian samples available on Earth to date.



## Sergey V. Krivovichev

St. Petersburg State University, Russia

### „Feldspar polymorphs: diversity, complexity, stability“

Sergey Krivovichev was born in 1972 and received his PhD and Doctor of Sciences degrees from St. Petersburg State University. He is currently a Head of the Federal Kola Science Centre of the Russian Academy of Sciences (Apatity, Russia) and Professor of Crystallography at St. Petersburg State University. During his career, he served as a President of International Mineralogical Association, Chief Editor of European Journal of Mineralogy and associate editor of several other mineralogical journals. His research interests include structural and topological diversity of minerals and inorganic compounds (with special emphasis on uranium, copper and lead oxocompounds), structural complexity and mineral evolution. He is Corresponding member of the Russian Academy of Sciences and foreign member of the Turin Academy of Sciences.



## Anna Vymazalová

*Czech Geological Survey, Prague, Czech Republic*

### „Platinum-group minerals, from natural to synthetic“

Anna Vymazalová received her MSc diploma followed by PhD (2005) at Faculty of Science, Charles University in Prague, Czech Republic. During her studies she completed two terms courses in Economic Geology at Imperial College in London, UK. Since 2001 she is employed as a Researcher at the Czech Geological Survey in Prague and currently she is the Head of the Department of Rock Geochemistry. She has been an active member of SGA (Society for Geology Applied to Mineral Deposits) and since 2004 she serves as a Vice President for Student Affairs on SGA Council. Her research interests are focused on ore and experimental mineralogy; precious metals (PGE), their formation, genesis of mineral deposits and various aspects associated with exploitation and processing of deposits. She has completed several short courses and workshops on mineralogy and mineral deposits and actively participated at several international projects and conferences. Her research has been focused on detail experimental investigation of ternary systems involving PGE, intermetalides and chalcogenides, their phase relations and mineralogical application. She

has been also actively involved in a description of new mineral species. She described (or participated on a description) of about twelve new platinum-group minerals.



## Juraj Majzlan

*Friedrich Schiller University Jena, Germany*

### „Different ways of incorporating elements into crystal structures in which they do not fit“

Juraj Majzlan studied mineralogy at the Comenius University in Bratislava and completed his Diploma thesis on orogenic Sb-Au deposits in 1996. After short research work on ore deposits in Bratislava, Budapest, and Copenhagen, he started his PhD at the University of California at Davis, dealing with thermodynamics of iron and aluminum oxides, completed in 2002. As a Hess postdoctoral fellow, he investigated acid mine waters at the Princeton University, using spectroscopic techniques. The next position in Freiburg (Germany) allowed him to continue in thermodynamics, spectroscopy, and crystallography of acid mine drainage, but also to return to field work. Since 2009, he is a full professor at the University in Jena (Germany), with a focus on environmental mineralogy, thermodynamics of minerals, geobiology, and ore deposits. He is the secretary of European Mineralogical Union and member of editorial boards of Mineralogical Magazine and Chemie der Erde – Geochemistry. Apart from publishing scientific papers, he translated two textbooks into Slovak and holds talks for pupils in the state of Thuringia.



## Sergey S. Lobanov

*GFZ German Research Center for Geosciences, Potsdam, Germany*

### „Optical spectroscopy at combined high P and T conditions and its applications to thermal and electrical transport in the deep mantle“

Sergey S. Lobanov received PhD from V.S. Sobolev Institute of Geology and Mineralogy (Novosibirsk, Russia), and then accepted a postdoctoral (2012) and subsequently a research scientist (2015) position at the Geophysical Laboratory, Carnegie Institution of Washington. At Carnegie, he used state-of-the-art light-based probes, to make important contributions in the areas of volatiles chemical reactivity, optical and transport properties of mantle minerals, and exoplanet mineralogy. In 2017, he moved on to Stony Brook University (New York State) as a Research Assistant Professor where he deepened his spectroscopic expertise while working with world-renowned chemists on novel metal organic frameworks, compounds that hold great promise for air purification. In 2018, he relocated to Germany to take on a new challenge as a Helmholtz Young Investigators Groups Leader at the German Research Center for Geosciences (GFZ). At GFZ, he established a new research group (CLEAR) to study properties of the deep Earth via unconventional ultra-fast time-resolved spectroscopic techniques. In cooperation with GFZ scientists, his group's near-future research will enable new models of the core-mantle interaction, help understand the effect

of iron spin transitions on the properties of the mantle, and provide new knowledge on the speciation of volatiles within planets.

His primary goal as a geoscientist is to understand the connection between the core, mantle, and crust on various geologic time scales in order to help decipher Earth's complex history. Planetary-scale geological processes, such as mantle convection and geodynamo action, operate at great depths and are governed by properties of minerals at high pressures (P) and temperatures (T). Accordingly, the structural, transport, and electronic properties of minerals at high P-T have been at the frontier of geosciences and one of the major subjects of his research. In order to understand Earth's deepest geological processes, he derives high quality mineral physics data using in situ measurements at high-P and -T.



# CONFERENCE SCHEDULE



	9/9	9/10	9/11	9/12	9/13	9/14		
8.00–9.00			Participant registration					
9.00–9.40	Workshop I (Jana 2006)	Workshop I (Jana 2006)	Conference opening	Keynote lecture	Keynote lecture			
			Keynote lecture					
9.40–10.40			Talks	Talks	Talks			
10.40–11.10			Coffee break	Coffee break	Coffee break			
11.10–12.40			Talks	Talks	Talks			
12.40–14.00			Lunch break	Lunch break	Lunch break			
14.00–14.40			Keynote lecture	Keynote lecture	Keynote lecture			
14.40–15.25			Talks	Talks	Talks			
15.25–15.45			Coffee break	Coffee break	Coffee break			
15.45–16.45					Talks	Talks	Talks	
							Summary & closing	
16.45–18.00			Ice-breaker party (17.00–19.00)	Poster session	Poster session			
18.00–19.00								
19.00–24.00						Conference dinner		

Workshop II (Gemstone deposits)

## SEPTEMBER 11, 2019

---

08.00-09.00 **PARTICIPANT REGISTRATION**

09.00-09.15 **CONFERENCE OPENING**

### THEME: ENVIRONMENTAL MINERALOGY AND GEOCHEMISTRY

*Chair: Jan Filip*

09.15-09.55 **Juraj Majzlan: Different ways of incorporating elements into crystal structures in which they do not fit**

09.55-10.10 **Tamara Đorđević: Arsenic in roméite-group minerals formed by weathering of realgar-rich tailings (Lojane mine, North Macedonia)**

10.10-10.25 **Alexandra M. Plumhoff: Fractionation of copper, oxygen and hydrogen isotopes between malachite and aqueous solution**

10.25-10.40 **Paulina Maziarz: Halloysite-supported iron oxide particles for As(V) removal: adsorption mechanism investigation by the XPS and Mössbauer spectroscopy**

10.40-11.10 **COFFEE BREAK**

### THEME: MINERALOGY

*Chair: Ferdinando Bosi*

11.10-11.25 **Charles A. Geiger: The Magnetic Behavior of Olivine and Garnet Substitutional Solid Solutions**

11.25-11.40 **Marcin Stachowicz: Fluorite a supposedly ordinary mineral. On charge-shift bonding, nonspherical charge distribution and boundary of ions**

11.40-11.55 **Peter Bačík: The site-occupancy assessment in beryl based on bond-length constraints**

11.55-12.10 **Monika Kubernátová: Crystal chemistry of Pb-rich tourmaline from pegmatite in Minh Tien, Vietnam**

12.10-12.25 **Andreas Ertl: Oxidized Mg- and Fe-rich tourmaline with significant amounts of Sr and Pb**

12.25-12.40 **Pavel Uher: Evolution of borate minerals (ludwigite group and szaibélyite): from contact metamorphic to hydrothermal stages (Vysoká – Zlatno skarn, Slovakia)**

12.40-14.00 **LUNCH BREAK**

**Carsten Laukamp: extra talk during lunch break 13:00-14:00**

Australia's National Virtual Core Library - unlocking mineralogical information from drill core to support research and mineral exploration

### THEME: REMOTE SENSING AND NEAR-SURFACE MINERALS

*Chair: Giovanni Andreozzi*

14.00-14.40 **Janice Bishop: Characterizing the surface of Mars through remote spectral identification of minerals**

14.40-14.55 **Carsten Laukamp: Mid- and Thermal Infrared Reflectance Spectral Signatures of Non-sulfide Zn-ores**

14.55-15.10 **Sari Romppanen: Optimized time-resolved photoluminescence detection of rare earth elements in apatites and calcites**

15.10-15.25 **Dominik Talla: The FTIR and Raman spectroscopic study of kieserite, MgSO<sub>4</sub>·H<sub>2</sub>O, an important sulfate in our Solar system, across its cosmochemically relevant solid solutions**

15.25-15.45 **COFFEE BREAK**

15.45-16.00 **Simone Bernardini: Oxidation state of manganese in oxide minerals by Raman spectroscopy**

16.00-16.15 **Monica LeGras: How to use infrared reflectance spectroscopy of pyroxenes and pyroxenoids for critical metals exploration and mining**

16.15-16.30 **Elena Zhitova: Low-temperature sulphate mineralization of modern hydrothermal systems of Kamchatka, Russia**

16.30-16.45 **Tomas Hrstka: Using Orange Software visual programming and machine learning for deposited dust particles identification**

16.45-19.00 **POSTER SESSION**

## SEPTEMBER 12, 2019

---

### THEME: HP-HT EXPERIMENTAL MINERALOGY AND SPECTROSCOPY

Chair: Henrik Skogby

- 09:00-09.40 **Sergey Lobanov: Optical spectroscopy at combined high P and T conditions and its applications to thermal and electrical transport in the deep mantle**
- 09.40-09.55 **Sergey Britvin:** Phosphides of schreibersite-nickelphosphide series as indicators of crystallization history of meteorites
- 09.55-10.10 **Liudmila Gorelova:** High-pressure behavior of hingganite-(Y),  $YBeSiO_4(OH)$
- 10.10-10.25 **Mara Murri:** How to determine a unique entrapment condition of host-inclusion systems from UHPM rocks using Raman elastic geobarometry
- 10.25-10.40 **Nicola Campomenosi:** Using polarized Raman spectroscopy to detect strain gradient in optical anomalous host-inclusion mineral systems
- 10.40-11.10 **COFFEE BREAK**

### THEME: MINERAL SPECTROSCOPY

Chair: Charles Geiger

- 11.10-11.25 **Anastasiya Kalugina:** The Raman estimation of composition of garnets in natural diamonds
- 11.25-11.40 **Ingrin Jannick:** Specific OH infrared signatures in pyroxenes from mantle xenoliths: characteristics and possible bands assignments
- 11.40-11.55 **Elena Zhitova:** Crystal chemical characterization of carbonate and chloride layered double hydroxides
- 11.55-12.10 **Karolina Rybka:** The effect of M(II)/M(III) molar ratio on the LDH structure derived from chemicals and minerals: a spectroscopic study using FTIR, Raman and XPS
- 12.10-12.25 **Maciej Manecki:** Compositional analysis of  $PO_4$ ,  $AsO_4$ , and  $VO_4$  in Pb-apatites with Raman spectroscopy
- 12.25-12.40 **Daria Kiseleva:** Raman spectroscopy in the studies of archaeological bone and tooth diagenesis
- 12.40-14.00 **LUNCH BREAK**

### THEME: URANIUM MINERALOGY

session dedicated to Dr. Jiří Čejka on the occasion of his 90<sup>th</sup> birthday

Chair: Jakub Plášil

- 14.00-14.40 **Peter C. Burns: New landscapes of uranium mineralogy**
- 14.40-14.55 **Vladislav Gurzhiy:** Structural complexity of natural and synthetic uranyl compounds with S- and Se-centered oxyanions
- 14.55-15.10 **Travis A. Olds:** Paddlewheelite, a new uranyl carbonate mineral from the Jáchymov District, Bohemia, Czech Republic
- 15.10-15.25 **Gwladys Steciuk:** Crystal structure of uranyl molybdate mineral calcurmolite solved from electron diffraction data
- 15.25-15.45 **COFFEE BREAK**
- 15.45-16.00 **Dmitry A. Zamyatin:** Thermally induced structural, chemical and textural rearrangement of metamictized zircon with high concentration of impurity elements: Raman, PL, EPMA, EBSD
- 16.00-16.15 **Dariusz Malczewski:** Activation energy of annealed, partially metamict davidite by  $^{57}Fe$  Mössbauer spectroscopy
- 16.15-16.30 **Emily Nienhuis:** The role of 4+ cations on the structure and crystallization of nepheline and related phases from sodium aluminosilicate glasses
- 16.30-16.45 **Gioacchino Tempesta:** Laser-induced breakdown spectroscopy (LIBS) as a tool for Li distribution in zoned tourmaline in thin section
- 16.45-18.00 **POSTER SESSION**
- 19:00-24:00 **CONFERENCE DINNER**

## SEPTEMBER 13, 2019

---

### THEME: EXPERIMENTAL MINERALOGY

Chair: František Laufek

- 09:00-09.40 **Anna Vymazalová: Platinum-group minerals, from nature to synthetic**
- 09.40-09.55 **Francesco Di Benedetto:** A new solvothermal approach to obtain nanoparticles in the  $\text{Cu}_3\text{SnS}_4$ - $\text{Cu}_2\text{FeSnS}_4$  join
- 09.55-10.10 **Gregory Ivanyuk:** Endemic titanosilicates of the Kola alkaline complexes and their functional synthetic analogs
- 10.10-10.25 **Andrea Giaccherini:** Spectroscopic and structural analysis of ultra-thin  $\text{Cu}_2\text{S}/\text{CdS}$  semiconducting devices
- 10.25-10.40 **Michela Botticelli:** New insights on the discrimination of synthesized ochres by  $\mu$ -FTIR: Mars yellow and calcinated red ochres recognition criteria
- 10.40-11.10 **COFFEE BREAK**

### THEME: GEMOLOGY

Chair: Lee Groat

- 11.10-11.25 **Tashia Dzikowski-Hutter:** A Gemmological Approach to Distinguishing Natural from Synthetic Rubies: LA-ICP-TOF mass spectrometry provides new insights
- 11.25-11.40 **Myint Myat Phyo:** U-Pb age dating of zircon and zirconolite inclusions in marble hosted gem-quality ruby and spinel from Mogok, Myanmar
- 11.40-11.55 **Laura Medeghini:** Provenance studies of emerald: evaluation of Raman approach
- 11.55-12.10 **Hao A.O. Wang:** Multi-element Analysis of Sapphires and Emeralds by LA-ICP-Time-Of-Flight-MS for Country of Origin Determination
- 12.10-12.25 **Myint Myat Phyo:** Detailed Inclusion Study of Gem-Quality Spinel from Mogok, Myanmar: Geikielite  $\text{MgTiO}_3$  as exsolution lamellae
- 12.25-12.40 **Evgeny Vasilev:** Enigma of the cuboid diamonds: inverse distribution of optical centres within the crystal volume
- 12.40-14.00 **LUNCH BREAK**

### THEME: CRYSTALLOGRAPHY

Chair: Jan Cempírek

- 14.00-14.40 **Sergey V. Krivovichev: Feldspar polymorphs: diversity, complexity, stability**
- 14.40-14.55 **Andrey A. Zolotarev, jr:** Crystal structure of dmisteinbergite,  $\text{CaAl}_2\text{Si}_2\text{O}_8$
- 14.55-15.10 **John McCloy:** Rare earth environments in silicate, borate, borosilicate, and transition metal phases obtained from glass-ceramics
- 15.10-15.25 **Taras Panikrovskii:** Crystal structure model of tiettaite and its Na-deficient analogue: novel type of microporous octahedral-tetrahedral framework
- 15.25-15.45 **COFFEE BREAK**
- 15.45-16.00 **Richard Pažout:** Substitution ranges of new mineral staročeskéite  $\text{Ag}_{0.7}\text{Pb}_{1.6}(\text{Bi}_{1.35}\text{Sb}_{1.35})_2\text{7O}_{56}$
- 16.00-16.15 **Maria G. Krzhizhanovskaya:** Crystalline borosilicates of alkali and alkaline-earth metals: hierarchy, fundamental building blocks and thermal expansion
- 16.15-16.45 **ECMS 2019:** a summary & closing  
Student's awards, next ECMS, farewell

## LIST OF POSTERS

---

- P-01 **Giovanni B. Andreozzi:** Diamond-magnesiochromite host-inclusion system recording old deep lithosphere conditions at Udachnaya (Siberia)
- P-02 **Simone Bernardini:** Raman spectra of natural manganese oxides
- P-03 **Małgorzata Cegielka:** Accessory mineral assemblage in various types of Karkonosze granite (West Sudetes)
- P-04 **Fabrice Dal Bo:** Crystal chemistry of the rinkite-(Ce)-nacareniobsite-(Ce) series
- P-05 **Francesco Di Benedetto:** An EPR study of silica radicals in lung tissues with evidence of silicosis
- P-06 **Francesco Di Benedetto:** Multi-analytical characterisation of a medieval red mosaic glass tessera of from the first facade of the Duomo of Florence
- P-07 **Tomáš Flégr:** Chemical evolution of tourmaline in elbaite-subtype pegmatites of the Bohemian Massif
- P-08 **Shijia Gao:** Scientific Development and Digitization of the Gemological Collection from Abraham Gottlob Werner
- P-09 **Andrea Giaccherini:** A microXRF study of silicon and its behaviour in lung tissues with evidence of silicosis
- P-10 **Andrea Giaccherini:** Spectroscopic analysis of nanocrystalline  $Cu_3SnS_4$ : evidence of a low temperature transition
- P-11 **Viktor Goliáš:** Non-destructive Alpha spectroscopy as a tool for distinguishing equilibrium state on uranium minerals
- P-12 **Jana Havláková:** Thermally induced solid-state transformations of  $Fe_2O_3$  polymorphs in reducing and inert atmospheres
- P-13 **Yu-Hsuan Cheng:** Electron microscopic study of burial diagenetic greigite and smythite in Gutingkeng Mudstone, SW Taiwan
- P-14 **Alina Izatulina:** Crystal chemistry of natural and synthetic oxalates of divalent cations
- P-15 **Ryou Kariya:** Emission mechanism of the cathodoluminescence in a series of scheelite-powellite
- P-16 **Jakub Kotowski:** Monazite and tourmaline from the Albian (Lower Cretaceous) sands from the Miechów Synclitorium (southern Poland) as a tool in provenance study
- P-17 **Maryna Kutsevol:** Mineralogy of silicified zones of the Southern Buh area silicate nickel deposits
- P-18 **František Laufek:** Synthesis and crystallographic study of laflammeite ( $Pd_3Pb_2S_2$ ) and thalhammerite ( $Pd_9Ag_2Bi_2S_4$ )
- P-19 **Daive Lenaz:** Raman spectroscopy and the  $K_2O$  content of glauconites
- P-20 **Eugen Libowitzky:** Non-destructive investigation of natural, treated, and synthetic amber by handheld XRF and ATR-FTIR spectroscopy
- P-21 **Daniela Mauro:** Sulfate assemblages from the Monte Arsiccio pyrite ore deposit (northern Tuscany, Italy): spectroscopic data on unusual mineral species
- P-22 **Elmira Mohammadi:** Synthesis, Characterization, and Application of Greigite, Pyrite, and Violarite Nanoparticles
- P-23 **Lucy M Mottram:** A preliminary investigation of Fe speciation in minerals by Fe K-edge XANES using a laboratory based spectrometer
- P-24 **Kira Musiyachenko:** The complexity behind the simple Ti oxide structure
- P-25 **Adil Nawaz:** Petrographic, Geochemical and mineralogical investigations of Koga and Jambil carbonatites from Peshawar Plain Alkaline Igneous Province (PPAIP), Pakistan
- P-26 **Krzysztof Nejbart:** Geochemical signatures and scandium mineralization potential of NYF member of the Julianna Pegmatite System, Sudetes
- P-27 **Hirotsugu Nishido:** Provenance study of eolian sediments by cathodoluminescence spectral analysis of quartz grains for a stratigraphic interpretation in the Gobi desert
- P-28 **Hirotsugu Nishido:** Cation site preference in apatite estimated by cathodoluminescence spectroscopy for U-Pb dating
- P-29 **František Novotný:** Magmatic-hydrothermal evolution of tourmaline from the elbaite pegmatite Dolní Rožínka, Czech Republic
- P-30 **Liudmyla Omelchenko:** Effect of electron irradiation on pseudogap in  $YBa_2Cu_3O_7$ - single crystals
- P-31 **Elizaveta A. Pankrushina:** Statistical analysis of temperature-dependent Raman spectra of minerals
- P-32 **Tereza Peterková:** Trace element chemistry of mica and quartz during magmatic-hydrothermal transition in the evolved granitic system of the eastern Krušné hory/Erzgebirge

- P-33 **Rezeda M. Ismagilova:** High-temperature crystal chemistry of szenicsite  $\text{Cu}_3(\text{MoO}_4)(\text{OH})_4$ , lindgrenite  $\text{Cu}_3(\text{MoO}_4)_2(\text{OH})_2$ , cupromolybdate  $\text{Cu}_3\text{O}(\text{MoO}_4)_2$  and copper trimolybdate  $\text{CuMo}_3\text{O}_{10}\cdot\text{H}_2\text{O}$
- P-34 **Caterina Rinaudo:** Micro-Raman spectroscopy, technique allowing in depth identification/characterization of asbestiform minerals
- P-35 **Michal Roll:** Origin of secondary uranyl-carbonate minerals at Giftkies mine, Jáchymov, Czechia: possible climate implications?
- P-36 **Anastasiya Ryanskaya:** A combined XRD and micro-Raman study of biogenic phosphates of fossil and subfossil animal bones
- P-37 **Jiří Sejkora:** Three natural As modifications from the Příbram uranium and base-metal district, Czech Republic
- P-38 **Yuliya V. Shchapova:** Lattice dynamics of crystalline and radiation-damaged zircon by the data of low-temperature Raman spectroscopy
- P-39 **Jürgen Schreuer:** Elastic properties of monoclinic alkalifeldspars
- P-40 **Henrik Skogby:** Tourmaline OH contents studied by FTIR spectroscopy and proton-proton scattering analysis
- P-41 **Lenka Skřápková:** Role of dissolution-reprecipitation in deciphering mineral evolution trends in lepidolite-subtype pegmatites
- P-42 **Marcin Syczewski:** The clay minerals/phosphogypsum-based ceramic composite as a useful adsorbent for the uranium uptake
- P-43 **Gioacchino Tempesta:** Pigments characterization by spectroscopic methods of three Apulian precious parchments (Privilegium XV-XVII) from State Archives of Bari
- P-44 **Makiko Tomita:** Emission centers in barite estimated by cathodoluminescence spectrometry
- P-45 **Jaromír Tvrđý:** Zincoberaunite from Krásno, Czech Republic
- P-46 **František Veselovský:** Mineralogy of stibnite deposit at Chřič near Rakovník (Czech Republic)
- P-47 **Yuto Yamauchi:** Temperature effects on cathodoluminescence of Ba- and Sr-feldspar
- P-48 **Adam Zachař:** Bohseite-bavenite from intragranitic NYF pegmatites of the Třebíč pluton

# ORAL PRESENTATIONS



## The site-occupancy assessment in beryl based on bond-length constraints

**Peter Bačík** (presenting author)

Department of Mineralogy and Petrology, Faculty of Natural Sciences, Comenius University in Bratislava, Ilkovičova 6, Mlynská dolina, SK-842 15 Bratislava, Slovakia,  
Earth Science Institute, Slovak Academy of Sciences, Dúbravská cesta 9, SK-845 28 Bratislava, Slovakia

Co-author(s): Jana Fridrichová

Department of Mineralogy and Petrology, Faculty of Natural Sciences, Comenius University in Bratislava, Ilkovičova 6, Mlynská dolina, SK-842 15 Bratislava, Slovakia

Beryl hexagonal structure has a 3D framework of  $\text{AlO}_6$  octahedra,  $\text{SiO}_4$  and  $\text{BeO}_4$  tetrahedra and channels surrounded by  $\text{SiO}_4$  tetrahedral rings. The site preference for each cation based on the bond-valence calculations was determined and compared with analytical data (65 beryl structures and spectroscopic data).

Tetrahedral  $\text{SiO}_4$  six-membered rings normally have no substitutions which results from very compact Si-O bonds in tetrahedra (average of 1.606 Å from single-crystal refinement, calculated 1.624 Å). Any substitution except Be (calculated 1.635 Å) would require significant tetrahedral ring distortion.

The Be tetrahedron should also be negligibly substituted based on bond-valence calculation and empirical data (1.659 Å), but LiBe-1 substitution was already described. The tetrahedral Li-O bond-length is 1.952 Å which is almost 20 % larger than Be-O. Smaller bond lengths were calculated for Cr, V,  $\text{Fe}^{3+}$ ,  $\text{Mn}^{3+}$ , Mg and Al suggesting that these cations could also substitute for Be. Moreover, tetrahedral  $\text{Fe}^{2+}$ -O bond length is only slightly larger than that of Li. However, based on Electron Paramagnetic Resonance (EPR) data, Li can occupy the tetrahedral site slightly shifted from the Be site (0.43, 0.34, 0.17) [1]. Since there are two neighbouring Li sites near Al site and assuming their occupancy by all mentioned cations, this could explain observed  $\text{Fe}^{2+}$ - $\text{Fe}^{3+}$  intervalence charge transfer observed in optical absorption spectra (OAS) of beryl.

Octahedral site is also very compressed due to dominant Al with short bond lengths (1.606 Å from SREF, calculated 1.624 Å). All typical octahedral cations form longer bonds resulting in the octahedron expansion.

There are two channels sites in beryl, smaller in the centre of each tetrahedral ring and larger between the pair of rings. Smaller 2b site is surrounded by six ring oxygens but presence of cations at this site requires  $\text{H}_2\text{O}$  molecule at the neighbouring to satisfy charge and bond-valence requirements. Consequently, the coordination of this site is 8 (or 7). Bond-length calculations revealed that only Na, Ca, Li and REE are proper to occupy 2b site with average 2b-O distance of 2.48 Å (half of channel diameter),  $\text{Fe}^{2+}$  and  $\text{Fe}^{3+}$  are too small, K, Cs, Rb and Ba are too large. This calculation contradicts the possibility of Fe present in the channels as suggested by some spectroscopic (OAS, EPR, Mössbauer) studies. The 2a site coordination is 12, the average bond length (calculated from Cs-rich beryls) is 3.38 Å. This is very large distance, larger than calculated Cs-O bond length (3.31 Å). This allows the presence of simple molecules as  $\text{H}_2\text{O}$ ,  $\text{CO}_2$  or  $\text{NH}_4$ , easily recognized by the IR and Raman spectroscopy. Among cations, the large size of the site results in preferring Cs at this site, which is in fact the most abundant cation at this site in natural samples.

This work was supported by the Slovak Research and Development Agency under the Contract no. APVV-18-0065.

### References

[1] Andersson, L.O. (2006) Phys. Chem. Minerals 33, 403–416.

## Oxidation state of manganese in oxide minerals by Raman spectroscopy

Simone Bernardini (presenting author)

Department of Science, Roma Tre University, Via della Vasca Navale 84, 00146 Rome, Italy

Co-author(s): Fabio Bellatreccia, Giancarlo Della Ventura, Armida Sodo

Department of Science, Roma Tre University, Via della Vasca Navale 84, 00146 Rome, Italy

Manganese oxides (MnOx) are widespread over all geological environments, being ubiquitous, in particular, in soils and sediments. Moreover, they are major components of polymetallic nodules that cover large areas of the ocean floor [1]. Recently, MnOx have been also identified on Mars surface, suggesting a possible Earth-like environment during the Martian geological history [2, 3]. Since, fluids conditions (e.g. pH, Eh, P, T, microbial activity) strongly control their crystallization, each environment has its own MnOx paragenesis, characterized by typical oxidation state (OS) of Mn. Moreover, the OS of Mn in the bulk and near-surface material has an important role on the physical-chemical proprieties of MnOx (e.g. heavy metals absorption, magnetism and so on).

Therefore, the characterization of the OS of Mn is a central issue in scientific works where these materials are involved, both in environmental and technological investigations.

Diffraction methods, although mandatory for a proper structural characterisation of crystalline compounds, do not allow a direct and unambiguous determination of the OS of Mn; these techniques may actually provide only an indirect estimation, by comparing average observed  $\langle \text{Mn-O} \rangle$  bond distances with those expected for each Mn ionic species. On the other side, both coordination environment and OS can be successfully investigated by different spectroscopic techniques, such as XPS, ESR, EELS, XES and XANES [4-6].

Because Raman spectroscopy is sensitive to the short-range environment of cations, we examined the possibility to derive the OS of Mn in MnOx based on a careful and systematic interpretation of their Raman spectra.

Comparing structural and Raman data of many well-characterized Mn oxides, we show that there is a clear correlation between the OS of Mn and the wavenumber of some Raman bands. Two trends can be recognized: the first related to the  $\nu_1$  vibrational mode of  $\text{MnO}_6$  octahedra, between 500 and 670  $\text{cm}^{-1}$ , and the second related to the  $\nu_1$  vibrational mode of  $\text{MnO}_4$  tetrahedra, between 650 and 850  $\text{cm}^{-1}$ ; the band position along each trend is correlated with the OS of Mn. In more details, in octahedral coordination  $\text{Mn}^{2+}$  is characterized by a band at  $\sim 530 \text{ cm}^{-1}$ ,  $\text{Mn}^{3+}$  by a band at  $\sim 580 \text{ cm}^{-1}$  and  $\text{Mn}^{4+}$  by a band at  $\sim 630 \text{ cm}^{-1}$ . In tetrahedral coordination,  $\text{Mn}^{2+}$  is characterized by a band at  $\sim 650 \text{ cm}^{-1}$ . Jahn-Teller activated-modes in strongly distorted  $\text{Mn}^{3+}\text{O}_6$  octahedra can lead to the arising of bands that simulate all the OS.

Our results show that Raman spectroscopy allows a quickly, accessible and local evaluation of the OS of Mn in oxide minerals with a high level of reliability and high spatial resolution.

### References

- [1] Post, J.E. (1999) Proc. Natl. Acad. Sci. USA 96, 3447.
- [2] Lanza, L.N., et al. (2014) Geophysical Research Letters 41, 16, 5755.
- [3] Arvidson, R.E., et al. (2016) Am. Mineral. 101, 1389.
- [4] Ilton, E.S., et al. (2016) Applied Surface Science 366, 475.
- [5] Chalmin, E., et al. (2009) Contrib. Mineral. Petrol. 157, 111.
- [6] Manceaou, A., et al. (2012) American Mineralogist 97, 816.

## Characterizing the surface of Mars through remote spectral identification of minerals

Janice Bishop (presenting author)

SETI Institute & NASA-Ames

Spectrometers orbiting Mars are providing information about the surface composition including igneous minerals and alteration products. The CRISM instrument on the Mars Reconnaissance Orbiter is measuring visible/near-infrared (VNIR, 0.4–4  $\mu\text{m}$ ) spectra at 18 m/pixel surface resolution and has enabled mapping a variety of hydrated minerals, pyroxene, and olivine. Analyses of these data suggest distinct aqueous geochemical environments on Mars including paleolakes, evaporites, hot springs, and subsurface hydrothermal systems. Liquid water on the surface of Mars during its early history likely took many forms. Changes in the climate and geochemical environment of early Mars can now be estimated through analyses of minerals in surface outcrops. Minerals in alteration environments include a variety of phyllosilicates, monohydrated sulfates, polyhydrated sulfates, carbonates, zeolites, perchlorates, and poorly crystalline phases. Phyllosilicates are the most abundant alteration mineral and these are frequently observed with Al-rich phyllosilicates emplaced on top of Fe- or Mg-rich phyllosilicates. Recent advances in image calibration are enabling detection and discrimination of smaller outcrops of hydrated minerals as the spectral signal is improved. Small outcrops of mixed phyllosilicate/sulfate deposits have been found in several regions with abundant phyllosilicates. These could be remnants of salty evaporite ponds during a time when the climate was changing on early Mars.

### Mawrth Vallis Phyllosilicate Stratigraphy

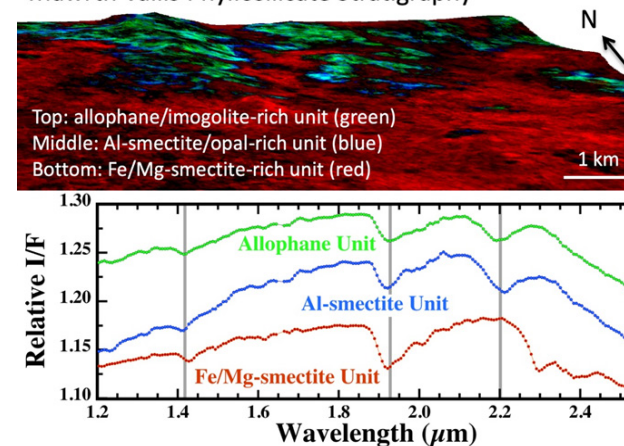


**Figure 1.** Phyllosilicate mineral stratigraphy determined from orbit using VNIR spectroscopy

Characterization of the minerals observed at Mars analog sites on Earth is enabling more precise mineral assignments in martian spectra. Smectites, hematite, and jarosite are formed at cinder cones and fumarole sites in volcanic environments. Gypsum and halite are observed in evaporite settings and can be mixed with opal, kaolinite, alunite, and jarosite. Hot springs at Yellowstone contain carbonates in alkaline systems and silica, ferric oxides/hydroxides, and jarosite/alunite in acidic systems. Diagenetic environments include mixtures of smectite, illite, chlorite, talc, serpentine, zeolite, and/or carbonate. Alteration in glacial environments results in higher abundances of poorly crystalline phases and fewer crystalline clays. Lab and field spectra of such analog samples is improving our ability to discern minerals on Mars in complex, natural mixtures. Orbital spectral data is also compared with the mineralogy detected in situ by martian rovers as a form of ground truthing. Smectites, hematite, gypsum, and abundant amorphous material have been found at Gale crater through XRD measured by the CheMin instrument. Mössbauer and Mini-TES spectra were used to identify hematite, goethite, silica, and carbonate at Gusev crater and to identify hematite, jarosite, and other sulfates at Meridiani Planum. Smectites, hematite, carbonate, jarosite, and hydrated sulfates were detected at these sites through orbital spectroscopy. Support from NASA's MDAP and NAI programs are greatly appreciated.

## New insights on the discrimination of synthesized ochres by $\mu$ -FTIR: Mars yellow and calcinated red ochres recognition criteria

**Michela Botticelli** (presenting author)

Dept. of Earth Sciences, „Sapienza“ University of Rome, P.le Aldo Moro, I-00185 Rome, Italy

Co-author(s): António Candeias<sup>1</sup>, Adriana Maras<sup>2</sup>

<sup>1</sup>HERCULES Laboratory, University of Evora, Largo Marquês de Marialva, 8, 7000-089 Évora, Portugal

<sup>2</sup>Dept. of Earth Sciences, „Sapienza“ University of Rome, P.le Aldo Moro, I-00185 Rome, Italy

The discrimination of synthetic and natural red ochres is an intriguing topic, being the synthesis of these pigments probably known since Prehistory [1, 2]. The present work is a systematic study to define the best, less invasive methodology in the discrimination of synthetic and natural red ochres. After the laboratory synthesis of Mars yellow and the collection of commercial or museum samples, all yellow samples were heated following two different pathways to obtain synthetic red ochres. The sample-set has been characterized by different analytical techniques: X-ray powder diffraction (XRPD), scanning electron microscopy coupled with energy dispersive spectroscopy (SEM-EDS), thermal analysis and Fourier transform infrared spectroscopy ( $\mu$ -FTIR). The synthetic pathway was also reproduced and followed through differential thermal analysis (DTA and TG). This multi-analytical approach was set to understand which technique – or a combination of more than one – has higher efficiency in the distinction of synthetic and natural red ochres. XRD remarked the different origin of precursory samples. SEM-EDS showed typical morphological features of Mars yellow that are partially retained even after heating, leading to the recognition of both Mars pigments. DTA and TG highlighted that the process sensibly differs from Mars yellow to natural ochres. Mars yellow is in fact characterized by a double-peak with minima at 551 and 577 K, while dehydration is a single-step process in natural ochres. Finally,  $\mu$ -FTIR proved to be very effective to discriminate a soft heating from the hard one. In particular, hydroxyl and  $\text{FeO}_6$  bands in the fingerprint region were the most useful for the task. Distinctive features of Mars products were for the first time characterized thanks to this combined methodology.

### References

- [1] Helwig K. (2014) in Artists' pigments: a handbook of their history and characteristics, 4. National Gallery of Art and Archetype Publications.  
[2] Salomon H., et al. (2015) J. Archaeol. Sci. 55, 100.

## Phosphides of schreibersite-nickelphosphide series as indicators of crystallization history of meteorites

**Sergey Britvin** (presenting author)

Saint Petersburg State University, Russia

Co-author(s): Maria Krzhizhanovskaya, Andrey Zolotarev, Liudmila Gorelova

Saint Petersburg State University, Russia

Natural phosphides – the minerals containing phosphorus in the oxidation state lower than zero – are typical constituents of space matter though rarely found on Earth [1]. Phosphides related to ternary Fe-Ni-P system comprise the dominant part of this mineral group. The most common phosphide, schreibersite,  $(\text{Fe,Ni})_3\text{P}$ , belongs to the earliest known meteoritic minerals [2] whereas its nickel-dominant analogue, nickelphosphide,  $(\text{Ni,Fe})_3\text{P}$ , was recognized as a distinct species for almost 170 years later [3]. In spite of compositional simplicity, the minerals related to schreibersite-nickelphosphide join exhibit complex crystal chemistry, due to presence of three independent metal sites in their crystal structure. Doenitz [4] first demonstrated the non-random distribution of Fe and Ni among M1, M2 and M3 sites of schreibersite structure. Further studies of these minerals were mainly devoted to iron-dominant (schreibersite) side of  $\text{Fe}_3\text{P-Ni}_3\text{P}$  series, whereas studies of nickelphosphide were performed only on synthetic counterpart of natural nickelphosphide [5]. In the course of ongoing research of natural phosphides, we carried out structural study of the minerals related to schreibersite-nickelphosphide series originated from more than 40 meteorites of different chemical and structural groups. The study involved both methodological and scientific aspects. It was established that distribution of Fe ( $Z = 26$ ) and Ni ( $Z = 28$ ) among M1, M2 and M3 sites of  $\text{Fe}_3\text{P-Ni}_3\text{P}$  solid solutions can be quantitatively determined using conventional X-ray single crystal methods, without implementation of resonant scattering techniques. It was found that site substitution schemes along the join  $\text{Fe}_3\text{P-Ni}_3\text{P}$  are more complex than it was supposed in the previous works. In particular, nickelphosphide halve of the series exhibits substantial sensitivity towards Fe/Ni distribution, depending on the origin of the mineral. The results of the present study could provide some new implications related to crystallization histories of meteorites and their parent bodies.

This work was supported by the Russian Science Foundation (grant No 18-17-00079). The authors thank Centre for X-ray Diffraction Studies and Geomodel Centre of Saint Petersburg State University for providing instrumental and computational resources.

### References

- [1] Berzelius, A.J. (1832) K. Sven. vetensk. akad. handl. 106–119.  
[2] Britvin, S.N., et al. (1999) Zapiski VMO 128, 64–72 (Russian).  
[3] Britvin, S.N., et al. (2015) Sci. Rep. 5, 8355.  
[4] Doenitz, F.D. (1970) Z. Kristall. 131, 222–236.  
[5] Skála, R., Drábek, M. (2003) Mineral. Mag. 67, 783–792.

## New Landscapes of Uranium Mineralogy

**Peter C. Burns** (presenting author)

Department of Civil and Environmental Engineering and Earth Sciences Department of Chemistry and Biochemistry Center for Sustainable Energy University of Notre Dame 301 Stinson Remick Hall, Notre Dame, IN 46556, USA

Actinides are of great societal importance: they are the fuel of nuclear energy, are important for international security and nuclear non-proliferation, are essential for medical isotope production, are major components of nuclear waste, and are serious environmental contaminants at many sites related to the nuclear fuel cycle and weapons production. Uranium, the heaviest actinide that naturally occurs in appreciable quantities, produces a vast array of chemically and structurally complex uranium minerals. This presentation focuses on highlights of the past decade of studies of the uranium mineralogy of two classic localities - Jáchymov, Czech Republic and Shinkolobwe, Democratic Republic of Congo, as well as a relatively new emerging classic locality – Red Canyon, Utah (USA). More than 20 new uranyl minerals have been described from these localities over the past decade. Those from Red Canyon have vastly increased the structural and chemical diversity of uranyl sulfate minerals, those from Jáchymov have demonstrated tremendous and unprecedented structural complexity, and those from Shinkolobwe have further expanded the group of uranyl oxyhydrate minerals and provided unexpected examples of uranium minerals containing uranium the extremely rare pentavalent oxidation state.

## Using polarized Raman spectroscopy to detect strain gradient in optical anomalous host-inclusion mineral systems

**Nicola Campomenosi** (presenting author)

Department of Earth Science, Environment & Life, University of Genova, Corso Europa 26, 16132 Genoa, Italy

Co-author(s): Mattia Luca Mazzucchelli<sup>1</sup>, Boriana D. Mihailova<sup>2</sup>, Ross J. Angel<sup>1,3</sup>, Matteo Alvaro<sup>1</sup>

<sup>1</sup>Department of Earth and Environmental Sciences, University of Pavia, Via A. Ferrata, 1 27100 Pavia, Italy

<sup>2</sup>Department of Earth Sciences, University of Hamburg, Grindelallee 48, D-20146 Hamburg, Germany

<sup>3</sup>IGG-CNR Padova, Italy

Optical anomalies in mineral systems can develop as a response of the contrast in the elastic properties between different phases constrained within a confined space. Key evidence of this, for example, is the development of induced birefringence haloes in a cubic host crystal surrounding pressurized mineral inclusions. From an optical point of view, this phenomenon has been widely described since it is a quite common feature in diamond-bearing systems [1]. In this study, we present a new and complementary technique in defining these issues using polarized Raman spectroscopy. Indeed, our experimental results on zircon and quartz inclusions within two different garnet hosts, show that the ratio between the Raman intensity of spectra collected under cross and parallel polarized scattering geometry (i.e. depolarization ratio), for fully symmetric phonon modes, and their intensity maps, represent a powerful tool in visualizing the stress decay from the host-inclusion boundary. This has been also confirmed by selected numerical models. Furthermore, we show how tensor analysis and elementary group theory can be exploited to define the stress induced symmetry of the host crystal which in turn give us information on the symmetry of the acting stress field. Further, we demonstrate experimentally that such a technique is more sensitive in detecting strain gradient in crystals with respect to the commonly used approach of measuring variation in phonon frequencies. Finally we would like to emphasize the possibility to use this complementary approach also in other mineralogical context.

This work was supported by ERC-StG TRUE DEPTHS grant (number 714936) and MIUR-SIR Mile Deep grant (number RBSI140351) to M. Alvaro. N. Campomenosi was also supported by the University of Genova

### References

[1] Howell, D. (2012) Eur. J. Mineral. 24, 575–585

## A new solvothermal approach to obtain nanoparticles in the $\text{Cu}_3\text{SnS}_4$ - $\text{Cu}_2\text{FeSnS}_4$ join

Francesco Di Benedetto (presenting author)

Department of Earth Sciences, University of Florence, Florence (Italy)

Co-author(s): Andrea Giaccherini<sup>1</sup>, A. Griesi<sup>2</sup>, Giordano Montegrossi<sup>3</sup>, M. Romanelli<sup>4</sup>, G. O. Lepore<sup>5</sup>, A. Lavacchi<sup>6</sup>, Georg Amthauer<sup>7</sup>, Günther J. Redhammer<sup>2</sup>, G. Tippelt<sup>8</sup>, G. Cucinotta<sup>8</sup>, M. Mannini<sup>8</sup>, Stefano Martinuzzi<sup>8</sup>, A. Caneschi<sup>7</sup>

<sup>1</sup>Dept. of Industrial Engineering, DIFE, University of Florence, Italy

<sup>2</sup>Istituto Italiano di Tecnologia Center for Nanotechnology Innovation @NEST, Pisa, Italy

<sup>3</sup>Istituto di Geoscienze e Georisorse, CNR, Florence, Italy

<sup>4</sup>Dept. of Earth Sciences, University of Florence, Italy

<sup>5</sup>Operative Group in Grenoble, Istituto Officina dei Materiali, CNR c/o ESRF, Grenoble, France

<sup>6</sup>Istituto di Chimica dei Composti Organometallici, CNR, Sesto Fiorentino, Italy

<sup>7</sup>Department of Chemistry and Physics of Materials, University of Salzburg, Austria

<sup>8</sup>Dept. of Chemistry, University of Florence, Italy

In the field of the renewables, a large effort has been devoted in the last years to obtain conventional and new materials for solar energy conversion by using methods which couple a good efficiency and scalability with energetic and environmental concerns. This research has obviously included the so-called kesterites, materials considered interesting for the thin film solar cell technology, which consists of relatively abundant and harmless elements:  $\text{Cu}_{3-x}\text{Fe}_x\text{Zn}_y\text{Sn}(\text{S},\text{Se})_4$ .

In this study, we undertook the synthesis of terms of the kuramite-stannite ( $\text{Cu}_3\text{SnS}_4$ - $\text{Cu}_2\text{FeSnS}_4$ ) join by means of a two-step solvothermal approach, which is able to provide nanocrystalline products in an easy, low temperature, and fast way.

The sample with the highest Fe concentration was characterised by means of a multi-analytical approach, aimed to assess not only its final structural, chemical and micromorphological features, but also the redox speciation of the two transition metal cations, i.e. Cu and Fe, in relation to the overall charge balance. Namely, EPR, Mössbauer and XAS spectroscopies and SQUID magnetometry were involved.

The main results point out an excellent control of the structural features, and a good Fe content in the sample, leading to the following formula unit:  $\text{Cu}_{1.9}\text{Fe}_{0.6}\text{SnS}_4$ . According to this composition, a relevant fraction of oxidised Cu and Fe ions were hypothesized. The overall finding of the multi-analytical characterisation point to a complex redox balance, where inferring the site occupancy is non trivial: the charge balance, in fact, can only be achieved taking into account the presence of both Cu(II) and Fe(III) but also vacancies; moreover, Fe is distributed over two different crystallographic sites.

## Arsenic in roméite-group minerals formed by weathering of realgar-rich tailings (Lojane mine, North Macedonia)

Tamara Đorđević (presenting author)

Institut für Mineralogie und Kristallographie, Universität Wien, Althanstr. 14, 1090 Wien, Austria

Co-author(s): Uwe Kolitsch<sup>1,2</sup>, Todor Serafimovski<sup>3</sup>, Goran Tasev<sup>3</sup>, Blažo Boev<sup>3</sup>, Michael Stöger-Pollach<sup>4</sup>

<sup>1</sup>Mineralogisch-Petrographische Abteilung, Naturhistorisches Museum, Burgring 7, 1010 Wien, Austria

<sup>2</sup>Institut für Mineralogie und Kristallographie, Universität Wien, Althanstr. 14, 1090 Wien, Austria

<sup>3</sup>Department of Mineral Deposits, Faculty of Natural and Technical Sciences, University "Goce Delčev"-Štip, Goce Delčev 89, 2000 Štip, North Macedonia

<sup>4</sup>University Service Centre for TEM, Technische Universität Wien, Wiedner Hauptstr. 8-10, 1040 Wien, Austria

Realgar and stibnite are the primary sources of arsenic and antimony contamination of the soils and water at the Sb-As-Cr Lojane mine (abandoned since 1979) in North Macedonia. The waste material comprises various waste dumps, an unprotected flotation tailings dump, and waste from a smelter. We have studied the association of As and Sb in realgar and stibnite weathering products from material sampled at the subsurface of the realgar-rich (up to 60 wt% realgar), fine-grained (20 to 100  $\mu\text{m}$ ) and porous tailings which contain significant amounts of stibnite (up to 13.5 wt%) [1].

Besides minor scorodite, arsenolite, annabergite, native sulfur, iron oxy-hydroxides, pickeringite, and alunogen, the weathering of the tailings material produces a chemically inhomogeneous Sb-As-Fe-Ca-(Ni)-oxide/hydroxide as the most widespread secondary phase. In this phase the As:Sb ratio varies from ca. 2:1 to 1:2.2 and the Fe content is variable. The phase mostly forms thin coatings around realgar and stibnite grains, but Sb-dominant variants also form larger homogeneous grains up to 500  $\mu\text{m}$ , characterized by broad dehydration cracks.

Using a combination of SEM-EDS, TEM, and Raman spectroscopy, this poorly crystalline to amorphous weathering product was determined to be an (often As-dominant) member of the roméite-group minerals (RGM) which themselves belong to the large pyrochlore supergroup of minerals [2] with general stoichiometry  $\text{A}_2\text{B}_2\text{X}_6\text{Y}$ , where A = non-framework cations (ideally 8-coordinated), B = octahedrally coordinated framework cations, X = framework anions and Y = non-framework anions. Although B sites are likely to be fully occupied, A sites may be partially vacant. The total number of cations per formula unit depends on valence determination, as does the amount of H needed for charge balance, and hence minimum  $\text{H}_2\text{O}$  content.

The crystallographic position of arsenic in the RGM in our samples is not fully clear. Although  $\text{As}^{5+}$  may occupy the octahedrally coordinated B-position in the roméite structure, it strongly prefers a tetrahedral coordination. The distorted A-centered polyhedron in RGM is too large for the  $\text{As}^{5+}$  cation. These crystal-chemical preferences explain that the As is hosted mostly in the X-ray amorphous phases. However, EDS point analyses clearly document that the roméite-type phase may incorporate considerable arsenic. Besides the intense Raman band at  $\sim 520\text{ cm}^{-1}$  assigned to the Sb-O symmetric stretching mode and the band at  $\sim 466\text{ cm}^{-1}$  assigned to the Sb-O antisymmetric stretching mode, Raman spectra of RGM-phases show additional weaker and broader bands in the region  $835\text{--}915\text{ cm}^{-1}$ . These bands correspond to the  $\text{AsO}_4$  stretching vibrations [3] and thus additionally confirm the presence of  $\text{As}^{5+}$  in the structure.

### References

- [1] Đorđević, T., et al. (2019) Can. Mineral. 57, 1–21.
- [2] Bosi, F., et al. (2017) Mineral. Mag. 81, 1287–1302.
- [3] Bahfenne, S., et al. (2010) Appl. Spec. Reviews 45, 101–129.

## A Gemmological Approach to Distinguishing Natural from Synthetic Rubies: LA-ICP-TOF mass spectrometry provides new insights

**Tashia Dzikowski-Hutter** (presenting author)  
SSEF Swiss Gemmological Institute, Switzerland

Co-author(s): Hao Wang, Pierre Lefèvre, Wei Zhou, Michael S. Krzemnicki  
SSEF Swiss Gemmological Institute, Switzerland

Identifying the subtle differences between natural, synthetic, and treated natural or synthetic rubies (Cr-bearing variety of  $\text{Al}_2\text{O}_3$ ) can be difficult due to the overlap of physical properties and some trace elements, the presence of similar inclusions or growth features, or the absence of inclusions or growth features. A gemmological approach to distinguishing natural from synthetic rubies involves a combination of meticulous microscopic observations (to examine inclusions and growth features), in addition to Raman spectroscopy (to identify inclusions), and ED-XRF spectrometry as well as LA-ICP-MS (to determine trace element compositions). The presence of rounded to elongated bubbles with or without curved growth lines or colour zones in addition to the presence of Cr and the absence of Ga and other trace elements, can easily identify a flame fusion synthetic ruby. Misidentification can occur in three situations: 1) when natural inclusions in rubies such as phlogopite, negative crystals, healed fissures, and iron staining are confused with platinum flakes, gas bubbles, or flux residue in flux melt synthetic rubies, 2) when natural rubies are heated with a flux and it is not known if the flux residue in healed fissures is from flux melt synthesis or a side effect of the heating process, or 3) when synthetic stones are heated with a flux to produce natural-looking inclusions. Trace element composition is extremely important when these potentially confusing inclusions are present or in the absence of any inclusions or growth features. V, Cr, Ga, and Fe are typically useful for distinguishing natural from synthetic rubies, however Ga may also be present in some flux synthetic rubies. Pt and Rh in addition to other exotic elements are present on average in higher concentrations in synthetic rubies. These elements are often present in the starting material or synthesizing apparatus. Time-of-flight mass spectrometry (LA-ICP-TOF-MS) is especially powerful to identify flux-melt synthetic rubies (and other synthetic minerals), as it provides fast and simultaneous chemical data of nearly the full range of isotopes. It is even possible using this technique to fully chemically characterize flux residues of exotic composition from specific synthetic ruby producers (e.g. Ramaura synthetic ruby from J.O.Crystal Inc. USA uses a REE-rich flux for their synthesizing process) without using a pre-selection of analysed isotopes, as would be necessary with conventional quadrupole mass spectrometry (LA-ICP-Q-MS). This multi-faceted approach combined with critical examination of all data is necessary to distinguish samples with similar characteristics.

## Oxidized Mg- and Fe-rich tourmaline with significant amounts of Sr and Pb

**Andreas Ertl** (presenting author)  
Institut für Mineralogie und Kristallographie, Geozentrum, Universität Wien, Althanstrasse 14, 1090 Vienna, Austria

Co-author(s): George R. Rossman<sup>1</sup>, Dan Topa<sup>2</sup>

<sup>1</sup>Division of Geological and Planetary Sciences, California Institute of Technology, Pasadena, California 91125-2500, USA

<sup>2</sup>Zentrale Forschungslaboratorien, Naturhistorisches Museum, Burgring 7, 1010 Vienna, Austria

A near-rim zone of an oxidized Mr- and Fe-rich high-pressure tourmaline from an eclogite (Kreuzeck Mountains, Eastern Alps, Austria) contains 0.6 wt% SrO, 0.6 wt%  $\text{Cr}_2\text{O}_3$  and 0.5 wt%  $\text{PbO}_2$ . Optical absorption spectroscopy was used to estimate the percentage of  $\text{Fe}^{2+}$ . For this purpose the band near 1120 nm was used, because it is the band that is best separated from other bands. To estimate the proportion of the two oxidation states, the intensity of the  $\text{Fe}^{2+}$  bands in the investigated tourmaline was compared to the intensity of the  $\text{Fe}^{2+}$  bands in two zones of a previously very well characterized Fe-bearing elbaite from the Himalaya Mine [1] assuming that a Beer's Law calibration applies equally to all the crystals. The result infers that in the investigated tourmaline only ca. 20% of the total iron is in the 2+ oxidation state. It can be presumed that this high-pressure tourmaline crystallized under oxidizing conditions, which would also be amenable to the mobilization of Sr. Advantages of using optical absorption spectroscopy for such an estimation are that it can be obtained much faster compared to Mössbauer spectroscopy and the estimation can be done on small, individual areas of a crystal, down to 100 x 100 nm.

The sum of (Na + Ca + Sr + K) for the different zones shows that the [9]-coordinated X site is completely filled up by these occupants. Because in this tourmaline ca. 80% of the total Fe is oxidized, it is likely that also Pb is oxidized to  $\text{Pb}^{4+}$ . In a [6]-coordination  $\text{Pb}^{4+}$  has an effective ionic radius, which is very similar to Mg and  $\text{Fe}^{2+}$ . Therefore we assigned these small amounts of Pb in tourmaline to the [6]-coordinated Y site and not to the X site.

This work was supported by the Austrian Science Fund (FWF) project no. P31049-N29.

### References

[1] Ertl, A., et al. (2010) Am. Mineral. 95, 24–40.

## The Magnetic Behavior of Olivine and Garnet Substitutional Solid Solutions

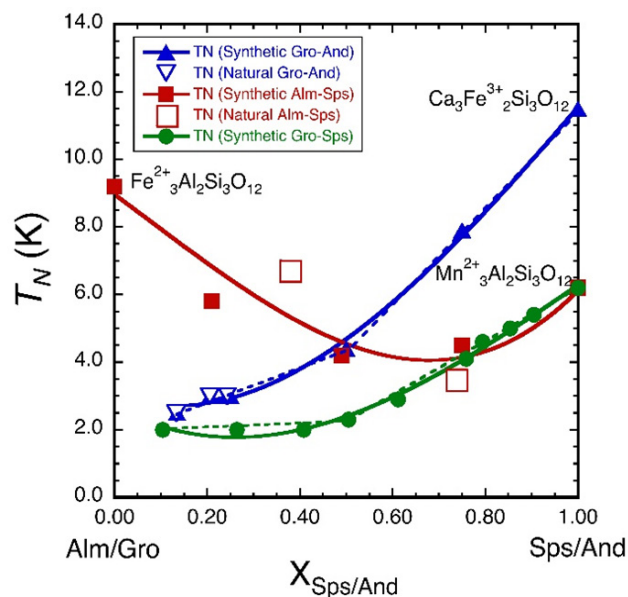
Charles A. Geiger (presenting author)

University of Salzburg; Department Chemistry and Physics of Materials

Co-author(s): Michael Grodzicki, Edgar Dachs

University of Salzburg; Department Chemistry and Physics of Materials

The low-temperature magnetic properties and Néel temperature,  $T_N$ , of four silicate substitutional solid solutions containing paramagnetic ions will be discussed. The four systems are: fayalite-forsterite olivine,  $\text{Fe}^{2+}_x\text{SiO}_4\text{-Mg}_{2-x}\text{SiO}_4$ , and the garnet series, grossular-andradite,  $\text{Ca}_3(\text{Al}_x\text{Fe}^{3+}_{1-x})\text{Si}_3\text{O}_{12}$ , grossular-spessartine,  $(\text{Ca}_x\text{Mn}^{2+}_{1-x})\text{Al}_2\text{Si}_3\text{O}_{12}$ , and almandine-spessartine,  $(\text{Fe}^{2+}_x\text{Mn}^{2+}_{1-x})\text{Al}_2\text{Si}_3\text{O}_{12}$ . Local magnetic behavior of the transition-metal-bearing end members is taken from published neutron diffraction results and computational studies.  $T_N$  values are from calorimetric heat capacity,  $C_p$ , and magnetic susceptibility measurements. These end-members, along with more transition-metal-rich solid solutions, show a paramagnetic to anti-ferromagnetic phase transition. It is marked by a  $C_p$  I-anomaly that decreases in temperature and magnitude with increasing substitution of the diamagnetic component. For olivines,  $T_N$  varies between 65 K and 18 K and  $T_N$  for the various garnets is less than 12 K. Local magnetic behavior can involve one or more superexchange interactions mediated through oxygen atoms.  $T_N$  behavior shows a quasi-plateau-like effect for the systems fayalite-forsterite, grossular-andradite and grossular-spessartine. More transition-metal-rich crystals show a stronger  $T_N$  dependence compared to transition-metal-poor ones. The latter may possibly show superparamagnetic behavior.  $(\text{Fe}^{2+}_x\text{Mn}^{2+}_{1-x})\text{Al}_2\text{Si}_3\text{O}_{12}$  garnets show fundamentally different magnetic behavior. End-member almandine and spessartine have different and complex interacting local superexchange mechanisms and intermediate compositions show a double-exchange magnetic mechanism. For the latter,  $T_N$  values show negative deviations from linear interpolated  $T_N$  values between the end members. Double exchange occurs seldomly in oxides, and this may be the first documentation of this magnetic mechanism in a silicate.  $T_N$  behavior may possibly be used to better understand the nature of macroscopic thermodynamic functions,  $C_p$  and  $S^\circ$ , of both end-member and substitutional solid solutions phases.



## Spectroscopic and structural analysis of ultra-thin $\text{Cu}_2\text{S}/\text{CdS}$ semiconducting devices

Andrea Giaccherini (presenting author)

Department of industrial engineering, University of Florence, Italy

Co-author(s): Francesco Carlà<sup>1</sup>, Francesca Russo<sup>2</sup>, Annalisa Guerri<sup>2</sup>, Giordano Montegrossi<sup>3</sup>, Enrico Berretti<sup>4</sup>, Alessandro Lavacchi<sup>5</sup>, Emanuele Salvietti<sup>6</sup>, Patrick Marcantelli<sup>7</sup>, Stefano Martinuzzi<sup>2</sup>, Maurizio Passaponti<sup>2</sup>, Walter Giurlani<sup>2</sup>, Lorenzo Poggini<sup>2</sup>, Mathieu Gonidec<sup>8</sup>, Roberto Felici<sup>2</sup>, Tommaso Baroni<sup>8</sup>, Francesco Di Benedetto<sup>8</sup>, Massimo Innocenti<sup>2</sup>

<sup>1</sup>Diamond Light Source, Chilton, Didcot, UK

<sup>2</sup>Department of chemistry, University of Florence, Italy

<sup>3</sup>CNR-IGG, Firenze, Italy

<sup>4</sup>CNR-ICCOM, Firenze, Italy

<sup>5</sup>ICMCB, CNRS, Pessac, France

<sup>6</sup>ICMCB, University of Bordeaux, Pessac, France

<sup>7</sup>CNR-SPIN, Roma, Italy

<sup>8</sup>Department of earth sciences, University of Florence, Italy

The development of micro and nano p-n junctions technology drove the research on information and communication technologies as well as photovoltaics and light emission diodes. For instance, in the basic component of your computer or in the camera of your smartphone there are billions of transistors and for each of them 5 p-n junctions [1]. The current production processes of these devices are complex and energy hungry (Czochralski growth, ion implantations and growth of metals and metal-oxides layers by means of ultra-high vacuum methods). On the contrary, electrodeposition from aqueous solutions reduces wastes, energy consumption and safety constraints. Indeed, electrodeposition from aqueous solutions succeed in growing high-quality layers of semiconducting crystalline chemical compounds [2] while failing the direct growth of p-n junctions. Still, we succeed in the growth of a p-n junction by means of Electrochemical Atomic Layer Deposition (E-ALD) [3] of CdS [4] and  $\text{Cu}_2\text{S}$  [5] without any intermediate manipulation. We investigated the structure and the growth process by means of operando surface X-ray diffraction and ex-situ X-ray photoelectron spectroscopy. We found that we can grow an ordered  $\text{Cu}_2\text{S}/\text{CdS}$  p-n junction avoiding the intermixing between the n and p layers. The focused ion beam and scanning electron microscopy confirmed the total thickness of 18 nm. The fact that the device is thinner than the depletion layer of bulk heterojunctions induces an unusual bending of the electronic structure bands. This feature explains the unexpected light absorption properties of the devices reckoned by means of diffuse reflectance spectroscopy. Eventually, our device responds to the direct current stimulus according to the Shockley model. At the moment, these facts show E-ALD as the only electrochemical techniques suitable for the direct growth of p-n junctions ensuring a scalable and environmentally friendlier 'life cycle' [6].

### References

- [1] Veendrick, H.J.M. (2017) Nanometer CMOS ICs.
- [2] Ojo, A.A., Dharmadasa, I. M. (2018) Coatings 8, 8, 262.
- [3] Huang, B.M., et al. (1995) J. Electrochem. Soc. 142, 9, 3007–3016.
- [4] Ceconi, T., et al. (2001) J. Electron Spectros. Relat. Phenomena 114–116, 563–568.
- [5] Innocenti, M., et al. (2011) Electrochim. Acta 58, 1, 599–605.
- [6] Innocenti, M., et al. (2016) SPIE Newsroom, 2–4.

## High-pressure behavior of hingganite-(Y), $\text{YBeSiO}_4(\text{OH})$

**Liudmila Gorelova** (presenting author)

Saint Petersburg State University, University Embankment 7/9, St. Petersburg, 199034 Russia

Co-author(s): Anna Pakhomova<sup>1</sup>, Sergey Krivovichev<sup>2,3</sup>, Anatoly Kasatkin<sup>4</sup>, Leonid Dubrovinsky<sup>5</sup>

<sup>1</sup>Deutsches Elektronen-Synchrotron (DESY), Petra III, Notkestraße 85, Hamburg, 22607 Germany

<sup>2</sup>Saint Petersburg State University, University Embankment 7/9, St. Petersburg, 199034 Russia

<sup>3</sup>Kola Science Centre, Russian Academy of Sciences, Fersman str. 14, Apatity, 184209 Russia

<sup>4</sup>Fersman Mineralogical Museum of the Russian Academy of Sciences, Leninskiy pr. 18, 2, 119071, Moscow, Russia

<sup>5</sup>Bayerisches Geoinstitut, University of Bayreuth, Universitätsstraße 30, Bayreuth, 95447 Germany

Hingganite-(Y),  $\text{YBeSiO}_4(\text{OH})$ , belongs to the gadolinite group [1], which contains such common minerals as datolite and gadolinite. Recent discovery of  $\text{SiO}_5$  polyhedra in the high-pressure modifications of datolite  $\text{CaBSiO}_4(\text{OH})$  [2] has inspired us to investigate hingganite as its structural analogue. The recent studies of beryllosilicate hurlbutite,  $\text{CaBe}_2\text{P}_2\text{O}_8$  [3], led to the discovery of unusual five- and six-fold oxygen-coordinated beryllium.

Under ambient conditions, hingganite is monoclinic ( $\text{P}2_1/c$ ). Its crystal structure consists of the  $[\text{BeSiO}_4(\text{OH})]^{2-}$  layers of corner-sharing  $\text{SiO}_4$  and  $\text{BeO}_4$  tetrahedra with  $\text{YO}_8$  polyhedra in the interlayer space [4]. The layers are based upon four- and elongated eight-membered rings of tetrahedra.

The high-pressure behavior of hingganite-(Y) was studied using in situ single-crystal X-ray diffraction in a diamond anvil cell at the Extreme Conditions Beamline P02.2 of PETRA III (DESY, Hamburg, Germany). For the study, we have used crystals of natural hingganite-(Y) from the Ploskaya mount, Kola Peninsula, Russia, obtained from a private collection of the fourth author, with the size of  $0.010 \times 0.010 \times 0.005 \text{ mm}^3$ . The experiments were performed at ambient temperature up to 50 GPa with the pressure step no more than 5 GPa (12 pressure points in total).

In the studied pressure range, hingganite-(Y) shows no phase transition, in contrast to datolite, which underwent a displacive phase transition with the formation of  $\text{SiO}_5$  polyhedra at the pressure above 33 GPa [2]. However, above 40 GPa,  $\text{SiO}_4$  tetrahedra in hingganite-(Y) undergo significant distortion with increasing bond lengths, showing the tendency of silicon to increase its coordination number from four to five or six. The distance from Si to the fifth O atom decreases continuously and above 45 GPa equals 2.07 Å. However, the DFT calculations and the analysis of theoretical electron-density distributions at the last pressure point do not confirm the existence of the fifth Si–O bond. The absence of the expected phase transition in hingganite-(Y) can be explained by the lower, compared to datolite, compression: the bulk modulus  $K_0$  is 124(1) and 106(4) GPa for hingganite-(Y) and datolite, respectively. The directions of the minimal and maximal compression are also different: along the b and c axis the compressibility of both minerals is similar, whereas along the a axis (i.e., perpendicular to the plane of the layers) the compression of datolite is twice as intense as that of hingganite-(Y).

This study was supported by the Russian Science Foundation 19-77-00038.

### References

- [1] Bačík, P., et al. (2017) *Eur. J. Mineral.* 29, 1067–1082.
- [2] Gorelova, L.A., et al. (2018) *Inorg. Chem. Front.* 5, 1653–1660.
- [3] Pakhomova, A., et al. (2019) *Nat. Comm.* (accepted).
- [4] Lulu, X., Zhizhong, P. (1986) *Chin. J. Geochem.* 5, 280–285.

## Structural complexity of natural and synthetic uranyl compounds with S- and Se-centered oxyanions

**Vladislav Gurzhiy** (presenting author)

Department of Crystallography, St. Petersburg State University, University Emb. 7/9, St. Petersburg, 199034, Russian Federation

Co-author(s): Jakub Plášil

Institute of Physics ASCR, v.v.i., Na Slovance 2, Praha 8, 18221, Czech Republic

Within the last few years, uranium mineralogy and crystal chemistry has witnessed a true Renaissance, due to the discoveries of exceptional suites of new uranium minerals in Jáchymov, Czech Republic and San Juan County, Utah, U.S. The diversity of new natural species is of particular interest since most of them do not have direct synthetic analogues and therefore are new to the synthetic inorganic chemistry as well. Most of the new uranium minerals are the products of secondary low-temperature hydrothermal processes, which are often associated with crystallization of very complex mineral species such as ewingite,  $\text{Mg}_8\text{Ca}_8(\text{UO}_2)_{24}(\text{CO}_3)_{30}\text{O}_4(\text{OH})_{12}(\text{H}_2\text{O})_{138}$ , the most structurally complex mineral known today. The structural architectures of novel natural phases, for instance, uranyl sulfates, show many similarities to synthetic uranyl sulfates, chromates, molybdates and selenates. In most of them, uranyl ions are inter-linked via tetrahedral  $\text{TO}_4$  groups ( $\text{T} = \text{S}, \text{Cr}, \text{Se}, \text{Mo}$ ) into finite clusters, chains or layers, in which interaction between adjacent uranyl groups is mediated by the hexavalent  $\text{T}^{6+}$  cations.

In order to evaluate an influence of various crystal-chemical factors (such as dimensionality of the U-bearing units and its hydration state) on the structure and symmetry of uranyl complexes and on the structural architecture of minerals in general, the structural and topological complexity was studied in terms of the information-based approach developed in [1-3] and recently developed in [4]. The structural complexity is quantitatively estimated as a Shannon information content per atom ( $I_c$ ) and per unit cell ( $I_{c,\text{total}}$ ). The amount of Shannon information reflects diversity and relative proportion of different objects, e.g., the number and relative proportion of different sites in an elementary unit cell of a crystal structure.

This work was supported by St. Petersburg State University and Russian Science Foundation (grant № 18-17-00018).

### References

- [1] Krivovichev, S.V. (2012) *Acta Cryst.* A68, 393–398.
- [2] Krivovichev, S.V. (2013) *Mineral. Mag.* 77, 275–326.
- [3] Krivovichev, S.V. (2014) *Angew. Chem. Int. Ed.* 53, 654–661.
- [4] Gurzhiy, V.V., Plášil, J. (2019) *Acta Cryst.* B75, 39–48.

## Using Orange Software visual programming and machine learning for deposited dust particles identification

**Tomas Hrstka** (presenting author)

*Institute of Geology, Academy of Sciences of the Czech Republic, v. v. i., Prague, 165 00, Czech Republic*

Co-author(s): Roman Skala<sup>1</sup>, Marko Toplak<sup>2</sup>, Jaroslav Moravec<sup>3</sup>

<sup>1</sup>Institute of Geology, Academy of Sciences of the Czech Republic, v. v. i., Prague, 165 00, Czech Republic

<sup>2</sup>University of Ljubljana, 1000 Ljubljana, Slovenia

<sup>3</sup>SIRET Research Group, Department of Software Engineering, Faculty of Mathematics and Physics, Charles University, Prague, 118 00, Czech Republic

Machine learning (ML) and artificial intelligence (AI) are now routinely used in many industrial and research applications. We are presenting the concept of automated identification of deposited dust particles by the means of data clustering and machine learning. In this case study, SEM-EDS spectral data has been used for classifying unknown mineral species through the means of combined unsupervised and supervised learning. Different classification models and their precision and accuracy were evaluated. As a part of this project we have implemented the support of necessary data formats in the latest version of the Orange software package. This now provides a solid platform for real big size data testing on 100K + data points using the full 3000+ parameters. We have also created a dataset with 100K + entries which can be used to evaluate different approaches of ML and AI for automated identification on mineral matter in the deposited dust samples. The availability of the training data is the key aspect of the potential use of any ML. With the produced dataset this approach is now fully applicable to real life projects. It also provides a huge potential of applying the concept/methodology to other mineral related data-sets from related spectroscopy techniques and/or their combinations (e.g. WDS spectra, Raman spectra, LIBS spectra, XRF spectra).

This study was financed through Strategy AV21/4 project and with help of Institute of Geology of the CAS, v. v. i. research plan RVO 67985831. Finally, we would also like to thank SGS Minerals for their support of this study.

## Endemic titanosilicates of the Kola alkaline complexes and their functional synthetic analogs

**Gregory Ivanyuk** (presenting author)

*Kola Science Center of the Russian Academy of Sciences*

Co-author(s): Victor N. Yakovenchuk, Yakov A. Pakhomovskii, Taras L. Panikorovskii, Ekaterina A. Selivanova, Sergei V. Krivovichev

*Kola Science Center of the Russian Academy of Sciences*

Alkaline and alkaline-ultrabasic massifs of the Kola province contain a number of endemic titanosilicates with cation-exchange properties (zorite-chivruaiite, sitinakite, ivanyukite-group minerals), gas separation molecular sieves (zorite), photo-catalysts (all above listed minerals), natural precursors of other functional compounds (minerals of the lintsite family), etc. All these minerals have been hydrothermally synthesized and used in industry for different purposes under the names of ETS-4 (analog of zorite), IE-911 (sitinakite), SIV (ivanyukite-Na), AM-4 and SL3 (lintisite and its protonated forms) [1-3].

In nature, framework titanosilicates often form partial to full pseudomorphs after earlier titanium silicates and oxides (titanite, titanomagnetite, loparite, astrophyllite, lamprophyllite, murmanite, etc.) under the influence of late Na-rich low-temperature hydrothermal solutions, so we can use similar technologies to obtain corresponding synthetic materials from Ti ores such as (apatite)-nepheline-titanite ores of the Khibiny massif and loparite-rich malignite/ijolites of the Lovozero massif. Both kinds of ores can be altered by sulfuric-acidic or hydrochloric-acidic technologies, resulting in titanyl sulfate or amorphous titanosilicate gels, respectively, as precursors for the subsequent synthesis of functional titanosilicates [4]. The synthesis includes mixing of Ti-precursors with Na-rich alkaline solution ( $\pm$  K, Si) and hydrothermal synthesis at 180–210 °C for 0.5–3 days.

Synthesized materials can be used for radioactive waste utilization into titanate ceramics, extraction of noble metals from industrial solutions (including electrolytes), for production of self-cleaning building materials and other purposes [4, 5].

The research is supported by the Kola Science Center of Russian Academy of Sciences (0226-2019-0009) and the Russian Foundation for Basic Research (18-29-12039).

### References

- [1] Men'shikov, Y.P., et al. (2006) *Am. Mineral.* 91, 922–92.
- [2] Yakovenchuk, V.N., et al. (2011) *Am. Mineral.* 96, 1624–1629.
- [3] Yakovenchuk, V.N., et al. (2009) *Am. Mineral.* 94, 1450–1458.
- [4] Gerasimova, L., et al. (2018) *Minerals* 8, 446.
- [5] Britvin, S.N., et al. (2016) *Theor. Found. Chem. Eng.* 50, 598–606.

## Specific OH infrared signatures in pyroxenes from mantle xenoliths: characteristics and possible bands assignments

**Ingrin Jannick** (presenting author)

Univ. Lille, CNRS, INRA, ENSCL, UMR 8207, UMET, Unité Matériaux et Transformations, F 59 000 Lille, France

Co-author(s): Samantha Azevedo-Vannson, Lydéric France

CRPG, UMR 7358, CNRS, Université de Lorraine, Vandoeuvre-lès-Nancy, France

Spectral signatures of infrared OH bands in pyroxenes from mantle xenoliths provide important information on water speciation in mantle lithospheres. We identified two characteristic types of spectral signatures in pyroxenes from mantle xenoliths: (a) Cpx and opx dominated by OH bands at 3595, 3517  $\text{cm}^{-1}$  and 3571, 3517  $\text{cm}^{-1}$ , respectively. (b) Cpx and opx dominated by OH bands at 3635, 3445  $\text{cm}^{-1}$  and 3602, 3417  $\text{cm}^{-1}$ , respectively. To understand the origin of these signatures and the nature of H-defects associated with them it is essential to isolate and characterize each specific bands that compose the spectra.

We present a low-temperature polarized infrared analysis of end-member signatures of these pyroxenes and identify the characteristics of the individual bands that compose their specific patterns. Possible bands assignments are discussed as well as possible strategies to implement identification.

## The Raman estimation of composition of garnets in natural diamonds

**Anastasiya Kalugina** (presenting author)

Novosibirsk State University, 1 Pirogova st., 630090, Novosibirsk, Russia

Co-author(s): Dmitry Zedgenizov

Novosibirsk State University, 1 Pirogova st., 630090, Novosibirsk, Russia

V.S.Sobolev Institute of Geology and Mineralogy, 3 Koptuyuga ave., 630090, Novosibirsk, Russia

Garnets ( $(\text{Mg,Fe,Ca})_3(\text{Al,Cr})_2[\text{SiO}_4]_3$ ) of peridotitic (P-type) and eclogitic (E-type) parageneses are the common inclusions in diamonds [1]. Raman spectroscopy is non-destructive high resolution technique to examine inclusions in minerals. In this study we present the approach based on large dataset (170 different garnets in diamonds from several localities of Siberian craton). The composition of garnets was analyzed using EPMA (JEOL JXA-8100). Raman spectra of the garnets were recorded on Horiba LabRAM HR800 Raman spectrometer with 532-nm laser.

The observed garnets have wide variations of chemical composition. P-type garnets are high-Cr (3.91–15.9 wt.%), high-Mg (18.3–23.9 wt.%) with Ca-content (0.92–8.22 wt.%) and low Fe-content (5.94–8.44 wt.%). E-type garnets are low-Cr (<0.2 wt.%), low-Mg (7.76–15.9 wt.%) and Ca-rich (3.93–13.4 wt.%) with Fe-content (12.4–20.3 wt.%). It is known that positions of three most intensive Raman modes (rotational  $R[\text{SiO}_4]$ , bending  $\nu_2$  and stretching  $\nu_1 A_{1g}$ -symmetry Si-O vibrations) may be described as a linear combination of weighted frequencies by ratio of different end-members [2–5]. The studied garnets show shifts for these modes in wide ranges ( $R[\text{SiO}_4]$  – 361.2–365.2  $\text{cm}^{-1}$ ,  $\nu_2$  – 554.5–558.7  $\text{cm}^{-1}$ ,  $\nu_1$  – 910.9–921.7  $\text{cm}^{-1}$  for P-type garnets and  $R[\text{SiO}_4]$  – 355.9–361.2  $\text{cm}^{-1}$ ,  $\nu_2$  – 557.8–559.2  $\text{cm}^{-1}$ ,  $\nu_1$  – 918.5–919.3  $\text{cm}^{-1}$  for E-type garnets. High-Cr P-type garnets display the splitting of  $\nu_1$ -mode and appearance of low-intensive peak  $\sim 930 \text{ cm}^{-1}$ . The shifts of intensive modes in garnet inclusions generally correlated with chemical composition. P-type garnets display the positive ( $r=81$ ) and negative ( $r=83$ ) correlations between position of  $\nu_1$  and Mg and Ca contents, respectively. For P-type garnets  $\nu_2$ -mode correlates with Al ( $r=89$ ) and Cr ( $r=85$ ) contents. E-type garnets show similar correlations between  $\nu_1$ -mode and Mg ( $r=86$ ) and Ca ( $r=97$ ) contents. Both P-type and E-type garnets don't show strong correlation between position of rotational mode ( $R[\text{SiO}_4]$ ) and composition, except weak negative dependence with Fe content in E-type garnets. The most expressed correlations may be used to evaluate the garnet composition by Raman spectroscopy. From observed dependences of  $\nu_1$ -mode, we derived two systems of equations for P-type and E-type garnets to estimate composition of the garnets ( $SD=3-4$  for P-type and  $SD=4$  for E-type (in % of prp-alm-gro components)). Al and Cr content in P-type garnets is proposed to estimate using the dependences of  $\nu_2$ -mode ( $SD_{\text{Al}} \sim 0.05$ ,  $SD_{\text{Cr}} \sim 0.06$  (in f.u.)).

This work was supported by the Russian Science Foundation (16-17-10067).

### References

- [1] Nixon, P.H. (1987) Mantle Xenoliths, J. Wiley & Sons.
- [2] Hofmeister, A.M., Chopelas, A. (1991) Phys. Chem. Miner. 17, 503–526.
- [3] Kolesov, B.A., Geiger, C.A. (1997) J. Raman Spectrosc. 28, 659–662.
- [4] Kolesov, B.A., Geiger, C.A. (1998) Phys. Chem. Miner. 25, 142–151.

## Raman spectroscopy in the studies of archaeological bone and tooth diagenesis

**Daria Kiseleva** (presenting author)

*Institute of Geology and Geochemistry, Ural Branch of Russian Academy of Sciences, Ekaterinburg, Russia*

Co-author(s): Daria Kiseleva<sup>1</sup>, Elizaveta Pankrushina<sup>1</sup>, Sergei Votyakov<sup>1</sup>, Svetlana Sharapova<sup>2</sup>, Lyudmila Koryakova<sup>2</sup>, Pavel Kosintsev<sup>3</sup>

<sup>1</sup>Institute of Geology and Geochemistry, Ural Branch of Russian Academy of Sciences, Ekaterinburg, Russia

<sup>2</sup>Institute of History and Archaeology, Ural Branch of Russian Academy of Sciences, Ekaterinburg, Russia

<sup>3</sup>Institute of Animal and Plant Ecology, Ural Branch of Russian Academy of Sciences, Ekaterinburg, Russia

Bone and tooth is a composite material made up of both organic (collagen) and inorganic components (carbonated hydroxylapatite, HAp). Due to their strength and hardness obtained via biomineralization process, they can survive through the history and serve as a source of palaeontological and archaeological information. However, their post-mortem preservation depends upon a number of complex processes including transformation after the deposition in the archaeological or geological strata, a process known as diagenesis [1]. Tooth enamel is more resistant to diagenesis due to low porosity and low organic content.

Increase in crystallinity (crystallite size and lattice perfection) is used as the parameter characterizing the degree of diagenetic alteration of ancient degraded bones, as well as decrease in carbonate content and collagen loss [1].

Bone collagen is the most often targeted molecule for the direct radiocarbon dating, stable isotope (C, N) and DNA analyses of skeletal remains. However, there are a number of contexts where collagen is not preserved (e.g., in arid and tropical environments or after burning), leaving only bioapatite phase, or rather the carbonate of bones and teeth to perform radiocarbon dating and stable carbon isotope analysis [2].

An understanding of the structural features of mineralized tissues is fundamental for diagenesis studies. Raman spectroscopy as a rapid and non-destructive screening method both to determine collagen quality and content [3] and to identify the diagenetic alteration of fossil bioapatite assigned for oxygen isotopic analysis of phosphate [4] in archaeological and paleontological bones. The 960 cm<sup>-1</sup> (phosphate anion stretching in the bone mineral) and 1636 cm<sup>-1</sup> (amide carbonyl stretching in the collagen) peaks were found to be very sensitive to variations in apatite chemistry, particularly with respect to common diagenetic components, and to distinguish between well and poorly-preserved collagen, respectively. In present work a number of human and animal archaeological bones and teeth collected from the Bronze age sites were investigated by Raman spectroscopy. Raman spectra were obtained using Horiba Jobin Yvon LabRam-HR Evolution based on a confocal Raman microscope, with 632.8 nm He–Ne laser excitation. The degrees of bioapatite crystallinity and collagen quality were determined. This allowed the impact of sampling to be minimized for the preservation of archaeological collection and the analytical strategies to be optimized. The work was carried out at the Geoanalyst Center for Collective Use and supported by RSF grants No. 16-17-10283 (Raman spectroscopy, E.A. Pankrushina) and 16-18-10332-P (archaeological sample collection and historiographical interpretation, S.V. Sharapova and L.N. Koryakova).

### References

- [1] Kendall, C., et al. (2018) *Palaeogeogr. Palaeoclimatol. Palaeoecol.* 491, 21–37.
- [2] Zazzo, A. (2014) *Palaeogeogr. Palaeoclimatol. Palaeoecol.* 416, 168–78.
- [3] France, C.A.M., et al. (2014) *J. Archaeol. Sci.* 42, 346–355.
- [4] Thomas, D.B., et al. (2011) *Palaeogeogr. Palaeoclimatol. Palaeoecol.* 310, 62–70.

## Feldspar polymorphs: diversity, complexity, stability

**Sergey V. Krivovichev** (presenting author)

*Kola Science Centre, Russian Academy of Sciences, 184209 Apatity, Russia*

*St. Petersburg State University, University Emb. 7/9, 199034 St. Petersburg, Russia*

Feldspars are the most common rock-forming minerals of the Earth's crust. According to the current nomenclature, the feldspar group includes mineral species with the general formula  $M[\text{AlnSi}_{4-n}\text{O}_8]$ , where  $M = \text{K, Na, Rb, NH}_4, \text{Ca, Sr, Ba}$ ;  $n = 1, 2$ . The crystal structures of 'classical' feldspars (albite, anorthite, orthoclase, microcline, sanidine, etc.) are based upon three-dimensional framework of  $\text{TO}_4$  tetrahedra linked by sharing common O corners and forming specific crankshaft-type chains. Under variation of temperature and pressure and depending upon exact chemical composition, they display phase transitions characterized by tilting of tetrahedra [1]. However, polymorphism in feldspars is not restricted to the changes in conformation of framework, but also includes recombination of tetrahedral groups and formation of different topological arrangements such as found in svyatoslavite (and probably kumdykolite), dmisteinbergite (and hexacelsian), and paracelsian. The application of high-pressure results in formation of feldspar polymorphs with different topologies based upon sixfold (octahedral) and fivefold (trigonal bipyramidal) coordinations of T atoms (e.g., lingunite with a hollandite-type structure [2]).

In our contribution, we will summarize the current state of knowledge on the polymorphism of feldspars, including high-temperature and high-pressure polymorphs, and metastable phases [3].

### References

- [1] Angel, R.J., et al. (2012) *Amer. Mineral.* 97, 765–778.
- [2] Gillet, P., et al. (2000) *Science* 287, 1633–1636.
- [3] Ferrero, S., et al. (2016) *Contrib. Mineral. Petrol.* 171, 3.

## Crystalline borosilicates of alkali and alkaline-earth metals: hierarchy, fundamental building blocks and thermal expansion

**Maria G. Krzhizhanovskaya** (presenting author)

Department of Crystallography, Institute of Earth Sciences, Saint Petersburg State University, University Emb. 7/9, 199034 St. Petersburg, Russia

Co-author(s): Rimma S. Bubnova<sup>1</sup>, Stanislav K. Filatov<sup>2</sup>

<sup>1</sup>Grebenshchikov Institute of Silicate Chemistry of the Russian Academy of Sciences, Adm. Makarov Emb., 2, St. Petersburg, 199034, Russia

<sup>2</sup>Department of Crystallography, Institute of Earth Sciences, Saint Petersburg State University, University Emb. 7/9, 199034 St. Petersburg, Russia

This paper presents a brief review on structure hierarchy, the main fundamental building blocks (FBBs) and some thermal characteristics of alkaline and alkaline-earth crystalline borosilicates [1]. Low-dimensional borosilicate anions are typical for borosilicates with considerable contents of non-tetrahedrally coordinated cations. There are only six types of borosilicate anions containing boron in  $\text{BO}_3$  triangles, which are almost never connected to silicon tetrahedra. The lower the ratio “non-tetrahedral / tetrahedral cation”, the higher dimensional layered and framework anions form. Most Si-dominant borosilicates ( $\text{B}/\text{Si} \leq 1$ ) with a low content of non-tetrahedrally coordinated cations have 3D-framework structures formed by boron and silicon atoms in tetrahedral coordination only. As with aluminosilicates, 3D-borosilicate structures contain a great variety of rings of tetrahedra, which are the main FBBs of borosilicate structures. The most common rings of tetrahedra are 4-, 6- and 8-membered. An ordered distribution of Si and B is typical for borosilicates. There are many OH-containing borosilicates, especially among the structures with 0D-, 1D- and 2D-anions; conversely, they almost never have  $\text{H}_2\text{O}$  molecules in the crystal structure. OH-groups are often involved in the coordination of boron. Non-tetrahedral alkali and alkaline-earth cations are coordinated by oxygen or hydroxyl groups with usual coordination numbers: lithium is 4-coordinated, sodium is mostly 6-coordinated, 8-coordination is typical for calcium. Other large cations have irregular coordinations with more than 8 oxygen atoms. Over the last 20 years we studied about a hundred borate, silicate and borosilicate natural and synthetic compounds. The most unusual examples of borosilicates’ thermal behavior are described in [2, 3]. The typical features of high-temperature behavior are summarized for about three dozens of borosilicates [1].

The study was supported by the Russian Foundation of Basic Research No. 17-03-00887. XRD measurements were performed in the Research Center of XRD studies of St. Petersburg State University.

### References

- [1] Krzhizhanovskaya, M.G., et al. (2019) Phys. Chem. Glasses, in press.
- [2] Krzhizhanovskaya, M.G., et al. (2016) Eur. J. Mineral. 28, 15–21.
- [3] Krzhizhanovskaya, M.G., et al. (2018) Phys. Chem. Mineral. 45, 463–473.

## Crystal chemistry of Pb-rich tourmaline from pegmatite in Minh Tien, Vietnam

**Monika Kubernátová** (presenting author)

Department of Geological Sciences, Faculty of Science, Masaryk University

Co-author(s): Jan Cempírek

Department of Geological Sciences, Faculty of Science, Masaryk University

The Minh Tien pegmatite in northern Vietnam is an elbaite-subtype granitic pegmatite with a mixed LCT+NYF (after [1]) geochemical signature. The studied sample from the pegmatite core contains amazonitic K-feldspar, albite, tourmaline, lepidolite (up to 3.1 wt.%  $\text{Rb}_2\text{O}$  and 1.0 wt.%  $\text{Cs}_2\text{O}$ ) and accessory cassiterite (up to 2.3 wt.%  $\text{Ta}_2\text{O}_5$  and 1.9 wt.%  $\text{Nb}_2\text{O}_5$ ), tusionite, manganocolumbite ( $X_{\text{Mn}} \sim 94\text{--}97$ ,  $X_{\text{Nb}} \sim 93\text{--}94$ ), zircon, thorite, Pb-rich mica and stokesite. The amazonite is locally of gem quality and, together with gem tourmaline, is mined from weathered outcrop and alluvial deposits [2–4].

Tourmaline composition was studied using electron microprobe. The tourmaline occurs in several color varieties (black, blue, pink) and in four textural types; its composition corresponds to fluor-liddicoatite, fluor-elbaite, and rarely also a new Pb-analogue of fluor-liddicoatite. It forms primary crystals with sector zoning (Tur 1; Fe, Mn, Pb-rich fluor-elbaite to Na, Pb-rich fluor-liddicoatite), irregular aggregates of tourmaline and quartz (Tur 2; Na-rich fluor-elbaite to Na, Pb-rich fluor-liddicoatite) on fissures and in inter-granular space of Tur 1 and feldspars, further as Pb-poor zones (Tur 3; Pb-poor fluor-liddicoatite and Ca-rich fluor-elbaite) around the Tur 2 aggregates, and as tiny domains of Pb-rich tourmaline (Tur 4; Pb-rich fluor-liddicoatite and Pb-dominant analogue of fluor-liddicoatite) on outer borders of the Tur 3 zones.

In the primary tourmaline, contents Fe and Zn correlate positively whereas they both show a negative correlation with Mn during progress of fractional crystallization. The tourmaline contains elevated amounts of tetrahedral boron, which increases with raising lead contents. Lead substitution in tourmaline is not related to a specific X-site occupancy, as high Pb content was observed in both Ca-rich and Ca-poor zones; the highest Pb (up to 5.87 wt.% PbO) is present in tourmalines with high X-site vacancy, high Ca and low Na contents, in zones and crystals up to 25  $\mu\text{m}$  in size. Decrease of temperature, as well as recrystallization of earlier tourmaline generations seem to decrease the Pb contents in Ca-Na tourmaline, as they decrease from the Tur 1 to the Tur 3 with a very low Pb-content. However, the X-site vacancy-rich Tur 4 that crystallized from final residual fluids is the richest in Pb.

The primary lead enrichment in tourmaline is related to alteration of amazonite. Textural relations show that the Pb-rich tourmaline (Tur 1) formed contemporarily with lepidolite during metasomatic albitization of K-feldspar, and the further three generations formed during hydrothermal reaction of Li, B, F-rich fluids with Tur 1, K-feldspar and albite.

### References

- [1] Černý, P., Ercit, T.S. (2005) Can. Mineral. 43, 2005–2026.
- [2] Wilson, W.E. (2007) Mineral. Rec. 38, 453–457.
- [3] Sokolov, M., Martin, R.F. (2009) Estudios Geológicos 19, 352–353.
- [4] Nhung, N.T., et al. (2017) Gems Gemol. 190–203.

## Australia's National Virtual Core Library - unlocking mineralogical information from drill core to support research and mineral exploration

**Carsten Laukamp**

CSIRO Mineral Resources, Kensington, Australia

Drill cores provide us with valuable information about the critical zone and resources it contains. Whether Geological Surveys invest in stratigraphic drill holes to better understand geological successions, or exploration companies want to test targets or mining companies want to characterise their mineral resource, it all revolves around drill core. The National Virtual Core Library (NVCL), part of AuScope's national earth science infrastructure program (<http://www.auscope.org.au/nvcl/>), has made it its prime objective to provide internet access to the vast resource of geological information from the upper 1 – 2 km of our Earth's crust. Thousands of meters of drill core material are stored in drill core libraries of the Australian State and Territory Geological Surveys and core sheds of numerous companies across Australia. The NVCL provides the research community with access to high-resolution RGB imagery, hyperspectral and associated geoscience data through AuScope's data infrastructure and discovery portal (<http://www.auscope.org.au/auscope-grid/>). Drill cores are sourced from various geological environments and mineral deposit types across the Australian continent. Visible near to shortwave infrared (VNIR-SWIR; 380 to 2500 nm) and thermal infrared (TIR; 6000 to 14500 nm) reflectance spectra are collected at approximately 1 cm resolution using the 800 spectral channel HyLogger™ systems (Schodlok et al., 2016) located at six NVCL nodes operated by State and Territory Geological Surveys. The combined VNIR-SWIR-TIR reflectance spectra allow the characterisation of all major rock-forming minerals, creating one of the world's largest collections of publicly available mineralogical data with associated high-resolution drill core imagery.

This paper describes material, hardware, human and database infrastructure underlying the NVCL and provides examples of the manifold geoscience questions that can be addressed by using NVCL data. For example, NVCL-derived hyperspectral data are used for characterising mineral footprints associated with hydrothermal ore deposits, identifying alteration mineral assemblages in bed- and cover rocks. The availability of mineralogical data from more than 3000 drill cores across the Australian continent allows the comparison of geological provinces and mineral deposit styles beyond state and territory boundaries. A combination of the RGB imagery with mineralogical, geochemical and/or geophysical data is evaluated for objective, automated mapping of bedrock lithologies, alteration minerals and regolith stratigraphy. Numbers of drill cores and data types available through the NVCL are steadily increasing, providing researchers, Geological Surveys and industry with new information to discover the geology and resource potential of Australia.

## Mid- and Thermal Infrared Reflectance Spectral Signatures of Non-sulfide Zn-ores

**Carsten Laukamp** (presenting author)

CSIRO Mineral Resources, Kensington, Australia

Co-author(s): Monica LeGras<sup>1</sup>, Bobby Pejčić<sup>2</sup>, Maria Boni<sup>3</sup>

<sup>1</sup>CSIRO Mineral Resources, Kensington, Australia

<sup>2</sup>CSIRO Energy, Kensington, Australia

<sup>3</sup>University of Naples, Italy

The economic value of non-sulfide Zn ores varies with the geologic setting as well as the ore and gangue mineralogy. The complexity of the respective mineral assemblages commonly requires detailed and time-consuming micro-analytical techniques to understand the formation of the respective ore body and to inform Zn ore processing. Reflectance spectroscopy can potentially be used to extrapolate these findings across scales by mineral assemblages from mine faces, blast hole samples and conveyor belts, improving ore body knowledge required for more efficient mining.

The visible-near infrared and shortwave infrared reflectance spectra of non-sulfide Zn-ores were summarised by [1]. The published visible-near to short-wave infrared (400 to 2500 nm) spectral signatures exhibit overtones and combination bands of a subset of fundamental infrared functional groups located in the mid (MIR; 2500 to 6000 nm) and thermal infrared (TIR; 6000 to 14500 nm) wavelength ranges. Cost-effective TIR-capable mineral characterisation technologies, such as handheld FTIRs or the hyperspectral drill core scanner HyLogger3 [2], have the potential to rapidly and objectively identify non-sulfide Zn-ores. The aim of this paper is to present mid- and thermal infrared reflectance spectral signatures and the most diagnostic functional groups of selected non-sulfide Zn-ores.

Smithsonite ( $\text{ZnCO}_3$ ) exhibits two major absorption peaks in the TIR at around 6550 and 11372 nm. Both can be attributed to  $\nu_2\text{CO}_3$  [3] and occur in other major carbonate phases. However, the wavelength position of the 11372 nm is sensitive to the amount of Zn versus other substituting cations. In the MIR, smithsonite shows a major absorption feature at around 3970 nm with a shoulder at 3856 nm. Both tentatively attributed to a combination of  $\text{CO}_3$ -related stretching fundamentals and overtones. Handheld FTIR reflectance spectra of willemite ( $\text{Zn}_2\text{SiO}_4$ ) show major absorption peaks at 10111, 10493 and 10707 nm, which can be assigned to  $\nu_3\text{SiO}_4$  after comparison with transmission measurements reported by [4]. A fourth major absorption peak at around 11468 nm can be attributed to  $\nu_1\text{SiO}_4$  and is potentially sensitive to estimating the replacement of the tetrahedrally coordinated Si by Ge [4]. In contrast to other silicates that show clear overtones of the fundamental Si-O stretching vibrations in the MIR, no absorption features for willemite could be observed in this wavelength range. Instead, commonly co-occurring carbonates such as smithsonite display  $\text{CO}_3$ -related overtones at around 4000 nm.

Reflectance spectra of tarbuttite ( $\text{Zn}_2(\text{PO}_4)_2(\text{OH})$ ) display distinct absorption peaks at around 8900, 9479, 9804, 10417 and 10870 nm, which are all due to either antisymmetric or symmetric stretching fundamentals of  $\text{PO}_4$  [5]. The 8900 nm absorption peak shows a significant shift of about 70 nm between a tarbuttite sample from Skorpion (Namibia) and Broken Hill (Zambia), which could be due to replacement of Zn by other cations such as Cu.

Our study demonstrates that the mineral compositional complexity of the investigated non-sulfide Zn ores and their distinct absorption features in the MIR and TIR can be observed with commercially available field and drill core hyperspectral sensing technologies. This opens up the potential for rapid and cost-effective characterisation of ore types, including geochemical composition of non-sulfide Zn ores.

### References

- [1] McConachy, T.F., et al. (2007) *Geochemistry: Exploration, Environment, Analysis* 7, 139–151.
- [2] Schodlok, L., et al. (2016) *Australian Journal of Earth Sciences* 63, 929–940.
- [3] Chester, P., Elderfield, H. (1966) *Chemical Geology* 1, 277–290.
- [4] Tarte, P. (1962) *Spectrochimica Acta* 18, 467–483.
- [5] Braithwaite, R.S.W. (1988) *Mineralogical Magazine* 52, 126–129.

## How to use infrared reflectance spectroscopy of pyroxenes and pyroxenoids for critical metals exploration and mining

**Monica LeGras** (presenting author)

CSIRO Mineral Resources, Kensington, Australia

Co-author(s): Carsten Laukamp

CSIRO Mineral Resources, Kensington, Australia

Pyroxene and pyroxenoid minerals produce absorption features in the thermal infrared region (TIR; 6000 – 14500 nm; 1667 – 690 cm<sup>-1</sup>) of the electromagnetic spectrum, arising from the stretching vibrations of their Si-O bonds. The frequency and magnitude of these vibrations are influenced by the cations occupying the alternating M1 and M2 sites joining the Si-O chains. The identity of these cations defines the pyroxene and pyroxenoid species and the resulting spectral features are sufficiently varied in number, position and magnitude to distinguish individual species.

This study, part of Auscope's National Virtual Core Library's spectral reference library project, analyses a wide variety of pyroxene and pyroxenoid endmember and intermediate species including aegirine, augite, diopside, enstatite, ferrosilite, hedenbergite, jadeite, kosmochlor, omphacite, petedunnite, pigeonite, rhodonite, spodumene and wollastonite. For each of these mineral species, mono-mineralic reflectance spectra were obtained using a handheld FTIR spectrometer instrument, or a FTIR microscope in the case of very small or multi-phase specimens. The handheld instrument was selected as portability opens the technique to a range of applications outside the laboratory, including fieldwork and space exploration. X-ray Diffraction and Energy-Dispersive X-ray Spectroscopy were used as independent measures of the specimens' structure and chemistry.

Due to their structural similarity and chemical diversity, the pyroxene and pyroxenoid group minerals easily allow assignment of specific cations to the observable absorption features. The Christiansen minimum (point of lowest reflectance at higher frequencies to the most intense TIR absorptions) is also indicative of composition and species. Generally, the combined mass of the M1 and M2 cations determine the position of the Christiansen minimum, which shifts to longer wavelengths with increasing cation mass.

In mixtures, reflectance spectra can also be used to accurately quantify pyroxene abundance, using partial least-squares (PLS) modelling. An example is given using spodumene from the Goulamina Lithium Project, Mali. This may be of significant utility when mining Li, which has intrinsic analytical challenges.

Automated classification of pyroxene minerals was tested using The Spectral Assistant (TSA), a method which matches the unknown spectrum against a training library of reference spectra. TSA demonstrates strong potential for identifying the pyroxene minerals on both a group and species level. Automated classification such as this becomes necessary when dealing with spectral data, a great advantage of which lies in its rapid collection time and easy automation, resulting in the production of large volumes of data. It also allows data to be processed remotely. These experiments improve our use of infrared reflectance spectroscopy as a tool for mineral characterisation in exploration, mining, and lunar, meteoritic and planetary sciences.

## Optical spectroscopy at combined high P and T conditions and its applications to thermal and electrical transport in the deep mantle

**Sergey Lobanov** (presenting author)

GFZ German Research Center for Geosciences, Section 3.6, Telegrafenberg, 14473 Potsdam, Germany

Co-author(s): François Soubiran<sup>1</sup>, Nicholas Holtgrewe<sup>2</sup>, Alexander F. Goncharov<sup>2</sup>

<sup>1</sup>École Normale Supérieure de Lyon, Université Lyon 1, Laboratoire de Géologie de Lyon, CNRS UMR5276, 69364 Lyon Cedex 07, France

<sup>2</sup>Geophysical Laboratory, Carnegie Institution of Washington, Washington, DC 20015, USA

The vigor of mantle and core dynamics is governed by the heat flow across the core-mantle boundary ( $Q_{\text{CMB}}$ ). One major source of ambiguity in the  $Q_{\text{CMB}}$  is the unknown contribution of photons in cooling the core with previous attempts to evaluate radiative thermal conductivity grouping at  $\sim 1$  W/m/K and at  $> 5$  W/m/K [1-4], translating into a factor of two different  $Q_{\text{CMB}}$ . Spectroscopic measurements on high-quality single crystals at pressure-temperature (P-T) conditions representative of the lowermost mantle are needed to resolve the debate over the effectiveness of radiative heat transport. Such measurements are extremely difficult to carry out because of the sample's thermal emission dominating in the signal collected by the detector. Over the past years we developed methodologies that allowed overcoming these and other challenges thanks to the use of pulsed ultra-bright spectroscopic probes and time-resolved detectors. Here we report on the absorption spectra of single crystalline bridgmanite and ferropericlase, the two most abundant minerals in the Earth's mantle, measured in dynamically- and statically-heated diamond anvil cells at near core-mantle boundary P-T conditions. Light absorption in the visible spectral range is enhanced upon heating in both minerals but the rate of change in opacity with temperature is a factor of six higher in ferropericlase. As a result, bridgmanite in the lowermost mantle is moderately transparent but ferropericlase is highly opaque. Our measurements suggest a low ( $< \sim 1$  W/m/K) and largely temperature-independent radiative conductivity in the lowermost mantle, pointing to a steady  $Q_{\text{CMB}}$  of 9-11 TW at least over the past 1 Gy. In addition, we were able to reproduce the experimentally-observed spectroscopic behavior of ferropericlase by independent first-principles computations that access a much wider spectral range and allow constraints on the DC electrical conductivity of the lowermost mantle. We find that the DC conductivity of opaque ferropericlase is sufficiently high to implement core-mantle electromagnetic coupling which could be responsible for the reversible intradecadal variations in the length of day [5].

### References

- [1] Goncharov, A.F., et al. (2008) Nature 456, 231.
- [2] Keppler, H., et al. (2008) Science 322, 1529.
- [3] Goncharov, A.F., et al. (2015) Phys. Earth Planet. Inter. 247, 11.
- [4] Lobanov, S.S., et al. (2017) Earth Planet. Sci. Lett. 479, 43.
- [5] Holme, R., de Viron, O. (2013) Nature 499, 202.

## Different ways of incorporating elements into crystal structures in which they do not fit

**Juraj Majzlan** (presenting author)  
University of Jena

Most minerals deviate from their nominal composition because of substitutions at various structural sites. In some cases, the substitutions are simple, such as in the forsterite–fayalite series. In some cases, however, the substituting elements have markedly different sizes, charges, and coordination environments. Simple crystal structures are surprisingly tolerant to such substitutions and surprisingly ‘inventive’ when it comes to the placement of the foreign ions into the structure.

In our research, we have examined the placement of W, As or Mo into the structures of iron oxides. Hematite with its dense structure based on hexagonal closed-packed array of oxygen atoms, is a good host of these elements. For arsenic ( $As^{5+}$ ), hematite can be a host of nanoclusters with a local angelellite-like ( $Fe_4^{3+}(AsO_4)_2O_3$ ) structure [1]. The epitaxial relationship of angelellite and hematite can be justified structurally. Another such example is the intergrowth of hematite and nanolamellae of ferberite ( $FeWO_4$ ), detected in our recent research. In this case, just as for  $As^{5+}$ , epitaxial intergrowth between both phases is possible and explains the uptake of  $W^{6+}$  by hematite. Epitaxy is not always the solution. In a thorough analysis of X-ray absorption spectroscopy (XAS) data, Marshall et al. [2] reported that  $U^{6+}$  is hosted by hematite in a distorted octahedral environment. In other words, the host structure forces the element to adopt its architecture, and the charge is compensated by creation of vacancies. Hematite can also pick up ions like  $Ce^{4+}$  and force them to adopt octahedral coordination [3].

Uptake of  $W^{6+}$  by rutile appears to be of a different nature. In natural W-rich (up to 16 wt.%  $WO_3$ ) rutile crystals is  $W^{6+}$  placed on an octahedral site of the rutile structure, together with abundant Fe, V and Cr. The charge-compensating mechanism must be complex; the valence states of V and Cr, determined by X-ray absorption spectroscopy, do not correspond to an integer.

Uptake of foreign ions, seemingly unfit to enter a given structure, is not limited only to oxides. Pyrite, the most common sulfide, can host appreciable amount of mercury in marcasite-like inclusions, in metacinnabar nanoparticles, or as elemental mercury [4]. Among complex structures, sulfosalts are also superb examples of complex substitutions where one metal site could be replaced by two without significant changes to the overall architecture of the structure [5].

It is unlikely that substitutions of this kind are restricted only to simple structures. Yet, they are easier to detect in such structures. Future research in this field will certainly identify additional mechanisms of incorporation of foreign ions into many structures of minerals and synthetic phases.

### References

- [1] Bolanz, et al. (2013) *Env. Sci. Technol.* 47, 9140–9147.
- [2] Marshall, et al. (2014) *Env. Sci. Technol.* 48, 3724–3731.
- [3] Bolanz, et al. (2018) *Sci. Tot. Environ.* 622–623, 849–860.
- [4] Manceau, et al. (2018) *Env. Sci. Technol.* 52, 10286–10296.
- [5] Topa, et al. (2008) *Can. Mineral.* 46, 515–523.

## Activation energy of annealed, partially metamict davidite by $^{57}Fe$ Mössbauer spectroscopy

**Dariusz Malczewski** (presenting author)  
University of Silesia, Faculty of Earth Sciences, 41-200 Sosnowiec, ul. Bedzinska 60, Poland

Co-author(s): Agnieszka Grabias<sup>1</sup>, Maria Dziurawicz<sup>2</sup>  
<sup>1</sup>Institute of Electronic Materials Technology, 09-919 Warszawa, ul. Wólczyńska 133, Poland  
<sup>2</sup>University of Silesia, Faculty of Earth Sciences, 41-200 Sosnowiec, ul. Bedzinska 60, Poland

This study used  $^{57}Fe$  Mössbauer spectroscopy to determine the activation energy for thermal recrystallization of partially metamict davidite (multiple oxides)  $(La,Ce,Ca,Th)(Y,U)(Ti,Fe^{3+})_{20}O_{38}$  [1]. Radioactive elements in metamict minerals damage crystal structure primarily through progressive overlapping recoil nuclei collision cascades from  $\alpha$ -decay of  $^{238}U$ ,  $^{232}Th$ ,  $^{235}U$  and their daughter products. Metamict minerals are widely used in geochronology and can serve as natural analogues for the study of radiation effects in high-level nuclear waste (HLW). Analysis was performed on fragments of a davidite sample collected from the Bektau-Ata granitoid massif (Kazakhstan).  $^{57}Fe$  Mössbauer spectroscopy was carried out on the davidite sample after one-hour annealing under an argon atmosphere from 673 to 1373 K. Changes in the selected hyperfine parameters of the  $^{57}Fe$  Mössbauer spectra, (e.g., a ratio of amplitudes of a low energy peak to a high energy peak from the  $Fe^{3+}$  components) and line width ratios are sensitive indicators of thermally induced recrystallization. The activation energy,  $E_a$ , for recrystallization was determined based on the exponential dependence of the Mössbauer parameters upon temperature and using Arrhenius plots. Estimated  $E_a$  values of about 0.4 eV were significantly lower than those obtained for fully metamict gadolinite ( $REE_2Fe^{2+}Be_2Si_2O_{10}$ ;  $E_a = 1.95$  eV [2]) and for track annealing in zircon ( $ZrSiO_4$ ;  $E_a = 2.87$  eV [3]).

### References

- [1] Gatehouse, B.M., et al. (1979) *Am. Mineral.* 64, 1010–1017
- [2] Malczewski, D., Janeczek, J. (2002) *Phys. Chem. Minerals* 29, 226–232
- [3] Weber, W.J., et al. (1998) *J. Mater. Res.* 13, 1434–484

## Compositional analysis of $\text{PO}_4$ , $\text{AsO}_4$ , and $\text{VO}_4$ in Pb-apatites with Raman spectroscopy

Maciej Manecki (presenting author)

AGH University of Science and Technology, Kraków, Poland

Co-author(s): Bartosz Puzio, Urszula Solecka, Tomasz Bajda, Justyna Topolska

AGH University of Science and Technology, Kraków, Poland

Natural Pb apatites always contain simultaneous substitutions of  $\text{PO}_4$ ,  $\text{AsO}_4$ , and  $\text{VO}_4$  [1]. Several studies on synthetic analogs indicate that continuous solid solution exist in these series. Raman bands of  $\text{PO}_4$ ,  $\text{AsO}_4$ , and  $\text{VO}_4$  are relatively strong, distinct and with little coincidences. This allows for application of Raman spectroscopy for detection and quantification of the extent of substitution.

The extent of  $\text{PO}_4$ ,  $\text{AsO}_4$ , and  $\text{VO}_4$  substitutions in Pb-apatites affect Raman spectra in two distinct ways: the intensity of individual bands is proportional to the content of the ion and the position of the bands is systematically shifted. The shift of the position of the band is usually used as a measure of the extent of substitution. However, the ratio of the intensities of selected bands also exhibits excellent functional relationship with the composition. This was indicated for the first time by Giera et al. [2] in the study of hydroxylmimetite  $\text{Pb}_{10}(\text{AsO}_4)_6(\text{OH})_2$  – hydroxylpyromorphite  $\text{Pb}_{10}(\text{PO}_4)_6(\text{OH})_2$  solid solutions.

It is hypothesized that the ratio of the intensities of selected Raman bands can be applied as a measure of  $\text{PO}_4$ ,  $\text{AsO}_4$ , and  $\text{VO}_4$  substitutions in Pb-apatites. Several synthetic solid solution series have been synthesized from aqueous solutions and characterized using powder X-ray diffraction and scanning electron microscopy with EDS microanalyzer. The Raman spectra were recorded in three or four repetitions for each member of the series at room temperature using DXR Raman Microscope. Approximately 1g of the powder was placed on a glass slide and irradiated with a green laser (532 nm) set to 5 mW. A 25- $\mu\text{m}$  slit aperture was applied to minimize the impact of crystallographic orientation on the intensity of peaks [3]. The peak positions and intensities in Raman raw spectra were determined using OMNIC For Dispersive Raman software. Identical background treatment was applied.

The intensity of selected Raman bands measured successively in collected spectra varies significantly. However, their average ratio is constant for analyzed specimen and varies systematically with the composition. These ratios appear to be only very little affected by sample preparation or the conditions of the measurement and data processing. A high correlation between this relative intensity of selected bands and molar content of  $\text{PO}_4$ ,  $\text{AsO}_4$ , and  $\text{VO}_4$  can be used for quantitative estimation of the extent of substitution.

BP was funded by NCN research grant no. 2017/27/N/ST10/00776. US was financed with NCN research grant no. 2013/09/N/ST10/00677.

### References

- [1] Markl, G., et al. (2014) Am. Mineral. 99, 1133–1146.
- [2] Giera, A., et al. (2016) Spectr. Acta A: Molec. Biomolec. Spectr. 152, 370–377.
- [3] Dieing, T., et al. (2010) Confocal Raman Microscopy. Springer-Verlag Berlin.

## Halloysite-supported iron oxide particles for As(V) removal: adsorption mechanism investigation by the XPS and Mössbauer spectroscopy

Paulina Maziarz (presenting author)

AGH University of Science and Technology, al. Mickiewicza 30, 30-059 Krakow, Poland

Co-author(s): Jakub Matusik

AGH University of Science and Technology, al. Mickiewicza 30, 30-059 Krakow, Poland

In this study, halloysite was used as a host for Fe oxide particles (FeOx) deposition. The obtained materials were thermally treated, in order to determine changes in their structure and enhance the adsorption behaviour toward As(V). In particular, the X-ray photoelectron and Mössbauer spectroscopies combined with adsorption and desorption experiments were used to determine the mechanisms responsible for As(V) removal.

The halloysite used in the study was collected from Dunino deposit, located in Lower Silesia near Legnica (Poland). The halloysite-FeOx composites (HFe) were synthesized using chemical precipitation method. The composites were additionally thermally treated at 400°C for 3 h (HFeK). The adsorption experiments were carried out for the initial As(V) concentration in the range of 0.01-25 mmol/L (initial pH=5.0 and 20 g/L solid/liquid ratio). The  $\text{Na}_2\text{HAsO}_4 \cdot 7\text{H}_2\text{O}$  was used as As(V) source. The ionic strength effect was also studied for the NaCl as a background electrolyte (0.005-0.1 mol/L).

The XRD patterns of studied composites showed basal peak of halloysite at 7.20 Å. The success of FeOx synthesis was confirmed by appearance of peaks at 2.95 Å, 2.52 Å, 2.08 Å, 1.70 Å, 1.61 Å and 1.48 Å which can be identified as Fe oxides ( $\gamma\text{-Fe}_2\text{O}_3/\text{Fe}_3\text{O}_4$ ). However, the presence of the sextets in the Mössbauer spectra of the HFe samples confirmed that nanocrystalline  $\gamma\text{-Fe}_2\text{O}_3$  particles were formed during synthesis. The ionic strength experiment revealed that the increase of ionic strength resulted in the increase of adsorption capacity. This indicated the formation of inner-sphere complexes between As(V) and composites surface. The XPS spectra of Al2p and Si2p attributed to halloysite host revealed single peaks. Since, the significant changes between samples before and after adsorption were not observed, this revealed that local environment of Al and Si was not altered. The As3d region of the XPS spectrum was fitted to the sum of two peaks, that were ascribed to As(V) and As(III). The presence of two peaks indicated that beside inner-sphere complexes formation, the As(V) reduction with simultaneous Fe(II) oxidation took place as one of the adsorption mechanisms. Due to partial Fe(II) oxidation during calcination, in the case of HFeK composites the relative proportion of As(III) to As(V) was lower. This suggested that this mechanism took place to a smaller extent. The analyses of O1s spectra before and after adsorption allowed to directly identify and confirm chemisorption as one of the adsorption mechanisms. This was also in agreement with Mössbauer spectroscopy which indicated the increase of aluminosilicate structure stiffness due to As chemisorption.

This project was supported by the National Science Centre, Poland, under a research project awarded by Decision No. 2016/21/N/ST10/00390.

## Rare earth environments in silicate, borate, borosilicate, and transition metal phases obtained from glass-ceramics

**John McCloy** (presenting author)  
Washington State University, USA

Co-author(s): Hua Chen  
Inner Mongolia University of Science and Technology, China

Alumino-boro-silicate glass-ceramics containing alkali (Na), alkaline earth (Ca), rare earth (one of La . . . Lu, Y, or Sc) and transition metals (Zr and Mo) were formulated to test the effects of composition and rare earth (RE) cation size on the crystallization of simulated nuclear waste glass-ceramics. Six-oxide glasses were formulated in three series: 1) peralkaline (defined as  $\text{Na}_2\text{O}_{\text{excess}} = \text{Na}_2\text{O} - \text{Al}_2\text{O}_3 - \text{ZrO}_2 > 0$ ) with ~5 mol%  $\text{RE}_2\text{O}_3$ ; 2) metaluminous ( $\text{Na}_2\text{O}_{\text{excess}} \sim 0$ ) with 10 mol%  $\text{RE}_2\text{O}_3$  and 10 mol%  $\text{B}_2\text{O}_3$ ; and 3) peraluminous ( $\text{Na}_2\text{O}_{\text{excess}} < 0$ ) with 10 mol%  $\text{RE}_2\text{O}_3$  and 15 mol%  $\text{B}_2\text{O}_3$ . Glasses were melted and quenched, then re-heated and slow cooled to maximize crystallization. Glass-ceramics were characterized by X-ray diffraction (XRD) Rietveld refinement and electron probe microanalysis.

A statistical phase analysis of ~50 previously made thirty-oxide compositions suggested that the simplified peralkaline and metaluminous glasses should crystallize powellite [(Ca,Na,RE)MoO<sub>4</sub>] and oxyapatite [(RE,Ca,Na)<sub>10</sub>Si<sub>6</sub>O<sub>26</sub>], while the peraluminous glasses should crystallize powellite and RE-borosilicate [RE<sub>3</sub>BSi<sub>2</sub>O<sub>10</sub>].

However, other crystalline phases were identified on testing. In all Ce-containing glasses, cubic cerianite, (Ce,Zr)O<sub>2</sub>, was formed. ZrO<sub>2</sub>-based phases occurred in all peraluminous glasses due to insufficient sodium available to keep Zr dissolved in the glass. The ZrO<sub>2</sub> phase could be monoclinic (baddeleyite), tetragonal, and/or cubic, presumably depending on the amount of RE<sup>3+</sup> incorporated. In a few compositions, zircon ZrSiO<sub>4</sub>, formed rather than a zirconia phase.

A monoclinic keiviite-type phase, i.e. (Y,Yb)<sub>2</sub>Si<sub>2</sub>O<sub>7</sub>, formed rather than oxyapatite in glasses with the smallest RE<sup>3+</sup> cations. A RE borate phase REBO<sub>3</sub>, isostructural with vaterite (CaCO<sub>3</sub>) and having RE CN=8, was identified in peraluminous compositions with Dy, Y, Ho, and Tm. The borate phase occurred simultaneously with the silicate phase, either oxyapatite or keiviite.

The results of this study suggest that the glass formulation and RE size strongly influenced the RE environment in the glass and hence the crystal phases formed. The formation of RE borosilicate, versus separate RE borate and RE silicate phases, also suggested underlying differences in the glass structure. For formulations with high RE and B oxide concentration (peraluminous), large RE ions favor RE-borosilicate crystallization (RE CN=8,9), while small RE ions favor keiviite (RE CN=6). When RE and B oxide concentration is lower, oxyapatite is the favored crystal structure (RE CN=7,9) for most RE ions while the smallest RE ions form keiviite. A Mo phase (powellite) always forms, and a Zr phase forms in all peraluminous compositions, both containing some RE. Minor anomalies in the trends with RE ion size can be explained by tendencies to form some RE<sup>4+</sup> (Ce, Tb) or by electronic effects (Y, Sc).

## Provenance studies of emerald: evaluation of Raman approach

**Laura Medeghini** (presenting author)  
Department of Earth Sciences, Sapienza University of Rome, Italy

Co-author(s): Silvano Mignardi<sup>1</sup>, Caterina De Vito<sup>1</sup>, Pier Paolo Lottici<sup>2</sup>, Danilo Bersani<sup>2</sup>  
<sup>1</sup>Department of Earth Sciences, Sapienza University of Rome, P.le Aldo Moro 5, 00185 Rome, Italy  
<sup>2</sup>Department of Mathematical, Physical and Computer Sciences, University of Parma, Parco Area delle Scienze 7/a, 43124 Parma, Italy

Emerald is the more prestigious gem among the beryl-group minerals. Mineralogically, it is a cyclosilicate of Al and Be with general formula Be<sub>3</sub>Al<sub>2</sub>Si<sub>6</sub>O<sub>18</sub>. The presence of Cr<sup>3+</sup> and V<sup>3+</sup> determines the typical green color. The particular structure is composed by tetrahedra (Si<sub>6</sub>O<sub>18</sub>) forming six-member rings, stacked along c -axis, forming continuous channels where ions (alkali) and molecules (water) can be present [1-3].

Recent studies used spectroscopies in the provenance study of emeralds [4-6]. In particular, on the basis of shape and position of vibrational features associated to the Si-O vibration (1067-1072 cm<sup>-1</sup>) and those of water (3300-3800 cm<sup>-1</sup>), it could be possible define the genetic model for each deposit and consequently the emerald provenance.

The present work is aimed to define a non-invasive procedure that could be applied in provenance studies of emeralds. In particular, the results of a Raman study on samples from the main deposits exploited in antiquity such as Malyshevsk (Russia), Jos (Nigeria), Pajshir Valley (Afghanistan), Habachtal (Austria), Sikait, Zabara (Egypt) and Swat Valley (Pakistan) are reported.

The spectroscopic markers connected to the different deposits are compared to the genetic models proposed by Aurisicchio et al. [7]. Therefore, a comparison among spectroscopic and chemical data can give an overview about the potentiality of the Raman spectroscopy.

### References

- [1] Artioli, G., et al. (1993) Am. Mineral. 78, 762–768.
- [2] Aurisicchio, C., et al. (1988) Am. Mineral. 73, 826–837.
- [3] Aurisicchio, C., et al. (2012) Can. Mineral. 50, 1467–1488.
- [4] Hagemann, H., et al. (1990) Phys. Chem. Miner. 17, 395–401.
- [5] Moroz, I., et al. (2000) J. Raman Spectrosc. 31, 485–490.
- [6] Huong, L.T.T., et al. (2014) Gems Gemol. 50, 287–292.
- [7] Aurisicchio, C., et al. (2018) Ore Geol. Rev. 94, 351–366.

## How to determine a unique entrapment condition of host-inclusion systems from UHPM rocks using Raman elastic geobarometry

**Mara Murri** (presenting author)

Department of Earth and Environmental Sciences, University of Pavia, Italy

Co-author(s): Claudia Stangarone<sup>1</sup>, Andrey V. Korsakov<sup>2</sup>, Ross J. Angel<sup>3</sup>, Mauro Prencipe<sup>4</sup>, Boriana D. Mihailova<sup>5</sup>, Matteo Alvaro<sup>3</sup>

<sup>1</sup>Institute of Planetary Research DLR – German Aerospace Center

<sup>2</sup>V.S. Sobolev Institute of Geology and Mineralogy, SB RAS, Novosibirsk, Russia

<sup>3</sup>Department of Earth and Environmental Sciences, University of Pavia, Italy (Current address: IGG-CNR Padova, Italy)

<sup>4</sup>Earth Sciences Department, University of Torino, Italy

<sup>5</sup>Department of Earth Sciences, University of Hamburg, Germany.

Elastic geobarometry for host-inclusion systems can provide constraints to determine pressure and temperature conditions experienced by minerals during subduction or ultra-high-pressure (UHP) metamorphism. However, the most common experimental approaches and theories are developed only for crystals immersed in a fluid pressure transmitting medium (i.e. hydrostatic pressure), whereas inclusions entrapped in other minerals are subject to isotropic strains.

For this purpose, we investigated the effects of non-hydrostatic stresses on rock-forming minerals in order to understand how minerals respond to tectonic stresses. We focused our study on quartz and zircon because they represent the most common inclusions found in garnet from UHP metamorphic terrains and they have relatively simple structures.

Since experimental data under hydrostatic pressure do not provide us access to all the possible modifications and structural changes experienced by minerals in the Earth's interior, we carried out *ab initio* hybrid Hartree–Fock/Density Functional Theory simulations to determine the changes in elastic and vibrational properties for alpha-quartz and zircon under different applied strains. We calculated their structure, elastic parameters and Raman-active vibrational modes as a function of different applied strains to determine the phonon-mode Grüneisen tensor for each Raman-active mode. These results coupled with the elastic geobarometry theory [1] allow us to infer the imposed stress at the moment of inclusion entrapment. As an example, we used these results to calculate the entrapment conditions for quartz inclusions in garnet within an eclogite xenolith from Mir pipe. The estimated P-T conditions of elastic equilibration of the pair into the stability field of coesite at 3 GPa and temperatures between 925 and 1000°C [2].

This project has received funding from the European Research Council under the H2020 research and innovation programme (N. 714936 TRUE DEPTHS to M. Alvaro).

### References

[1] Angel, et al. (2015) *J. Met. Geol.* 33, 801–813.

[2] Alvaro, et al. submitted

## The role of 4+ cations on the structure and crystallization of nepheline and related phases from sodium aluminosilicate glasses

**Emily Nienhuis** (presenting author)

Washington State University, WA, USA

Co-author(s): Gabe Cocking<sup>1</sup>, Jose Marcia<sup>1</sup>, John McCloy<sup>1</sup>

<sup>1</sup>Washington State University, WA, USA

<sup>2</sup>University of Chemistry and Technology, Prague, Czech Republic

Vitrification is the decided means for disposal of High Level Nuclear Waste (HLW) at the Hanford site in Washington State, USA. Through vitrification, glass forming additives are mixed and melted with the nuclear waste to produce a durable glass waste form. The waste can have a wide range of compositions resulting in glasses containing high amounts of sodium and aluminum that tend to result in the crystallization of nepheline and other crystalline aluminosilicate phases. The compositional dependence of this crystallization has been a US Department of Energy priority for at least a decade. This talk summarizes the problem surrounding nepheline crystallization and highlights recent work on the substitution of Si with 4+ cations, such as Sn, Zr, and Ti, on the structure of the glass and the resulting glass-ceramics. Structural studies include X-ray and neutron PDF analysis paired with Raman spectroscopy, quantitative XRD, and EPMA. From these studies, the propensity for these 4+ cations to incorporate into the glass network as formers, or modifiers, and the effect of these species on crystallization of aluminosilicates will be discussed in terms of the relationship of physical properties as influenced by the short- and medium-range ordering of glass constituents.

## Paddlewheelite, a new uranyl carbonate mineral from the Jáchymov District, Bohemia, Czech Republic

Travis A. Olds (presenting author)

School of Mechanical and Materials Engineering, Washington State University, Pullman, WA, 99163, USA

Co-author(s): Jakub Plášil<sup>1</sup>, Anthony R. Kampf<sup>2</sup>, Fabrice Dal Bo<sup>3</sup>, Peter C. Burns<sup>3,4</sup>

<sup>1</sup>Institute of Physics, Academy of Sciences of the Czech Republic, v.v.i., Na Slovance 1999/2, 18221 Prague 8, Czech Republic

<sup>2</sup>Mineral Sciences Department, Natural History Museum of Los Angeles County, 900 Exposition Boulevard, Los Angeles, CA 90007, USA

<sup>3</sup>School of Mechanical and Materials Engineering, Washington State University, Pullman, WA, 99163, USA

<sup>4</sup>Department of Chemistry and Biochemistry, University of Notre Dame, Notre Dame, IN 46556, USA

Paddlewheelite,  $\text{MgCa}_5\text{Cu}_2[(\text{UO}_2)(\text{CO}_3)_{3/3+4}]\cdot 33\text{H}_2\text{O}$ , is a new uranyl carbonate mineral found underground in the Svornost mine, Jáchymov District, Bohemia, Czech Republic, where it occurs as a secondary oxidation product of uraninite. The conditions leading to its crystallization are complex, likely requiring concomitant dissolution of uraninite, calcite, dolomite, chalcopryrite, and andersonite. Paddlewheelite is named after its distinctive structure, which consists of paddle-wheel clusters of uranyl tricarbonate units bound by square pyramidal copper “axles” and a cubic calcium cation “gearbox.” Each paddle wheel shares edges with calcium polyhedra to form open sheets that are held together solely by hydrogen bonding interactions. The new mineral is monoclinic,  $Pc$ ,  $a = 22.052(4)$ ,  $b = 17.118(3)$ ,  $c = 19.354(3)$  Å,  $\beta = 90.474(2)^\circ$ ,  $V = 7306(2)$  Å<sup>3</sup> and  $Z = 4$ . Paddlewheelite is the second-most structurally complex uranyl carbonate mineral known after ewingite and its structure may provide insights into the insufficiently described mineral voglite, as well as Cu-U-CO<sub>3</sub> equilibrium in general.

## Crystal structure model of tiettaite and its Na-deficient analogue: novel type of microporous octahedral-tetrahedral framework

Taras Panikrovskii (presenting author)

Kola Science Centre of RAS, Fersman Str. 14, Apatity, Murmansk Region, 184209 Russia

Co-author(s): Gregory Yu. Ivanyuk, Victor N. Yakovenchuk, Ayya V. Bazai, Igor V. Pekov, Sergey V. Krivovichev

Kola Science Centre of RAS, Fersman Str. 14, Apatity, Murmansk Region, 184209 Russia

Tiettaite was discovered by A.P. Khomyakov [1] in a peralkaline (hyperagpaitic) pegmatite at Mt. Rasvumchor in the Khibiny alkaline massif (Kola Peninsula, Russia), as rounded aggregates up to 1 cm in diameter consisting of needle-shaped, fibrous and tabular individuals. The mineral was named from Lappish tietta which means “science” or “knowledge”. “Tietta” was also the name of the first scientific base of the USSR Academy of Sciences in Khibiny (1930–1938). Tiettaite was described with the simplified formula  $(\text{Na},\text{K})_{17}\text{FeTiSi}_{16}\text{O}_{29}(\text{OH})_{30}\cdot 2\text{H}_2\text{O}$  [1], but its crystal structure remained unknown.

In this work, we studied chemical composition and crystal structure of tiettaite from its new locality at Mt. Rasumchorr (pegmatite Rasvumchorr-2017 uncovered in an underground working of the Rasvumchorr apatite mine), and of a hydrated Na-deficient tiettaite-like phase extracted from the co-type specimen of tiettaite (sample No 7326 from the collection of the Bel'kov Museum of Geology and Mineralogy of Kola Science Centre of the Russian Academy of Sciences; donated by A.P. Khomyakov).

The empirical formula of a „Na-deficient tiettaite” from the Bel'kov Museum calculated on the basis of  $\text{Si} = 16$  is  $(\text{Na}_{6.01}\text{K}_{4.49})_{210.50}(\text{Fe}^{3+}_{1.41}\text{Ti}_{1.04}\text{Si}_{22.45}(\text{Si}_{16.00}\text{Al}_{0.17})_{216.17}\text{O}_{38.40}(\text{OH})_{6.60})\times 2.05\text{H}_2\text{O}$ . It demonstrates significant deficiency of Na in comparison with the holotype (12.51 apfu Na [1]) and recently collected samples  $(\text{K}_{3.59}\text{Na}_{12.86}\text{Ca}_{0.02})_{216.47}(\text{Fe}^{3+}_{1.79}\text{Al}_{0.08}\text{Mn}_{0.03}\text{Mg}_{0.03}\text{Ti}_{0.03})_{21.96}\text{Si}_{16}\text{O}_{41.34}(\text{OH})_{3.66}\cdot 2.17\text{H}_2\text{O}$ .

The quality of both studied single crystals was far from perfect due to the high mosaicity. This caused relatively high crystallographic agreement index ( $R_1 = 0.23$  for 606 independent reflections with  $|F_o| \geq 4\sigma_f$ ) and, thus, we consider our results as a crystal structure model only. However, the model is crystal chemically reasonable and show reasonable interatomic distances.

The mineral is orthorhombic, space group  $Cmnm$ ,  $a = 30.616(6)$ ,  $b = 10.808(2)$ ,  $c = 17.494(3)$  Å,  $V = 5788.7(2)$  Å<sup>3</sup> (as suggested by Khomyakov et al. [1]). Tiettaite possesses a novel structure type of minerals and inorganic compounds. The structure is based upon microporous framework consisting of branched  $[\text{Si}_{14}\text{O}_{39}]$  silicate tetrahedral chains extended along the  $c$  axis. The chains are linked into framework via dimers of  $(\text{Fe}^{3+}\text{O}_6)$  octahedra sharing a common edge. The simplified crystal chemical formula of tiettaite can be written as  $\text{K}_4\text{Na}_{12.5}\text{Fe}^{3+}_2[\text{Si}_{16}\text{O}_{41.5}(\text{OH})_{3.5}]^*\cdot 2\text{H}_2\text{O}$ .

The crystal structure of Na-deficient and hydrated tiettaite-like phase, which is more stable in atmospheric air, was solved and refined to  $R_1 = 0.15$  for 1599 independent reflections with  $|F_o| \geq 4\sigma_f$  [ $Cmnm$ ,  $a = 28.80(4)$ ,  $b = 10.952(14)$ ,  $c = 17.48(2)$  Å,  $V = 5515(1)$  Å<sup>3</sup>]. Compared to tiettaite, the  $a$  unit-cell parameter of this phase is shorter by  $\sim 2$  Å. The simplified crystal chemical formula of the Na-deficient phase is  $\text{K}_4\text{Na}_8\text{Fe}^{3+}_2[\text{Si}_{16}\text{O}_{37}(\text{OH})_8]^*\cdot 3.5\text{H}_2\text{O}$ .

Alkaline and alkaline-ultrabasic massifs of the Kola province contain a number of meso-, microporous silicates including endemic zeolites and titanosilicates [2, 3] with properties of cation-exchangers, gas separation molecular sieves, photo-catalysts, natural precursors of other functional compounds. It seems likely that tiettaite or its synthetic counterparts may possess interesting physical and chemical properties as well.

The research is supported by the Kola Science Center of Russian Academy of Sciences (0186-2019-0011), Russian Science Foundation (19-17-00038) and the Russian Foundation for Basic Research (18-29-12039 and 18-29-12007).

### References

- [1] Khomyakov, A.P., et al. (1993) Zapiski RMO 122, 1, 121–124.
- [2] Yakovenchuk, V.N., et al. (2011) Am. Mineral. 96, 1624–1629.
- [3] Yakovenchuk, V.N., et al. (2009) Am. Mineral. 94, 1450–1458.

## Substitution ranges of new mineral staročeskéite $\text{Ag}_{0.7}\text{Pb}_{1.6}(\text{Bi}_{1.35}\text{Sb}_{1.35})_{\Sigma 2.70}\text{S}_6$

Richard Pažout (presenting author)

University of Chemistry and Technology Prague, Czech Republic

A new sulfosalt mineral staročeskéite from the family of lillianite homologues was identified in samples of Bi-mineralization in the Kutná Hora ore district, Czech Republic. The simplified empirical formula based on electron probe microanalysis is  $\text{Ag}_{0.70}\text{Pb}_{1.60}(\text{Bi}_{1.35}\text{Sb}_{1.35})_{\Sigma 2.70}\text{S}_6$ . The mineral belongs to the lillianite homologous series with  $N = 4$ . The  $N$  value represents a number of octahedra in two neighbouring blocks in the structure (sites M1 and M2), where two main substitutions take place: 1.  $\text{Ag}^+ + \text{Bi}^{3+}, \text{Sb}^{3+} \leftrightarrow 2 \text{Pb}^{2+}$  and 2.  $\text{Bi}^{3+} \leftrightarrow \text{Sb}^{3+}$ .

Staročeskéite is orthorhombic, space group  $\text{Cmcm}$ , with  $a = 4.2539(8)$ ,  $b = 13.3094(8)$ ,  $c = 19.625(1)$  Å,  $V = 1111.1(2)$  Å<sup>3</sup>,  $Z = 4$ . The structure contains four sulphur sites and three metal sites [1]: one pure Pb site M3 in trigonal prismatic coordination and two mixed octahedral sites - each with three atom species: M1 (0.52Bi + 0.356Ag + 0.124Sb) and M2 (0.601Sb + 0.259Pb + 0.14 Bi). The type sample of staročeskéite is characterized by Bi:Sb ratio 1:1 ( $\text{Bi}/(\text{Bi} + \text{Sb}) = 0.50$ ) and the  $\text{Ag}^+ + \text{Bi}^{3+}, \text{Sb}^{3+} \leftrightarrow 2 \text{Pb}^{2+}$  substitution (L%) equal to 70 %.

Because there is a great variety of minerals (ten mineral species) of a similar and very close composition in the lillianite series with  $N = 4$  (Figure 1), it is necessary to determine the ranges of substitution (substitution limits) within which the mineral is defined.

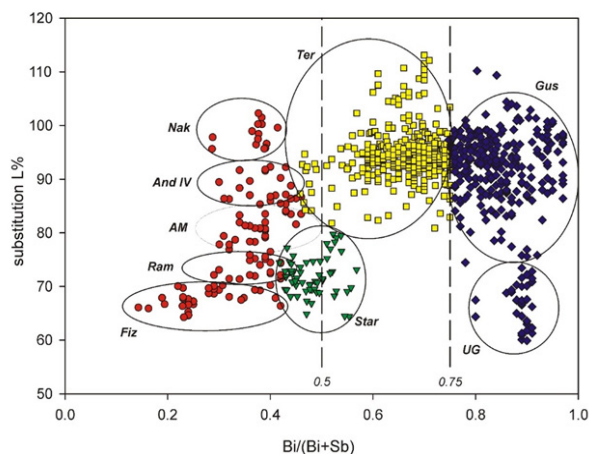


**Figure 1.** A great variety of mineral species from the series of lillianite homologues with  $N = 4$ : Star - staročeskéite, Gus - gustavite, UN - undersubstituted gustavite (Ag,Bi-rich lillianite), Ter - terrywallaceite, Fiz - Bi-rich fizelyite, Ram - Bi-rich ramdohrite, AM - mixture of several andorite minerals, And IV - Bi-rich andorite IV, Nak - nakaseite (Bi-rich Cu-bearing andorite VI). Oskarkempffite and clino-oskarkempffite with substitution above 120 % are not in picture.

Empirically it is possible to determine that the name staročeskéite would be valid for a lillianite structure with composition  $\text{Ag}_x\text{Pb}_{3-2x}\text{Bi}_y\text{Sb}_{2+x-y}\text{S}_6$  with the boundaries  $\frac{1}{2} \leq x \leq 0.8$ , and  $1 - \frac{1}{2}x \leq y \leq 2$ , where the parameter  $x = \text{Ag}$  content = L% and  $y = \text{total Bi}$  content. Thus the conclusion is that for staročeskéite to exist, there must be between 20 to 50 % occupation of M2 site by Pb, apart from fully occupied M3 site. Other Pb concentrations in M2 site result in different lillianite homologues with  $N = 4$  [2].

### References

- [1] Pažout, R., Dušek, M. (2010) Eur. J. Mineral. 22, 741–750.  
 [2] Pažout, R., Sejkora, J. (2018) Miner. Mag. 82, 4, 1–26.

## U-Pb age dating of zircon and zirconolite inclusions in marble hosted gem-quality ruby and spinel from Mogok, Myanmar

Myint Myat Phyo (presenting author)

Mineralogical Petrological Institute, University of Basel, Switzerland

Co-author(s): Marcel Guillong<sup>1</sup>, Leander Franz<sup>2</sup>, Alfons Berger<sup>3</sup>, Walter A. Balmer<sup>4</sup>, Hao A.O. Wang<sup>4</sup>, Michael S. Krzemiński<sup>4</sup>

<sup>1</sup>Institute of Geochemistry and Petrology, ETH Zürich, Switzerland

<sup>2</sup>Mineralogical Petrological Institute, University of Basel, Switzerland

<sup>3</sup>Geological Institute, University of Bern, Switzerland

<sup>4</sup>Swiss Gemmological Institute SSEF, Basel, Switzerland

The Mogok area of Myanmar is one of the finest ruby and spinel deposits, which attracts much research attention in order to understand its gemstone formation relevant to magmatic and metamorphic events. The age dating of such events provide not only critical information for gemstone formation, but also complementary evidence for origin determination in gem testing labs. Especially in recent decades, when conventional gemmological features overlap among gems from a growing number of deposits worldwide, geochronological age dating on zircon, titanite and other inclusions in gemstones, have become more and more popular. However, age determined from such inclusions often indicates a maximum possible formation age of gemstones.

In this study, we applied two experimental setups: LA-ICP-Time-Of-Flight-MS for multi-element information due to full mass spectrum acquisition and LA-ICP-Sector-Field-MS for analysis of small inclusions due to its higher sensitivity. U-Pb age dating has been conducted on zircon and zirconolite inclusions in marble hosted gem-quality rubies and spinels sampled from Mogok area. Besides, zircons from the hosting marble and from neighbouring gneisses were dated for additional information. In total, more than 100 zircons and zirconolites has been analysed.

Age dating results on zircon cores in ruby, spinel and marble range from Cretaceous (~100 Ma) to Eocene (~33 Ma). The age on zircon rims is concordant at Early Miocene-  $22.88 \pm 0.36$  Ma (Spinel) and  $22.26 \pm 0.18$  Ma (Ruby), are shown in Figure 1. Analyses of 41 zircons from a granulite facies garnet biotite gneiss from western Mogok show Pb-loss condition and yield upper intersect age at Precambrian (~990 Ma), whereas lower intersect is at Oligocene (~30 Ma). Core analyses from 25 zircons from garnet orthopyroxene gneiss, central Mogok showed Jurassic to Cretaceous age (~180–70 Ma) and analyses of their rims highlight Oligocene age (~30 Ma). These zircon core may form during old magmatic events in the area, as described in a former study [1]. Furthermore, concordia age of zirconolite inclusions as single grains in ruby falls at Early Miocene ( $18.06 \pm 0.09$  Ma), which is similar to the result of K-Ar age dating of biotite in granite from Mogok [2]. Finally, zirconolite forming a rim around zircon from a gem-bearing marble dated around 20–24 Ma.

## Detailed Inclusion Study of Gem-Quality Spinel from Mogok, Myanmar: Geikielite $\text{MgTiO}_3$ as exsolution lamellae

**Myint Myat Phyo** (presenting author)

Mineralogical Petrological Institute, University of Basel, Switzerland

Co-author(s): Eva Bieler<sup>1</sup>, Leander Franz<sup>2</sup>, Hao A.O. Wang<sup>3</sup>, Walter Balmer<sup>3</sup>, Michael S. Krzemenicki<sup>3</sup>

<sup>1</sup>Swiss Nano Imaging Lab, Swiss Nanoscience Institute, University of Basel, Switzerland

<sup>2</sup>Mineralogical Petrological Institute, University of Basel, Switzerland

<sup>3</sup>Swiss Gemmological Institute SSEF, Basel, Switzerland

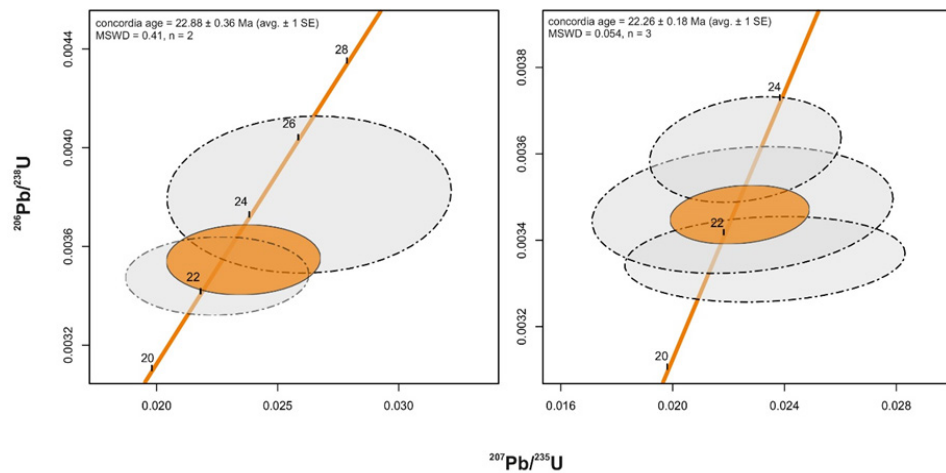


**Figure 1.** Concordia diagram of U-Pb ages, analysed on zircon rims from gemstones: spinel (concordant at  $22.88 \pm 0.36$  Ma) and ruby (concordant at  $22.26 \pm 0.18$  Ma)

Based on these investigations, we assume that ages obtained from zircon rims indicate age of granulite facies metamorphism event Late Oligocene to Early Miocene. This event may be responsible for the generation of gemstones. The wide range of zircon core ages may be due to multiple magmatic or metamorphic events in Mogok area prior to the gemstone formation. All these zircon inclusions probably came as detrital grains from others sources and were growing during the late granulite facies event.

### References

[1] Barley, M.E., et al. (2003) *Tectonics* 22, 1–11.

[2] Brook, M., et al. (1976) *Isotope Geology Unit Report*, Institute of Geological Sciences, UK.

Traditionally, the meticulous observation and analysis of inclusions is one of the most useful and accessible methods to deduct the origin of coloured gemstones. In this study, we analysed 100 gem-quality spinels from Mogok (Myanmar) in colour of pink to red, orangey red and purplish grey. Most of the samples (87) were collected by the first author at six different gem localities within the so-called Mogok Stone Tract [1], with additional 13 spinel samples from local gem markets. In addition to a detailed microscopic investigation of our samples, a large number of spinel inclusions were analysed by Raman microspectroscopy, scanning electron microscopy (SEM) for secondary electron (SE), variable pressure secondary electron (VPSE) and back-scattered electron (BSE) imaging. Chemical analyses of inclusions were carried out by SEM-EDS (energy dispersive spectroscopy) for inclusion characterization, as well as LA-ICP-TOF-MS (Laser Ablation Inductively Coupled Plasma Time-Of-Flight Mass Spectrometry) and LA-ICP-SF-MS (Sector-Field MS) for radiometric age dating.

In our study, we detected 16 minerals as inclusion which were not described before in Mogok spinel. These include (in alphabetical order): amphibole (pargasite), anatase, baddeleyite, boehmite, brucite, chlorite, clinohumite, clinopyroxene, diaspore, goethite, geikielite, halite, marcasite, molybdenite, periclase and pyrrhotite. Interestingly, geikielite ( $\text{MgTiO}_3$ ) was discovered as tiny, colourless flakes of maximum  $20\mu\text{m}$  diameter oriented along the crystallographic planes  $\{111\}$  of spinel (Figure 1). They probably formed as epigenetic precipitates along the spinel structure. This is similar to the geikielite-rich ilmenite exsolution lamellae described from chromite-chrome spinel in metacarbonates of the Oetztal-Stubai complex in Austria [2]. Furthermore, we observed mineral inclusions with exsolved phases (e.g. dolomite in calcite inclusions) and numerous multi-phase solid inclusions (e.g. calcite intergrown or aggregated with primary and secondary mineral). Most of these complex intergrowths are beyond the resolution of gemmological microscopes (10–70x magnification) and rarely detected by Raman.

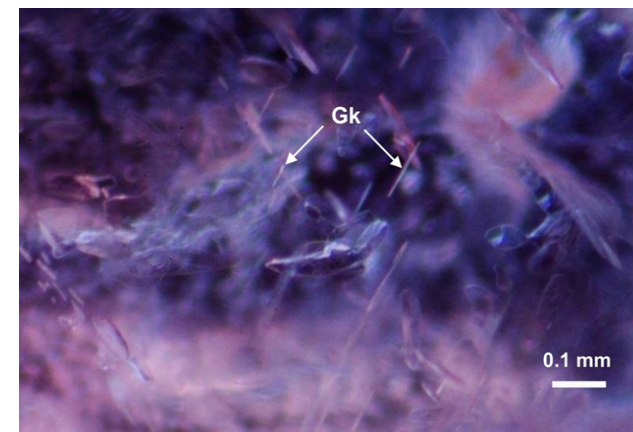


**Figure 1.** Geikielite (Gk,  $\text{MgTiO}_3$ ) inclusions oriented along the crystallographic planes  $\{111\}$  of spinel.

To conclude, in this study we demonstrate notable variation of inclusions found in gem-quality spinel from Mogok based on their specific local geographical (geological) occurrence. To our knowledge, this is the largest study about spinel inclusions found in this region so far. Not only does the result provide a detailed overview about Mogok spinels and their inclusions, but also valuable information to separate Mogok spinel from those found in other gem deposits worldwide.

#### References

- [1] Chhibber, H.L. (1934) The Geology of Burma.  
 [2] Mogessie, A., et al. (1988) Mineralogical Magazine 52, 229–236.

## Fractionation of copper, oxygen and hydrogen isotopes between malachite and aqueous solution

Alexandra M. Plumhoff (presenting author)

Institute of Geosciences, Friedrich-Schiller University Jena, Germany

Co-author(s): Ryan Mathur<sup>1</sup>, Rastislav Milovsky<sup>2</sup>, Juraj Majzlan<sup>3</sup>

<sup>1</sup>Department of Geology, Juniata College, Huntingdon, PA, USA

<sup>2</sup>Earth Science Institute, Slovak Academy of Sciences, Banská Bystrica, Slovakia

<sup>3</sup>Institute of Geosciences, Friedrich-Schiller University Jena, Germany

Studies of the equilibrium isotope properties of stable isotopes of minerals have been initiated principally because of their application to the solution of geochemical problems. Stable isotope fractionation factors can provide insights into the mineral formation pathways by establishing of the isotopic composition of the parent aqueous solutions. In this work, we examined malachite, a common secondary mineral in the oxidation zone of copper ore deposits and its isotopic fractionation with aqueous solution. The equilibrium isotope fractionations of oxygen, hydrogen and copper between malachite and aqueous solution were determined by precipitation experiments over the temperature range from 10 to 65 °C. The solid products were characterized by powder X-ray diffraction, infrared spectroscopy and thermogravimetric analysis and consisted of a single phase  $\text{Cu}_2\text{CO}_3(\text{OH})_2$ , corresponding to the mineral malachite. The isotopic fractionation factors for oxygen and hydrogen could be divided in two temperature regions (10–35 °C and 45–65 °C) (Tab. 1) due to a non-linear change in the isotopic values at around 40 °C. This change is related to the initial precipitation of georgeite (X-ray amorphous  $\text{Cu}_2\text{CO}_3(\text{OH})_2$ ) and the isotopic exchange of this mineral and the malachite formed from georgeite. The isotopic fractionation factor for copper is defined over the whole temperature range (10–65 °C) (Tab. 1) with a distinct temperature dependent fractionation and an average fractionation shift of  $\Delta^{65}\text{Cu}_{\text{sol-mal}} = 0.16 \pm 0.05 \text{ ‰}$ .

The calculated fractionation factors of oxygen and hydrogen were used to determine the oxygen and hydrogen isotopic composition of the formation waters of natural malachite samples from a number of localities worldwide. With  $\delta^{18}\text{O}_{\text{SMOW}}$  values of +22 to +29.5 ‰ and  $\delta\text{D}_{\text{SMOW}}$  values of -132 to -61 ‰ for the natural malachite and  $\delta^{18}\text{O}_{\text{SMOW}}$  values of -14.5 to -7 ‰ and  $\delta\text{D}_{\text{SMOW}}$  values of -107 to -36 ‰ for the formation water, it is to assume that all investigated malachite samples are supergene samples which formed from meteoric water. Even in massive malachite samples from Ural Mts. (Russia), no signs of other fluids were detected from the isotopic composition.

	temperature range	A	B
oxygen <sub>mineral-solution</sub>	10 – 35 °C	2.71 ± 0.16	4.06 ± 1.79
	45 – 65 °C	2.87 ± 0.33	0.96 ± 3.05
hydrogen <sub>mineral-solution</sub>	10 – 35 °C	0.21 ± 0.47	-27.47 ± 5.52
	45 – 65 °C	-1.47 ± 0.61	-22.29 ± 5.65
copper <sub>solution-malachite</sub>	10 – 65 °C	0.03 ± 0.01	-0.19 ± 0.14

Values for A and B of the equation for the isotopic fractionation factors of oxygen, hydrogen and copper in the form of  $1000 \ln \alpha = A (10^6 / T^2) + B$ , with T the temperature in Kelvin.

## Optimized time-resolved photoluminescence detection of rare earth elements in apatites and calcites

**Sari Romppanen** (presenting author)

University of Jyväskylä, Department of Chemistry, P. O. Box 35 FI-40014, Finland

Co-author(s): Heikki Häkkinen<sup>1</sup>, Saara Kaski<sup>2</sup>

<sup>1</sup>University of Jyväskylä, Department of Biological and Environmental Science, P. O. Box 35 FI-40014, Finland

<sup>2</sup>University of Jyväskylä, Department of Chemistry, P. O. Box 35 FI-40014, Finland

Photoluminescence (PL) is effective and fast way to analyse the occurrence of luminescence activators in minerals. Especially interesting are the rare earth element (REE) activators, which are considered as critical raw materials for the EU and important for the modern society and technology. REEs show several narrow luminescence bands at relatively constant emission wavelengths. The host mineral, however, may contain other interfering activators, like Mn<sup>2+</sup>-ions, which can hinder the detection of luminescence of REEs.

In this research, we demonstrate that by selecting optimal PL measurement parameters, including excitation wavelength and detection wavelength range, and applying time-resolved detection in the analysis of natural calcite and apatite samples, the different REEs can be recognized and the spectral interference can be minimized. Comparison of REE luminescence in apatite and calcite in carbonatite samples is presented.

## The effect of M(II)/M(III) molar ratio on the LDH structure derived from chemicals and minerals: a spectroscopic study using FTIR, Raman and XPS

**Karolina Rybka** (presenting author)

AGH University of Science and Technology, al. Mickiewicza 30, 30-059 Krakow, Poland

Co-author(s): Jakub Matusik

AGH University of Science and Technology, al. Mickiewicza 30, 30-059 Krakow, Poland

Layered double hydroxides (LDH) is a supergroup of crystalline non-silicate hydroxides with the following general formula:  $[M^{II}_{1-x}M^{III}_x(OH)_2]^{x+} [A^{n-}]_{x/n} \cdot x y H_2O$ . Due to similarities with clay minerals they are called 'anionic clays'. Their structure comprises positively-charged brucite-like layers balanced with the intercalated hydrated anions. LDH have perfect anion exchange properties, therefore they are promising materials for the wastewater treatment. Two most common LDH groups are hydrotalcites and pyroaurites with Mg/Al and Mg/Fe chemistry, respectively. They are rare in nature, however synthesis can be easily carried out in the laboratory conditions. However, the synthesis involving chemical reagents is expensive, therefore in this work, the synthesis was done by transformation of abundant minerals (magnesite [M] and dolomite [D]), which were a source of Mg. Mg/Al LDH and Mg/Fe LDH were synthesized via the co-precipitation method in different variants including three M(II)/M(III) molar ratios and two ageing times. The goal was to characterize these materials and to get insight into structural differences which may affect the sorption affinity towards aqueous anions.

For the synthesis, M and D were used as M(II) source, while  $AlCl_3 \cdot 6H_2O$  and  $FeCl_3 \cdot 6H_2O$  were used as M(III) source. Reference materials were synthesized from chemical reagents with  $MgCl_2 \cdot 6H_2O$  and appropriate Al and Fe chlorides. Firstly, M and D were dissolved in order to release M(II) in  $AlCl_3$  via the hydrolysis process in the case of Mg/Al LDH, or in HCl in the case of Mg/Fe LDH. Then, solution of both M(II) and M(III) was added dropwise to the 2 M NaCl solution, with constantly controlled pH=10 with NaOH aqueous solution. The formed precipitates were aged for 2 or 24 h, washed and dried at 60°C overnight. The obtained phases were investigated with XRD, FTIR, Raman spectroscopy and XPS.

The XRD confirmed the presence of hydrotalcite, with admixtures of gibbsite and calcite for the Mg/Al LDH and pyroaurite for the Mg/Fe LDH in all samples. The FTIR spectra showed bands attributed to the water content and carbonates, as well as lattice vibrations. Differences were observed in positions of bands related to carbonates in the region of 1510-1360  $cm^{-1}$  for the materials with different molar ratio. Two carbonate species were identified: monodentate carbonate and bicarbonate in the interlayer space of LDH. The results were confirmed by Raman spectroscopy, where different band positions were observed in the region of 1370-1320  $cm^{-1}$ . Both FTIR and Raman spectroscopy showed differences in the region related to lattice vibrations. The C1s XPS spectra displayed the presence of monodentate carbonates and bicarbonates in the samples. Moreover, a chemical shift of Mg1s was observed as a result of increasing content of Mg-O-Mg bonds with increasing molar ratio.

This research was supported by the National Science Centre, Poland under the project no. 2017/27/B/ST10/00898.

## Fluorite a supposedly ordinary mineral. On charge-shift bonding, nonspherical charge distribution and boundary of ions

Marcin Stachowicz (presenting author)

Institute of Geochemistry, Mineralogy and Petrology, University of Warsaw

A century after the X-ray investigations of fluorite by the Bragg, this experimental work goes beyond routine X-ray structural analysis based on Independent Atom Model. A modern approach, using an aspherical atomic model of electron density [1], Quantum Theory of Atoms In Molecules and Crystals [2], Electron Localisation Function [3], Non-Covalent Interactions [4] formalisms open new opportunities by enabling spatial quantification of electron density in the mineral structures that reflect the nature of interactions between atoms or ions.

On the basis of a multipole refinement of single-crystal X-ray diffraction data collected to a resolution of  $1.63 \text{ \AA}^{-1}$ , a quantitative experimental charge density distribution has been obtained for fluorite [5]. An Atoms-In-Molecules integrated experimental charges for Ca and F ions are  $+1.40e$  and  $-0.70e$ , respectively. The bonded radii along the Ca...F bond path are  $1.21 \text{ \AA}$  for calcium and  $1.15 \text{ \AA}$  for fluoride ions, and are established by the position of the Bond Critical Points. Moreover, the derived electron density distribution, maximum electron density paths, interaction lines, and bond critical points along Ca...F and F...F contacts revealed the character of these interactions. The Ca...F interaction is clearly a closed-shell and ionic in character. However, the F...F interaction has properties associated with the recently recognised type of interaction referred to as charge-shift [6] bonding. This conclusion is supported by the topology of Electron Localisation Function and Non-Covalent Interactions topological parameters.

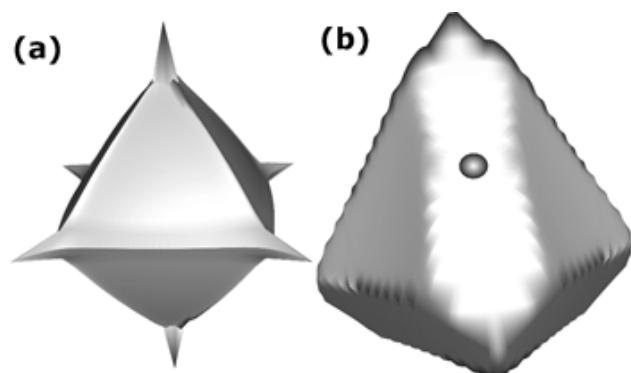


**Figure 1.** The atomic basins of calcium (a) and fluoride (b) ions in fluorite, with the volume of  $11.6 \text{ \AA}^3$  and  $14.4 \text{ \AA}^3$ , respectively.

### References

- [1] Hansen, N.K., Coppens, P. (1978) *Acta Crystallographica Section A: Crystal Physics, Diffraction, Theoretical and General Crystallography* 34, 909–921.
- [2] Bader, R.F.W. (1994) *Atoms in Molecules: A Quantum Theory*, 438 p. Clarendon Press.
- [3] Silvi, B., Savin, A. (1994) *Nature* 371, 683–686.
- [4] Johnson, E.R., et al. (2010) *Journal of the American Chemical Society* 132, 6498–6506.
- [5] Stachowicz, M., et al. (2017) *Acta Crystallographica Section B* 73, 643–653.
- [6] Shaik, S., et al. (2009) *Nature Chemistry* 1, 443–449.

## Crystal structure of uranyl molybdate mineral calcurmolite solved from electron diffraction data

Gwladys Steciuk (presenting author)

Institute of Physics, Academy of Sciences of the Czech Republic v.v.i, Prague 8, Czech Republic

Co-author(s): Radek Škoda<sup>1</sup>, Jakub Plášil<sup>2</sup>

<sup>1</sup>Department of Geological Sciences, Faculty of Science, Masaryk University, Brno, Czech Republic

<sup>2</sup>Institute of Physics, Academy of Sciences of the Czech Republic v.v.i, Prague 8, Czech Republic

We have determined the structure of uranyl molybdate mineral calcurmolite for the first time using precession electron diffraction tomography (PEDT) [1, 2]. Nanocrystals investigated in this study were extracted from the specimen that originates from the Rabejac uranium deposit, Hérault, France. Calcurmolite occurs there as fine yellow crystalline crusts composed of fine hundreds of individual long-prismatic crystals and is often associated with umohoite and uranophane (Figure 1a). Solving the structure of calcurmolite is in several ways challenging due to the poor crystallization and their crystal size; they are nano-sized (Figure 1b). In general, calcurmolite is among the alteration products that have remained overlooked or at least less-studied until now, thus unsuitable for a conventional structure analysis using X-rays. Nevertheless, with the development of electron diffraction techniques, we actually have tools to determine structures down to the nanoscale including the determination of the lightest atoms in the structures, hydrogens [3]. According to single-crystal data from the electron diffraction experiment, calcurmolite is triclinic, twinned and commensurately modulated. We described it in the superspace group  $P-1(a00)0$  with the unit cell  $a = 3.95 \text{ \AA}$ ,  $b = 11.26 \text{ \AA}$ ,  $c = 14.20 \text{ \AA}$ ,  $\alpha = 84.4^\circ$ ,  $\beta = 112.5^\circ$ ,  $\gamma = 133.9^\circ$  and  $q = 2/5a^*$  ( $V = 405 \text{ \AA}^3$ , and  $Z = 4$ ). Interestingly, the crystal structure is based upon sheets of  $U^{6+}$  and  $Mo^{6+}$ -polyhedra of the same topology recently found in baumoite characterized by the same U/Mo ratio [4] (Figure 1c). One cationic site partially occupied by Ca atom is located between the sheets, together with  $H_2O$  molecules. We have also documented that the structure contains a lower amount of Ca than considered previously.

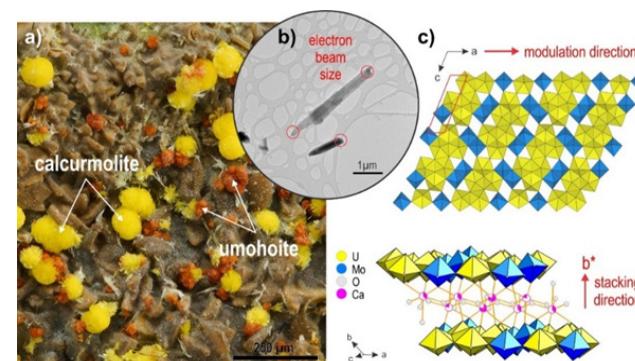


**Figure 1.** a) Uranyl mineral containing both calcurmolite and umohoite (picture from S. Wolfsried). b) Crystals used for the collection of PEDT data. c) Representation of the calcurmolite model with the U/Mo topology and the stacking arrangement.

### References

- [1] Vincent, R., Midgley, P.A. (1994) *Ultramicroscopy* 53, 271–282.
- [2] Kolb, U., et al. (2007) *Ultramicroscopy* 107, 507–513.
- [3] Palatinus, L., et al. (2017) *Science* 355, 166–169.
- [4] Elliott, P., et al. (2019) *Mineralogical Magazine* 1–18.

## The FTIR and Raman spectroscopic study of kieserite, $\text{MgSO}_4 \cdot \text{H}_2\text{O}$ , an important sulfate in our Solar system, across its cosmochemically relevant solid solutions

**Dominik Talla** (presenting author)

Institut für Mineralogie und Kristallographie, Althanstraße 14, 1090 Wien, Austria

Co-author(s): Manfred Wildner

Institut für Mineralogie und Kristallographie, Althanstraße 14, 1090 Wien, Austria

Kieserite,  $\text{MgSO}_4 \cdot \text{H}_2\text{O}$ , and related sulfate monohydrates, a mineral group with limited commercial applicability, has received wide attention following the discovery of its presence in significant quantities on Mars [1-3]. It is also presumed to exist on the icy moons of Jupiter and Saturn, governing, along with higher-hydrated sulfates, the melting equilibria leading to the formation of subsurface oceans and cryovolcanism [4, 5].

Despite the cosmochemical importance of this mineral group, no thorough spectroscopic study of potential solid solutions has been undertaken so far. We hereby present the comparison of FTIR- and Raman spectroscopic data, measured on synthetic samples, along four cosmochemically important binary solid solutions – the Mg/Fe, Mg/Ni, Mg/Mn and Mg/Co kieserite-type series – at ambient and low temperatures, as relevant for the planetary bodies.

All investigated solid solutions show Vegard-type behavior, i.e. the structural and spectral properties change along linear trends, depending on the ratio of Mg and the substituting transition metal cation. Two types of spectral behavior can be discerned, one related to the vibrations of the  $\text{H}_2\text{O}$  molecule, and the other to those of the sulfate group. While the substitution of any of the studied transition elements for Mg leads to a comparable shift of sulfate-related bands to lower wavenumbers, discernible mainly in the Raman spectra, the behavior of  $\text{H}_2\text{O}$ -related bands strongly depends on the particular substituting cation. While Fe contents mainly shift the symmetric  $\nu_{1(\text{H}_2\text{O})}$  stretching mode to higher wavenumbers (from 3182 to 3245  $\text{cm}^{-1}$ ), the incorporation of Ni has the opposite effect (decrease to 3057  $\text{cm}^{-1}$ ). Contents of Mn and Co have a minor impact on the spectral position of the  $\text{H}_2\text{O}$ -related absorption features.

The relation between the spectra and sample composition are important for the evaluation of orbiter and rover data from past and upcoming missions to Mars and elsewhere. A  $\nu_{1(\text{H}_2\text{O})}$  symmetric stretching band above 3182  $\text{cm}^{-1}$  indicates increased Fe contents, as relevant to Mars; conversely, its position at lower values indicates Ni contents, probable on the Galilean icy satellites. Mn and Co contents may be estimated from the position of the sulfate-related Raman bands.

The temperature during measurement has to be taken into consideration. While the sulfate-related bands are nearly unaffected by temperature variations, the  $\text{H}_2\text{O}$  stretching bands shift to lower wavenumbers upon cooling, thus complicating the interpretation of spectra acquired during space missions. Yet, even without exact knowledge of the temperature, at least semi-quantitative interpretations can be drawn regarding the composition of the kieserite at hand.

### References

- [1] Roach, L.H., et al. (2010) *Icarus* 206, 253–268.
- [2] Lichtenberg, K.A., et al. (2010) *J. Geophys. Res.* 115, E00D17.
- [3] Noel, A., et al. (2015) *Icarus* 251, 315–331.
- [4] Kargel, J.S. (1991) *Icarus* 94, 368–390.
- [5] McCord, T.B., et al. (2001) *Science* 292, 1523–1525.

## Laser-induced breakdown spectroscopy (LIBS) as a tool for Li distribution in zoned tourmaline in thin section

**Gioacchino Tempsta** (presenting author)

Dipartimento di Scienze della Terra e Geoambientali, Università degli Studi di Bari Aldo Moro, Bari, Italy

Co-author(s): Giovanna Agrosi<sup>1</sup>, Ferdinando Bosi<sup>2</sup>

<sup>1</sup>Dipartimento di Scienze della Terra e Geoambientali, Università degli Studi di Bari Aldo Moro, Bari, Italy

<sup>2</sup>Dipartimento di Scienze della Terra, Sapienza Università di Roma, Rome, Italy

Laser-induced breakdown spectroscopy (LIBS) represents a suitable method for qualitative and semi-quantitative analysis of light elements ( $Z < 10$ ), including Li. This method provides very rapid analysis with little sample damage, does not require any sample preparation and is relatively inexpensive. Compared with other techniques, the LIBS offers a direct experimental determination of Li, with a very low detection limit: up to 5 ppm [1]. Moreover, the use of microscope allows to probe a slightly poorer spatial resolution (6 to 8  $\mu\text{m}$ ) that make LIBS suitable for Li analysis in zoned crystals. In this study, we performed LIBS analyses directly on thin sections of color zoned tourmalines from different pegmatitic dikes of Elba Island (Italy). The tourmaline supergroup minerals show a complex chemical composition, characterized by light elements difficult to measure at micrometric scale with conventional methods. In particular, the detection and quantification of Li in elbaite tourmalines represents important steps in relating the Li variation to crystal-chemical evolution of system. In our work, we found a speedy method to quantify Li with LIBS analyses. Lithium was previously detected and measured in several solids and minerals [1-4]. We obtained quantitative data generating a linear regression using the main Li emission line intensity (670.706 nm corresponding to resonance transition  $1s^2 2s > 1s^2 2p$ ) particularly sensitive to Li amounts [1]. The linear fit was made using spectra recorded on three standard-tourmalines from Brazil, Canada and Switzerland characterized by a known  $\text{Li}_2\text{O}$  contents ranging from 0.02% to 1.31% [5-7]. The validity and the goodness of linear fit were confirmed by  $\text{Li}_2\text{O}$ -measuring on two samples of tourmaline (tsilaisite and elbaite) with a known chemical composition [8].

### References

- [1] Fabre, C., et al. (2002) *Geochimica et Cosmochimica Acta* 66, 8, 1401–1407.
- [2] McMillan, N.J., et al. (2006) *Anal. Bioanal. Chem.* 385, 263–27.
- [3] Sweetapple, M. T., Tassios, S. (2015) *Am. Mineral.* 100, 2141–2151.
- [4] Mcmillan, N.J., et al. (2018) *Can. Mineral.* 56, 393–410.
- [5] Grew, E.S., et al. (2018) *Eur. J. Mineral.* 30, 205–218.
- [6] Bosi, F., et al. (2019) *Physics and Chemistry of Minerals* 46, 371–383.
- [7] Filip, J., et al. (2012) *Geochim. Cosmochim. Acta* 86, 239–256.
- [8] Bosi, F., et al. (2012) *Am. Mineral.* 97, 5-6, 989–994.

## Evolution of borate minerals (ludwigite group and szaibélyite): from contact metamorphic to hydrothermal stages (Vysoká – Zlatno skarn, Slovakia)

**Pavel Uher** (presenting author)

Comenius University, Bratislava, Slovakia

Co-author(s): Peter Bačík<sup>1</sup>, Vladimír Bilohuštin<sup>1</sup>, Peter Koděra<sup>2</sup>, Stanislava Milovská<sup>3</sup>, Tomáš Mikuš<sup>3</sup>

<sup>1</sup>Dept. of Mineralogy and Petrology, Comenius University, Ilkovičova 6, 842 15 Bratislava, Slovakia

<sup>2</sup>Dept. of Mineral Deposits, Comenius University, Ilkovičova 6, 842 15 Bratislava, Slovakia

<sup>3</sup>Earth Sci. Inst., Slovak Acad. Sci., Dumbierska 1, 975 01 Banská Bystrica, Slovakia

Borate minerals of the ludwigite group (LGM) and szaibélyite [MgBO<sub>2</sub>(OH)] in association with hydroxylclinohumite, clinochlore, serpentine, magnetite, spinel, carbonate and sulphide minerals, occur in a magnesian exoskarn in the R-20 borehole, located in the Vysoká – Zlatno Cu-Au porphyry-skarn deposit, central Slovakia. The skarn is developed along the contact of Miocene (~13 Ma) granodiorite to quartz-diorite porphyry and a Triassic dolomite-shale-psammitic-anhydrite sedimentary sequence. The minerals were investigated by electron probe micro-analyser (EPMA) and micro-Raman techniques.

The skarn minerals originated during two stages. (1) An early high-temperature, contact-metamorphic and metasomatic stage comprises coarse-crystalline massive black aggregates (>5 cm across) of LGM (types 1 to 3). In BSE images, LGM acicular crystals (£3 mm long) show regular concentric, rarely oscillatory or irregular zoning caused by distinct compositional variations during their growth or partial alteration. The variations of LGM show a crystallization sequence from early azoproteite with £17 wt% TiO<sub>2</sub> [~0.40 apfu Ti; £79 mol% of the Mg<sub>2</sub>(Mg<sub>0.5</sub>Ti<sub>0.5</sub>)O<sub>2</sub>(BO<sub>3</sub>) end-member], Ti-Al-rich members of LGM, “aluminoludwigite” [£14 wt% Al<sub>2</sub>O<sub>3</sub>; £0.53 apfu Al and £53 mol% of Mg<sub>2</sub>AlO<sub>2</sub>(BO<sub>3</sub>)], Al-rich ludwigite [Mg<sub>2</sub>Fe<sup>3+</sup>O<sub>2</sub>(BO<sub>3</sub>)] to Ti-Al-poor ludwigite in outer parts of crystals. The contents of other constituents in LGM attain elevated concentrations in some cases: 2.5–3.2 wt% SnO<sub>2</sub> (£0.04 apfu Sn), 0.4–1.0 wt% ZrO<sub>2</sub> (£0.02 apfu Zr), and £0.5 wt% V<sub>2</sub>O<sub>3</sub> (£0.01 apfu V) in Ti-Al-rich LGM compositions of type 1. The LGM compositional variations indicate the following main substitution mechanisms: Fe<sup>2+</sup> = Mg<sup>2+</sup> in M1-3 sites for all compositions, Mg<sup>2+</sup> + Ti<sup>4+</sup> (Sn<sup>4+</sup>, Zr<sup>4+</sup>) = 2(Fe<sup>3+</sup>, Al) in M4 site mainly for analyses including high Ti contents (type 1), and Al<sup>3+</sup> (V<sup>3+</sup>) = Fe<sup>3+</sup> in M4 site for compositions with a small amount of Ti but moderate to high Al contents (types 2 and 3).

(2) The late retrograde serpentinization and hydrothermal stage of the skarn form irregular veinlets and aggregates, including replacement of LGM by szaibélyite, formation of the latest generation of Fe-rich, Ti-Al poor ludwigite (type 4), and precipitation of dolomite, magnesite and sulphide minerals (valleriite, sphalerite, chalcopyrite).

Conditions for the precipitation of borates and associated minerals could be estimated at ~600–700 °C and 50–70 MPa (stage 1), and ~320–370 °C (stage 2).

The work was supported by the Slovak Research and Development Agency under the projects APVV-18-0065 and APVV-15-0050.

## Enigma of the cuboid diamonds: inverse distribution of optical centres within the crystal volume

**Evgeny Vasilev** (presenting author)

Saint-Petersburg Mining University, Russia

Co-author(s): Dmitry Zedgenizov

Sobolev Institute of Geology and Mineralogy, Novosibirsk, Russia

Studies the distribution of structural defects in the bulk of the diamond crystals allow researchers to resolve a wide range of problems. Some of them are: revealing of regularities of defects transformation, reconstructing of processes occurring in/with the crystals, and determining of growth conditions and the post-growth history. The internal defects, impurities, impurity-vacancy complexes in the diamond have different temperature ranges of stability. Single interstitial nitrogen atom N<sub>s</sub> is the simplest low-temperature nitrogen defect. They cause yellow coloration. During annealing N<sub>s</sub> turn into defects N<sub>3</sub>V; yellow color disappears. After further annealing or at a higher temperature, defects N<sub>3</sub>V and N<sub>4</sub>V appears. Defects N<sub>3</sub>V cause a blue luminescence.

In some diamond cuboids, the “inverse” distribution of defects is observed: low-temperature N<sub>s</sub> are noted in the crystal core, while N<sub>3</sub>V on the periphery of the crystals [1]. Such a distribution one can interpret as evidence of the possibility of the growth nature of N<sub>s</sub> defects [2]. However, there is an alternative explanation for the “inverse” distribution. In the central part of the cuboids, the yellow zone with a yellow luminescence (PL) is observed (Figure 1). The blue PL of N<sub>3</sub>V defects was noted in the colorless peripheral part of the crystals. A wide structured PL band with a maximum of 700 nm, a doublet of 883/885 nm and lines at 799.5, 819.6, 869.5, 930 of different intensities were recorded in the yellow core of the crystals. This PL is due to Ni-containing defects [3]. It was previously shown [3] that Ni atoms stabilize N<sub>s</sub> by compensating the charge and reduces their diffusion mobility. Apparently, in the studied crystals, the “inverse” distribution is a consequence of the stabilization of N<sub>s</sub> defects by Ni atoms, but not of the growth nature of N<sub>s</sub> defects.

The distribution of N<sub>3</sub>V within the crystal's volume does not correspond to the distribution of N<sub>s</sub> or Ni-related luminescence and therefore has a different nature. An inverse relationship is observed between the PL intensity of N<sub>3</sub>V centers and the absorbance of hydrogen-containing N<sub>3</sub>VH centers at 3107 cm<sup>-1</sup>. Earlier, we observed a similar distribution in a crystal with a high concentration of N<sub>4</sub>V centers [4]. We interpret this distribution as a consequence of the capture of the hydrogen atoms by the N<sub>3</sub>V centers and their conversion into the N<sub>3</sub>VH form that is inactive in PL but active in IR absorption. Thus, studying of the distribution of defects within the diamonds allows one to obtain new regularities of their transformation and to identify their nature. The origin for the change of Ni concentration during the cuboids growth is the aim of further researches.

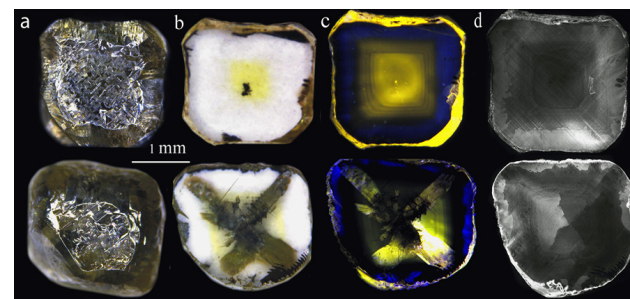


**Figure 1.** Studied cuboids: general view (a); polished plates: (b) transmitted light; (c) luminescence at 405 nm excitation after 450 nm edge filter; (d) cathodoluminescence

### References

- [1] Zedgenizov, D.A., et al. (2016) *Lithos* 265,125.
- [2] Palyanov, Y.N., et al. (1997) *Russian Geology and Geophysics* 38, 920.
- [3] Yelisseyev, A.P., Kanda H. (2007) *New Diam. Front. Carbon Technol.* 3, 127.
- [4] Vasilev, E.A., et al. (2019) *Min. Mag.* 3, 1.

## Platinum-group minerals, from natural to synthetic

Anna Vymazalová (presenting author)

Czech Geological Survey, Geologická 6, 152 00 Prague 5, Czech Republic

Co-author(s): František Laufek

Czech Geological Survey, Geologická 6, 152 00 Prague 5, Czech Republic

The Platinum-group elements (PGE) are of significant technological importance. The PGE are used primarily in industrial applications and have become widely established in chemical, electrical, and electronic engineering. About 50 % of world production of Pt and Pd is used in automobile industry (catalysts). The PGE exhibit various interesting physical, chemical and structural properties that place these compounds at the interface of chemistry, mineralogy, solid-state physics and material science. Therefore, there is still a demand for exploration and mining and to advance the understanding of the natural process that lead to their formation.

Up to date, there are 141 known Platinum-group minerals (PGM), approved by the Commission on New Minerals, Nomenclature and Classification (CNMNC) of the International Mineralogical Association (IMA). PGM (109) recognized by 2002 are summarized in [1], additional 23 PGM described since 2002 up to 2017 are listed in [2] and since 2017 up to now, according to our best knowledge, another 9 PGM were approved by the CNMNC. Among known 141 PGM there are: 71 Pd-dominant, 33 Pt-dominant, 13 Ir-dominant, 14 Rh-dominant, 6 Ru-dominant and 4 Os-dominant. The type localities are geographically located world-wide: 50 – Russia; 16 – JAR; 15 – China; 13 – Canada; 11 – USA; 7 – Brazil; 5 – D.R. Congo; 4 – Colombia; 3 – Finland, 2 – in Ethiopia, Indonesia, Papua New Guinea, and Greenland; 1 – has a type locality in Argentina, Bulgaria, Czech Republic, Dominican Republic, Germany, France (Guyana), Japan, Serbia, UK.

There is still a significant number of PGM that require re-examination, re-definition or additional data for better characterization, in particular, in terms of correct chemical formula, extent of solid solution, thermal stability and the crystal structure. The main reason for the lack of insufficient identification of PGM is their mode of occurrence (as minute inclusions), intergrowths with other PGM, often embedded in base-metal sulphides and in most cases of very rare occurrence. Therefore, in some cases further studies of synthetic analogues including crystal structure determination of PGM are desirable, ideally with natural minerals being investigated at the same time. Among recently described PGM the synthetic analogues were used in the description of the following mineral species: milotaite, pašavaite, jacutingaite, zaccariniite, kitagohaite, lukkulaisvaaraita, kojonenite, palladosilicide, norilskite, kravtsovite, vymazalováite, mitrofanovite, thalhammerite, nipalarside and orthocuproplatinum.

The Grant Agency of the Czech Republic (project No. 18-15390S) is greatly acknowledged.

### References

[1] Cabri, L.J. (2002) CIM Special 54, 177–210.

[2] Vymazalová, A., et al. (2017) Experimental Aspects of Platinum-Group Minerals, Elsevier, Amsterdam, 303–345.

## Multi-element Analysis of Sapphires and Emeralds by LA-ICP-Time-Of-Flight-MS for Country of Origin Determination

Hao A.O. Wang (presenting author)

Swiss Gemmological Institute SSEF, Basel, Switzerland

Co-author(s): Michael S. Krzemnicki, Susanne Büche, Ramon Schmid, Judith Braun

Swiss Gemmological Institute SSEF, Basel, Switzerland

Major, minor and trace element analysis of gemstones provides gem testing laboratories very important information, especially for country of origin determination of coloured gemstones [1]. Such information assists gemmologists to deliver scientifically based opinions as requested by the trade due to market value factors attributed to certain origins (e.g. sapphires from Kashmir), as well as the growing demand for traceability of gems due to political and ethical reasons.

One of the advanced testing methods, LA-ICP-MS, conventionally quantifies elemental composition based on a list of selected isotopes pre-defined before analysis. A drawback of this approach is, however, that the list of isotopes cannot be modified after analysis. Hence, a priori knowledge about multi-element content of the sample must be presumed. Making such assumption is often challenging in case of, for example, rarely occurring elements in gemstones, or trace element composition in solid or fluid inclusions. Moreover, the isotope of selection for a specific element cannot be changed in the post-data processing when unforeseen mass interferences are encountered after the measurement is done and the sample has left the lab. In this presentation, we apply LA-ICP-Time-Of-Flight-MS, a simultaneous multi-element quantification technique, and introduce the novel acquisition scheme of FIRST measure, THEN determine which isotopes are of interest. We would like to demonstrate how this paradigm-shift is useful for trace element analysis on gemstones and minerals.

In a real case study of blue sapphire analysis using LA-ICP-TOF-MS, rarely occurring trace elements such as Be, Zr, Nb, Hf, Th, etc. have been observed more frequently in Madagascar sapphires than Kashmir ones. In a recently tested sapphire, radioactive <sup>232</sup>Th was detected. Thanks to the full mass spectrum acquisition by LA-ICP-TOF-MS, without re-ablation, all of the Pb isotopes (<sup>204</sup>Pb, <sup>206</sup>Pb, <sup>207</sup>Pb, <sup>208</sup>Pb) were collected simultaneously, and indicated no common Pb contamination. Finally, the formation age of this sapphire was estimated to be around 500Ma, within the reference age of Madagascar sapphires (formed during the Pan-African orogeny) and is supporting the country of origin opinion – Madagascar – deduced by gemmologists using other gem testing techniques.

In a second case study of emerald, a dataset of 20 elemental concentrations (20 dimensions) in more than 700 analyses are projected onto a two-dimensional space using statistical dimension reduction. In this example, we demonstrate that non-linear machine learning algorithm (t-SNE, [2]) achieves a better separation of country of origin comparing to linear Principle Component Analysis (PCA), as shown in Figure 1. Both algorithms are unsupervised, meaning samples are grouped solely on their concentrations and without prior information about their origins. The present study reveals the potential of multi-element data combined with statistical evaluation to separate gemstones from different origins. It also provides a novel tool to distinguish various geological settings by visualizing multi-element similarities.

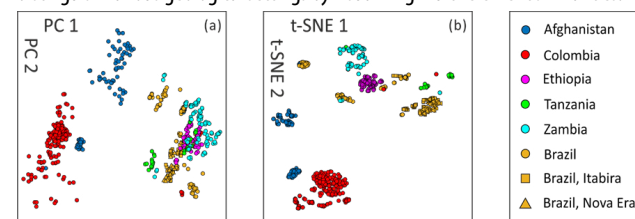


**Figure 1.** Visualization of multi-element (high dimensional) data in emeralds using a) linear PCA; and b) non-linear t-SNE, reduced from 20 element concentrations. Country of origin information (colour of scatter dots) is given after dimension reduction.

### References

[1] Wang, H.A.O., et al. (2016) J. Gemm. 35, 212–223.

[2] Van Der Maaten, L.J.P., Hinton, G.E. (2008) J. Mach. Learn. Res. 9, 2579–2605.

## Thermally induced structural, chemical and textural rearrangement of metamictized zircon with high concentration of impurity elements: Raman, PL, EPMA, EBSD

**Dmitry A. Zamyatin** (presenting author)

Zavaritsky Institute of Geology and Geochemistry UB RAS, 15 Vonsovskogo st., Ekaterinburg, 620016 Russia

Co-author(s): Sergey L. Votyakov, Yuiya V. Shchapova

Zavaritsky Institute of Geology and Geochemistry UB RAS, 15 Vonsovskogo st., Ekaterinburg, 620016 Russia

Petrogenetic and geochronological issues require study the mechanisms of the redistribution of impurity elements at elevated temperatures in the important geochronometer zircon. This paper is devoted to the study of the influence of lab annealing ( $T = 1400^{\circ}\text{C}$ , 96 h) on the internal texture, structural state, chemical composition, luminescent and vibrational properties of zircon K1098 from metamorphic rocks of the Taldyk block Mugodzhyr Hills (South Urals, Kazakhstan) [1].

Zircon grains consist of crystalline bulks and metamictized cores (Figure 1a,c,d,f). Cores yield very low BSE and CL intensities and significant content of Y, Yb, heavy REE, Hf, U, non-formula elements Fe, Ca, Al, water, F (electron microprobe Cameca SX100), which are signs of alterations of the zircon under the influence of aqueous fluid [2]. The degree of metamictization of not annealed zircon varies from mildly (in bulks) to strongly (in cores) damage according to Raman spectroscopy (Horiba LabRam HR800 Evolution spectrometer). Raman parameters plot off the progressive damage-accumulation trend (Figure 1g, pink). The band width  $\nu_3(\text{SiO}_4)$  in the not annealed zircon takes a value from 5 to 35  $\text{cm}^{-1}$ .

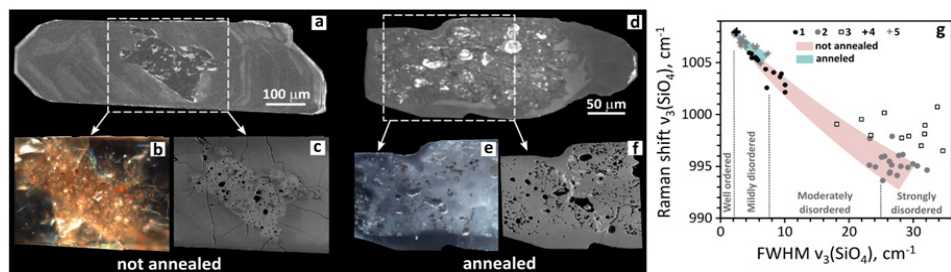


**Figure 1.** BSE (c, f), CL (a, d) and optic (b, e) images of not annealed (a–c) and annealed (d–f) zircons; g—Raman shift vs full width at half maximum of  $\nu_3(\text{SiO}_4)$  band in bulks (1, 4) and cores (2, 3, 5) of not annealed (1, 2, 3) and annealed (4, 5) zircon.

Thermal annealing significantly affects the properties of zircon: the color of the cores changes from brown to dull white (Figure 1b,e), cores retain many mineral inclusions, the CL brightness increases, the bands in the Raman and photoluminescence spectra narrow and vary in width and position (Figure 1g, green). The band width  $\nu_3(\text{SiO}_4)$  in the annealed zircon takes a value from 2 to 8  $\text{cm}^{-1}$ , which corresponds to mildly damaged state. In the annealed zircon, regions with high O content and pores are preserved, zones with extremely high concentrations of REE (Dy–Lu up to 3 and Y up to 9 wt.%) and BSE intensities appear. The observed broadening of vibrational and luminescent bands should be due to chemical disordering of the zircon matrix due to the high content of heterovalent impurities. According to EBSD (Jeol JSM-6390LV electron microscope with the NordlysNano attachment) in areas with a high BSE intensity, in addition to zircon saturated with impurities, a submicron-sized a non-typical zircon phase with a monoclinic structure is observed.

The work was carried out at the Common Use Center “Geoanalyst” with the financial support by the Russian Science Foundation (grant No.16-17-10283).

### References

- [1] Votyakov, S.L., et al. (2014) Dokl. Earth. Sci. 457, 3, 882–886.
- [2] Geisler, T., et al. (2007) Elements 3, 1, 43–50.

## Low-temperature sulphate mineralization of modern hydrothermal systems of Kamchatka, Russia

**Elena Zhitova** (presenting author)

Institute of Volcanology and Seismology, RAS, Russia  
 St. Petersburg State University, Russia

Co-author(s): Rezeda M. Ismagilova<sup>1</sup>, Vladimir V. Shilovskikh<sup>1</sup>, Anton A. Nuzhdaev<sup>2</sup>

<sup>1</sup>Institute of Volcanology and Seismology, RAS, Russia

<sup>2</sup>St. Petersburg State University, Russia

The surface of the geothermal fields of Southern Kamchatka is usually covered by efflorescences that originate in the conditions of elevated temperature up to  $\sim 100^{\circ}\text{C}$  and acid leaching of primary rocks with the release of elements for the subsequent formation of various exhalative minerals. This assemblage is represented mostly by water-soluble minerals, usually hydrated sulfates. Many of these hydrated sulphates have been identified on the Martian surface and allegedly indicate the presence of hydrothermal activity in the Mars history. These findings triggered recent crystal chemical studies of such hydrated sulphates at varying conditions using different analytical methods.

In the course of our study we have studied low-temperature mineralization of geothermal fields associated with Koshelevsky, Kambalny and Mutnovsky volcanos (Southern Kamchatka, Russia). The efflorescence samples have been studied using scanning electron microscopy and powder X-ray diffraction. The interesting peculiarity of low-temperature surface mineralization is widespread abundance of ammonium minerals. Among identified minerals are tschermigite, aluminopyracmonite, boussingaultite, clairite, mascagnite, koktaite, mohrite, buddingtonite, ammoniovoltaite and presumably ammoniojarosite and ammonioalunite. It is worth noting that ammoniovoltaite has been initially found at Kamchatka geothermal fields [1], whereas the majority of the rest of ammonium minerals have been first identified in Russia. It is also of interest that many ammonium minerals have been originally described in burning coal dumps and therefore their presence in nature have been doubted, for example, for koktaite, boussingaultite, mascagnite, mohrite and tschermigite [2]. The finding of these minerals at geothermal fields confirms their existence in natural environments.

This work has been supported by the President of Russian Federation Grant for Young Candidates of Sciences grant MK-3246.2019.5.

### References

- [1] Zhitova, E.S., et al. (2018) Miner. Mag. 82, 1057–1077.
- [2] Hazen, R.M., et al. (2017) Amer. Miner. 102, 595–611.

## Crystal chemical characterization of carbonate and chloride layered double hydroxides

**Elena Zhitova** (presenting author)

*Institute of Volcanology and Seismology, St. Petersburg State University, Russia*

Co-author(s): Chris Greenwell<sup>1</sup>, Sergey V. Krivovichev<sup>1,2</sup>, Igor V. Pekov<sup>3</sup>

<sup>1</sup>St. Petersburg State University, Russia

<sup>2</sup>Durham University, Russia

<sup>3</sup>Moscow State University, Russia

Layered Double Hydroxides (LDHs) are important technologically applied materials with general formula  $[M^{2+}_{1-x}M^{3+}_x(OH)_2]^{q+}(X^{n-})_{q/n} \cdot yH_2O$ , where  $M^{2+}$  and  $M^{3+}$  - metal cations, X - anion. Most of them are synthesized in laboratory, although around 40 natural species commonly possessing much better crystallinity are known. Their crystal structure consists of brucite-type octahedral layers built by  $M^{2+}(OH)_6$  and  $M^{3+}(OH)_6$  octahedra and interlayer space accommodating anion and water molecules. Due to the high demand for layered double hydroxides, their fast and reliable characterization by various widely available methods becomes very topical.

In the course of present study we have undertaken crystal chemical characterization of carbonate and chloride LDHs with  $M^{2+}:M^{3+} = 3:1$  and  $2:1$ , namely hydrotalcite, quintinite, iowaite and chlormagaluminite at varying temperature. The structure study of these minerals has revealed that the interlayer arrangement of chloride and carbonate species is different from each other, i.e. can be considered as more ordered in the case of chloride. This structural peculiarity is reflected by Raman and infrared spectroscopy by bands that occur in the  $3700\text{--}3000\text{ cm}^{-1}$  and  $900\text{--}100\text{ cm}^{-1}$  regions. Moreover the arrangement of interlayer anion plays a key role in the high-temperature behavior of these minerals: carbonate LDHs experience collapse of interlayer space for  $\sim 1\text{ \AA}$  at  $\sim 200\text{ }^\circ\text{C}$ , whereas chloride LDHs does not experience significant structural reconstruction.

The study has been supported jointly by the Russian Foundation for Basic Research and the Royal Society of London, agreement 19-55-10005.

## Crystal structure of dmisteinbergite, $CaAl_2Si_2O_8$

**Andrey A. Zolotarev, jr** (presenting author)

*Department of Crystallography, Institute of Earth Sciences, Saint Petersburg State University, University Emb. 7/9, 199034 St. Petersburg, Russia*

Co-author(s): Sergey V. Krivovichev<sup>1,2</sup>, Taras L. Panikorovskii<sup>2</sup>, Vladislav V. Gurzhiy<sup>1</sup>, M. A. Rassomahin<sup>3,4</sup>

<sup>1</sup>Department of Crystallography, Institute of Earth Sciences, Saint Petersburg State University, University Emb. 7/9, 199034 St. Petersburg, Russia

<sup>2</sup>Kola Science Centre, Russian Academy of Sciences, Fersmana 14, 184209 Apatity, Russia

<sup>3</sup>Natural Scientific Museum of the Ilmen State Reserve, RAS, Miass 456317, Russia

<sup>4</sup>Federal Research Center, Kola Science Center, RAS, Fersmana Str. 14, Apatity 184209, Russia

Dmisteinbergite,  $CaAl_2Si_2O_8$ , or “hexagonal anorthite” was first described from the burned dumps of the Chelyabinsk coal basin [1], together with svyatoslavite, an orthorhombic anorthite polymorph [2]. Dmisteinbergite crystallized from the gas phase under extremely reducing conditions at temperatures close to  $1000\text{ }^\circ\text{C}$ . The transformation of  $CaAl_2Si_2O_8$  metastable phases (dmshteinbergite and svyatoslavite) to a stable anorthite at temperatures close to melting temperatures occurs within a few minutes; therefore, in nature „hexagonal anorthite“ can be found in places formed under exceptional conditions only [3–8]. To date, there is no accurate experimental data of crystal structure of the “natural” dmisteinbergite, which is the purpose of the current work. The crystal structure of dmisteinbergite is based upon double layers of 6-membered rings of  $AlO_4$  and  $SiO_4$  tetrahedra [9]. More detailed topological analysis of Si-Al frameworks of  $CaAl_2Si_2O_8$  polymorphs is given by Krivovichev et al. [2]. The currently used high-symmetry structural model for the synthetic hexagonal anorthite with the space group  $P6_3/mcm$  indicates disordered distribution of Si and Al in tetrahedral sites [9]. The single-crystal X-ray diffraction data obtained by us showed that the more correct space group for dmisteinbergite is  $P312$  ( $a = 5.1123(2)$ ,  $c = 14.7420(7)\text{ \AA}$ ,  $V = 333.67(2)\text{ \AA}^3$ ,  $R_1 = 0.044$ ) due to the partial ordering of tetrahedral positions. There are four independent tetrahedral sites: two of which (T2 and T4) are predominantly occupied by Al ( $\langle T2-O \rangle = 1.714$ ;  $\langle T4-O \rangle = 1.745\text{ \AA}$ ) and two by Si (T1 and T3:  $\langle T1-O \rangle = 1.668$ ;  $\langle T3-O \rangle = 1.612\text{ \AA}$ ). It is likely that there are different degrees of order in the hexagonal  $CaAl_2Si_2O_8$  phases that depends on the specific conditions of their formation. Moreover, Raman spectra of dmisteinbergite differ from one another slightly due to the variable degree of Al-Si order in different samples similarly to anorthite [10].

The study was supported by the Russian Foundation for Basic Research (No. 19-05-00628). The experiments were carried out using facilities of XRD and Geomodel Resource Centers of St. Petersburg University.

### References

- [1] Chesnokov, B.V., et al. (1990) ZVMO 119, 5, 43–46.
- [2] Krivovichev, S.V., et al. (2012) Can. Mineral. 50, 585–592.
- [3] Simakin, A.G., et al. (2010) ZRMO 139, 3, 102–108.
- [4] Ma, C., et al. (2013) Am. Mineral. 98, 368–1371.
- [5] Fintor, K., et al (2013) Lunar and Planetary Science 44, 1152–1152.
- [6] Fintor, K., et al (2014) Meteoritics & Planetary Science 49, 5, 812–823.
- [7] Nestola, F., et al (2010) Am. Mineral. 95, 405–409.
- [8] Pierro, S.D., Gnos, E. (2016) Am. Mineral. 101, 71–81.
- [9] Takéuchi Y., Donnay G. (1959) Acta Cryst. 12, 465–470.
- [10] Freeman, J.J. (2008) Can. Mineral. 46, 1477–1500.

# POSTER PRESENTATIONS



## Diamond-magnesiochromite host-inclusion system recording old deep lithosphere conditions at Udachnaya (Siberia)

**Giovanni B. Andreozzi** (presenting author)

Dipartimento di Scienze della Terra, Sapienza University of Rome (Italy)

Co-author(s): Fabrizio Nestola<sup>1</sup>, Paolo Nimis<sup>1</sup>, Benedetta Perotto<sup>1</sup>, Luciano Secco<sup>1</sup>, Leonardo Pasqualetto<sup>1</sup>, Gabriele Zaffiro<sup>2</sup>, Mattia L. Mazzucchelli<sup>2</sup>, Francesco Princivalle<sup>3</sup>, Davide Lenaz<sup>3</sup>, Alla M. Logvinova<sup>4</sup>, Alessandra Lorenzetti<sup>5</sup>, Jeffrey W. Harris<sup>6</sup>

<sup>1</sup>Dipartimento di Geoscienze, Università degli Studi di Padova, Italy

<sup>2</sup>Dipartimento di Scienze della Terra e dell'Ambiente, Università degli Studi di Pavia, Italy

<sup>3</sup>Dipartimento di Matematica e Geoscienze, Università degli Studi di Trieste, Italy

<sup>4</sup>Nikolay V. Sobolev Institute of Mineralogy and Petrography, Russian Academy of Sciences Siberian Branch, Novosibirsk, Russia

<sup>5</sup>Dipartimento di Ingegneria Industriale, Università degli Studi di Padova, Italy

<sup>6</sup>School of Geographical and Earth Sciences, University of Glasgow, UK

Lithospheric diamonds (formed between 130 and 200 km) represent 99% of all mined diamonds. These diamonds may contain mineral inclusions, which can be used to derive inferences on the physical-chemical environments in which their host diamonds were formed. Magnesiochromite (mchr) is one of the most common of these inclusions, representing about 19% of reported inclusions in lithospheric diamonds worldwide. To determine the formation conditions of a mchr-bearing diamond from the Paleozoic Udachnaya kimberlite (Siberia), we adopted an original method based on elastic geobarometry.

When a mineral is trapped in a host at conditions  $P_{\text{trap}}$  and  $T_{\text{trap}}$  and then is exhumed to the Earth's surface, it may develop residual strains as a result of the contrast in elastic properties between the host and the inclusion. If  $T_{\text{trap}}$  is known independently and the residual strains are measured when the host is at room pressure,  $P_{\text{trap}}$  can be back-calculated as the condition at which mechanical equilibrium between the host and the inclusion is elastically restored.

To retrieve  $T_{\text{trap}}$ , we acquired FTIR spectra of the diamond host from Udachnaya. The software DiaMap [1] was used to deconvolute the spectrum in the 1001 to 1350  $\text{cm}^{-1}$  range and fit the individual nitrogen absorption bands. An average N content of 267 ppm and the concentration of A (pairs of N impurities) and B (clusters of four N impurities aggregated about a vacancy) defects were obtained, so that the diamond was classified as type-IaB. The N-aggregation state allowed to estimate a mantle residence  $T$  (assumed to be the same as  $T_{\text{trap}}$ ) of 1125–1140 °C for a diamond age of 3.5–2.0 Ga, typical for Udachnaya diamonds.

The residual pressure was retrieved by studying the mchr inclusion by single-crystal X-ray diffraction. Comparing its unit-cell volumes measured before and after its release from the host diamond, the obtained  $P_{\text{inc}}$  was 1.073(72) GPa.

Using the obtained  $T_{\text{trap}}$  and  $P_{\text{inc}}$ , an appropriate P-V-T Equation of State for mchr and diamond, and an elastic model, we disclosed the following entrapment conditions:  $P_{\text{trap}} = 6.5(2)$  GPa and  $T_{\text{trap}} = 1125(32)$ – $1140(33)$  °C. These conditions fall on a ~35 mW/m<sup>2</sup> geotherm, which is colder than most mantle xenoliths from the same depths, suggesting that cold cratonic conditions persisted for billions of years to at least 200 km in the local lithosphere.



**Figure 1.** Magnesiochromite single crystal included in lithospheric diamond

Given the relatively common occurrence of mchr inclusions in diamonds, this method can potentially be applied to a large number of diamonds from worldwide localities. This would in turn allow better insight into the depth distribution of lithospheric diamonds at global scale and, consequently, into the processes that control diamond formation in the Earth's mantle.

### References

[1] Howell, D., et al. (2012) Contrib. Mineral. Petr. 164, 1011–1025.

## Raman spectra of natural manganese oxides

**Simone Bernardini** (presenting author)

Department of Science, Roma Tre University, Via della Vasca Navale 84, 00146 Rome, Italy

Co-author(s): Fabio Bellatreccia, Annalaura Casanova Municchia, Giancarlo Della Ventura, Armida Sodo

Department of Science, Roma Tre University, Via della Vasca Navale 84, 00146 Rome, Italy

Manganese oxides/hydroxides (MnOx) are very important geomaterials, having a structure based on the linkage of the MnO<sub>6</sub> octahedra to form layers and tunnels able to accommodate large cations and water molecules [1]. They are widespread all over the world, their formation being strongly controlled by mineralizing fluid conditions (e.g. pH, Eh, ionic strength) as well as by microbial activity. As a consequence, each environment has its own typical MnOx paragenesis. Their wide occurrence (over time and space) allows their use as environmental indicators, as it is the case, for example, of marine nodules and crusts constituting a very powerful geological record. Moreover, MnOx are important phases controlling the partition of arsenic and heavy metals between solid materials and aqueous systems [2]. Recently they are attracting attention as nanostructured materials with very intriguing physicochemical properties (e.g. cathode materials in lithium and alkaline batteries) [3].

MnOx commonly occur as cryptocrystalline and fine-grained mixtures of different Mn-phases and additional minerals such as carbonates, silicates and Fe oxides/hydroxides. These features make their identification and proper characterization a challenge by standard X-ray diffraction methods because of their poor crystallinity. Typically, MnOx X-ray patterns are characterized by broad and weak Bragg reflections, which can be easily overlapped by the stronger reflections of other more crystalline phases in the sample.

FT-IR spectroscopy could be a very powerful technique to characterize MnOx minerals [4]. In fact, FT-IR spectroscopy yields reliable information on disordered and/or poor crystalline materials as Mn oxides typically are. However, FT-IR spectra usually show broad and overlapping absorption bands that do not always allow a simple and unique identification of the sample.

To overcome these difficulties, Raman spectroscopy has been shown to offer a valuable alternative tool for the investigation of these materials, being a fast and non-destructive method not requiring sample preparation. In literature, there are many incongruities regarding the Raman spectra of MnOx [5,6], due to their low Raman activity and the high sensitivity of manganese compounds to the laser heating, that may produce a significant degradation of the sample, as a function of the laser power and irradiation time [7].

The aim of this work is at providing reference Raman spectra of well-characterized MnOx, to be used for their proper characterization. With this purpose, a set of different MnOx (birnessite, chalcophanite, cryptomelane, groutellite, hausmannite, hollandite, lithiophorite, manganite, manganosite, pyrolusite, ramsdellite, romanechite and todorokite) were studied by Raman spectroscopy and the data were integrated with XRPD and FT-IR spectroscopy results.

Our work shows that some MnOx have characteristic Raman spectra, whereas integration of Raman data with other techniques is mandatory to characterize minerals that have almost identical Raman spectra<sup>[8]</sup>. With this respect, Raman spectroscopy is the only technique allowing an easy discrimination between hollandite [Ba(Mn<sup>4+</sup><sub>6</sub>Mn<sup>3+</sup><sub>2</sub>)O<sub>16</sub>] and cryptomelane [K(Mn<sup>4+</sup><sub>7</sub>Mn<sup>3+</sup>)O<sub>16</sub>].

In the case of samples consisting of finely intermixed Mn-phases, Raman mapping, because of its high spatial resolution, may also provide an efficient tool for their differentiation (Figure 1).

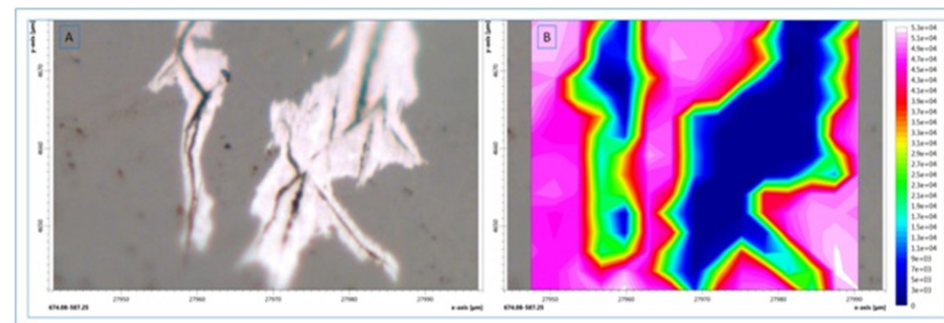


**Figure 1.** Spatial distribution of pyrolusite (blue) and manganite (pink) in the sample

### References

- [1] Post, J.E. (1999) Proc. Natl. Acad. Sci. U.S.A. 96, 3447.
- [2] Lafferty B.J., et al. (2011) Environ. Sci. Technol. 45, 9218.
- [3] Paik, Y., et al. (2001) Journal of the American Chemical Society 123, 7564.
- [4] Potter, R.M., Rossman, G.R. (1979) American Mineralogist 64, 1199.
- [5] Buciuman, F., et al. (1999) Physical Chemistry Chemical Physics 1, 185.
- [6] Julien, C., et al. (2004) Spectrochimica Acta 60, 689.
- [7] Bernard, M.C., et al. (1993) Journal of the Electrochemical Society 140, 11, 3065.
- [8] Bernardini, S., et al. (2019) Journal of Raman Spectroscopy 1–16.

## Accessory mineral assemblage in various types of Karkonosze granite (West Sudetes)

**Małgorzata Cegiełka** (presenting author)

University of Warsaw, Faculty of Geology, Institute of Geochemistry, Mineralogy and Petrology, Poland

Karkonosze pluton is one of the biggest Variscian magmatic bodies located in the West Sudetes. Currently there are six varieties of granitoids distinguished in the pluton: (i) the two-mica granite of Tanvald type, (ii) Fojtka granodiorite, (iii) porphyritic coarse- to medium-grained granite, which are subdivided into the Jizera and Liberec types in the Czech part [1], (iv) equigranular, medium-grained biotite granite (the Harrachov type; [1]), (v) fine-grained biotite granite often called the ridge [2] or Karkonosze granite [1], (vi) other mostly fine- to medium grained granitoids forming small bodies.

The main goal of this research is a detailed description of complex mineralogical assemblage comprising Karkonosze granite centered around types (ii), (iii) and (v). To obtain thorough characterization of mineral phases multiple analytical methods such as optical microscopy, scanning microscopy (SEM/EDS), electron microprobe analysis (EPMA) and X-ray diffraction (XRD), were used.

The samples were collected from 12 localities and there were multiple accessory mineral phases identified including zircon, monazite-(Ce), thorite, apatite, xenotime-(Y), allanite-(Ce), britholite-(Ce) and Nb-rich silicates. Such a variety gives us insight into conditions of crystallization and provides foundation for further research.

### References

- [1] Žák, J., Klomínský, J. (2007) *J. Volcanol. Geotherm. Res.* 164, 254–267.  
 [2] Borkowska, M. (1966) *Geol. Sudet.* 2, 7–119.

## Crystal chemistry of the rinkite-(Ce)-nacareniobsite-(Ce) series

**Fabrice Dal Bo** (presenting author)

Natural History Museum, University of Oslo, Norway

Co-author(s): Henrik Friis

Natural History Museum, University of Oslo, Norway

Following the nomenclature approved by the IMA's CNMNC, rinkite-(Ce) and nacareniobsite-(Ce) are included in the seidozerite supergroup which contains close to 50 minerals [1]. These sorosilicates are based on a central octahedral sheet (O sheet) and two adjacent heteropolyhedral sheets (H sheet) that combine to a layered HOH structure, thus forming the so called TS block (TS = Titanium Silicate). The O sheet is composed of 6- to 8-coordinated polyhedra connected by edge-sharing, while the H sheet consists of corner-sharing  $\text{Si}_2\text{O}_7$  groups and 5- to 7-coordinated polyhedra [1-3]. The seidozerite supergroup is divided based on the content of Ti (+ Nb + Zr +  $\text{Fe}^{3+}$  + Mg + Mn) in the TS block that varies between 1 and 4 atom per formula unit, thus giving the four groups: rinkite, bafertisite, lamprophyllite and murmanite groups. The rinkite group, formerly called rosenbuschite group [3], consists of 13 approved species. In addition to the TS block, the crystal structure of the rinkite-group minerals contains two peripheral (P) cation sites ( $A^p$ ). The general formula of the rinkite-group minerals is:  $A^p M^h M^o (Si_2O_7)(X_M^o)_2(X_A^o)_2$ ; where  $A^p = \text{Na, Ca+REE, Ca, Mn}$ ;  $M^h = \text{Ti, Zr, Y, Mn, Ca+REE, Ca+Y, Ca}$ ;  $M^o = \text{Ti, Zr, Nb, Fe, Mg, Mn, Ca, Na}$ ;  $X_M^o = \text{O, F, O+F, OH}$ ; and  $X_A^o = \text{F, H}_2\text{O}$ . Most studies into the crystal chemistry of the seidozerite supergroup have investigated a single of few specimens. From our fieldwork we have observed a range of habits and paragenesis of minerals that all traditionally have been identified as one species. This motivated us to investigate in details multiple samples of rinkite-(Ce) and nacareniobsite-(Ce) from different localities around the world, as well as the type material for both species. The results confirm the substitution  $\text{Ti}^{4+} \rightarrow \text{Nb}^{5+}$  and the charge balance mechanism  $\text{Ti}^{4+} + \text{Ca}^{2+} \rightarrow \text{Nb}^{5+} + \text{Na}^+$  occurring in the rinkite-nacareniobsite solid-solution [4-5]. We also note a higher content of REE in the Nb-rich species, i.e. nacareniobsite-(Ce) [6]. However, crystal structure refinements of some nacareniobsite-(Ce) samples show some discrepancy in the cationic occupancy of the  $M^o(2)$  site with a 8-fold coordination. The  $M^o(2)$  site is always reported as Na-dominant in the published structures of the rinkite-nacareniobsite series [4-5,7-8]. In the present work we report structural models in which Ca is dominant on the  $M^o(2)$  site, thus leading to a new hypothetical end-member with the formula  $(\text{Ca}_3\text{,REE})\text{Na}_2\text{CaNb}(\text{Si}_2\text{O}_7)_2(\text{O}_2)\text{F}_2$ . The substitution  $\text{F} \rightarrow \text{O}^{2-}$  is most probably occurring on the  $X_M^o$  site to compensate the excess of positive charges coming from the  $\text{Na}^+ \rightarrow \text{Ca}^{2+}$  substitution on the  $M^o(2)$  site. So far we have never observed Ca-dominant  $M^o(2)$  site in the crystal structure of Ti-dominant members of the rinkite-nacareniobsite series.

### References

- [1] Sokolova, E., Cámara, F. (2017) *Mineral. Mag.* 81, 1457–1484.  
 [2] Christiansen, C.C., et al. (1999) *N. Jb. Miner. Abh.* 175, 153–189.  
 [3] Christiansen, C.C., et al. (2003) *Can. Mineral.* 41, 1203–1224.  
 [4] Cámara, F., et al. (2011) *Mineral. Mag.* 75, 2755–2774.  
 [5] Sokolova, E., Hawthorne, F.C. (2008) *Can. Mineral.* 46, 1333–1342.  
 [6] Rønso, J.G., et al. (2014) *B. Geol. Soc. Denmark*, 62, 1–15.  
 [7] Galli, E., Alberti, A. (1971) *Acta Crystallogr.* B27, 1277–1284.  
 [8] Rastsvetaeva, R.K., et al. (1991) *Sov. Phys. Crystallogr.* 36, 349–351.

## An EPR study of silica radicals in lung tissues with evidence of silicosis

**Francesco Di Benedetto** (presenting author)

Department of Earth Sciences, University of Florence, Florence (Italy)

Co-author(s): Elena Belluso<sup>1,2,3</sup>, Silvana Capella<sup>1,2</sup>, Andrea Giaccherini<sup>4,5</sup>, Maurizio Romanelli<sup>4</sup>, Benedetta Ciuffi<sup>6</sup>, Giordano Montegrossi<sup>3</sup>, Alfonso Zoleo<sup>7</sup>, Fabio Capacci<sup>8</sup>

<sup>1</sup>Department of Earth Sciences, University of Torino, Torino, Italy

<sup>2</sup>Interdepartmental Centre for Studies on Asbestos and Other Toxic Particulates G. Scansetti, University of Torino, Torino, Italy

<sup>3</sup>Institute of Geosciences and Earth Resources, CNR, Unit of Torino, Torino, Italy

<sup>4</sup>Department of Earth Sciences, University of Florence, Florence, Italy

<sup>5</sup>Department of Industrial Engineering, University of Florence, Florence, Italy

<sup>6</sup>Department of Chemistry, University of Florence, Florence, Italy

<sup>7</sup>Department of Chemical Sciences, University of Padua, Padua, Italy

<sup>8</sup>Dipartimento di Prevenzione, PISLL, Health Agency of Tuscany (USL Toscana Centro), Florence, Italy

The study of inorganic radicals associated to the respirable crystalline silica (RCS) is relevant for the definition of the health issues (silicosis, lung cancer and self-immune diseases) related to occupational exposure contexts.

In this study, a continuous-wave (cw) and pulsed Electron Paramagnetic Resonance (EPR) investigation of human lung tissue samples of an individual diagnosed of silicosis has been carried out. This technique, in fact, is able to trace the presence of radicals and of selected paramagnetic metal ions. Both types of paramagnetic species were observed through the cw-EPR survey, but their spectra resulted heavily superimposed. Through the use of an opportune set of pulse sequence and temperature, we were able to discern the two species, attributing the metal ion contribution to Cu(II) and the radical to an inorganic species. From the time-domain patterns, Cu(II) is found to interact with nitrogen atoms, thus supporting its attribution to biological Cu. Preliminary considerations about the radical species suggest its similarity to the inorganic Si· radicals already described in the literature.

## Multi-analytical characterisation of a medieval red mosaic glass tessera of from the first facade of the Duomo of Florence

**Francesco Di Benedetto** (presenting author)

Department of Earth Sciences, University of Florence, Florence (Italy)

Co-author(s): Capozzoli Laura<sup>1</sup>, Suzuki Amelia<sup>2</sup>, Giaccherini Andrea<sup>3</sup>, Lepore Giovanni Orazio<sup>4</sup>, Montegrossi Giordano<sup>5</sup>, Lavacchi Alessandro<sup>1</sup>, Bracci Susanna<sup>6</sup>

<sup>1</sup>CNR-ICCOM, Sesto Fiorentino, Italy

<sup>2</sup>Dept. Earth Sciences, Università di Firenze, Florence, Italy

<sup>3</sup>DIEF, Università di Firenze, Florence, Italy

<sup>4</sup>CNR- IOM, c/o OGG ESRF, Grenoble, France

<sup>5</sup>CNR-IGG, Firenze, Italy

<sup>6</sup>CNR-ICVBC, Sesto Fiorentino, Italy

The cathedral in Florence was designed by Arnolfo di Cambio, famous architect and sculptor. The plans for the new cathedral, started in 1296, included the construction of the main façade which was begun but never completed. In 1587 the unfinished façade was completely dismantled with the purpose of building a new one.

A red opaque glass tessera belonging to medieval mosaics of the first façade, was investigated with the aim of providing more information on the glass manufacturing during the end of the Middle Age. The red/orange glass production has generated considerable interest due to the high complexity of the technical achievements and the multiple technological solutions used. The tessera was investigated by means of a multi-analytical approach, including micro-morphological and microchemical FEG-SEM investigations, and synchrotron radiation X-ray absorption and X-ray Fluorescence techniques.

Optical and scanning electron microscopy show that this red medieval tessera has a inhomogeneous microscopical structure due to the presence of some optically transparent stripes within the main red stripes in which a bimodal distribution (~30 and ~160 nm) of copper nanoparticles is responsible for the red colour. EDS raster microanalyses indicate that the tessera is a soda-lime-silica glass which has probably been produced with plant ash flux, with a particularly high MgO content (3.7 wt% MgO). Moreover, an anomalously high Fe-content (6 wt%) was observed. X-ray Absorption Spectroscopy (XAS) and mX-ray Fluorescence maps were performed to identify Fe and Cu speciation and distribution in the sample with the aim to verify if the formation of the copper nanoparticles is due to the reduction of copper oxides at the expenses of the oxidation of iron (II) species to iron (III) during the glass production process. The combined mXRF and XAS information reveal that the transparent and red stripes regions in the tessera exhibit different redox balance of the main species: Cu(I)/Cu<sup>0</sup> and Fe(II)/Fe(III). In the transparent stripes at least one half of the total Cu is present as Cu(I), and ~20% of the total Fe as Fe(II). In the red stripes Cu is almost completely reduced, and the Fe(II) content decreases to ~10%. Conversely, mXRF and XAS reveal a low concentration of MnO, homogeneously distributed throughout the whole sample, always present in its divalent state. A thermodynamic modelling of the chemical and redox evidences has been undertaken and a preliminary explanation will be provided.

## Chemical evolution of tourmaline in elbaite-subtype pegmatites of the Bohemian Massif

Tomáš Flégr (presenting author)

Department of Geological Sciences, Faculty of Science, Masaryk University, Kotlářská 2, 611 37, Brno, Czech Republic

Co-author(s): Jan Cempírek

Department of Geological Sciences, Faculty of Science, Masaryk University, Kotlářská 2, 611 37, Brno, Czech Republic

Tourmaline supergroup is regarded as a robust and versatile group of minerals, useful as an important tool to record the evolution of magmatic and metamorphic systems. In boron-rich granitic pegmatites, tourmaline is particularly useful as it frequently crystallizes in most zones and during most stages of pegmatite formation; thus it may reflect changes of melt and fluid chemical composition, and transition from magmatic to hydrothermal stage [1].

Elbaite subtype of rare-element granitic pegmatites was originally defined from the Moldanubian Zone of the Bohemian Massif [2]. Tourmaline is the dominant Li-bearing mineral; it is typically associated by (typically late-stage) borate minerals and B-bearing silicates, including hambergite, datolite, danburite, boromuscovite, tusionite also B-bearing polyolithionite [3]. Early tourmaline commonly belongs to the schorl-elbaite series with typical strong enrichment in Mn (and in some cases F), low vacancy and dominant Na. Schorl occurs in various forms in pegmatites border, wall and intermediate zones; however, elbaite is restricted to irregularly distributed pockets (from few mm to several dm in size) and late veinlets. Elbaite subtype pegmatites exhibits low activity of P, reduced F and high B, documented by presence of late-stage boron-rich minerals:

Recent data show that some elbaite subtype pegmatites can feature exceptional variability in chemical evolution of primary and secondary tourmalines, especially in composition of the late-stage, most fractionated generations. Tourmalines of the elbaite subtype pegmatite typically belongs to the alkali group [4], with minor importance of vacancy and rather scarce Ca, however some examples show exceptional enrichment in vacancy in primary and secondary tourmalines [5]. Influence of Ca is typical in latest stages of tourmaline formation (e. g. Řečice, Rudolfov, Dolní Rožínka), locally reaching composition of fluor-liddicoatite. Late hydrothermal tourmalines may also form in outer pegmatite zones, as recently documented by occurrence of Al – deficit, Fe<sup>3+</sup>, Ti – rich tourmaline replacing primary biotite. In the Řečice pegmatite, it shows composition close to bosite [6], in Dolní Rožínka it is Al-deficient schorl-dravite [7].

Besides the usual evolution of the primary tourmaline (from Mg-, Fe-, to Li,Al,Mn- and Li,Al-rich compositions), the elbaite-subtype pegmatites are therefore characterized by significant B(±F)-rich late-magmatic to hydrothermal stage.

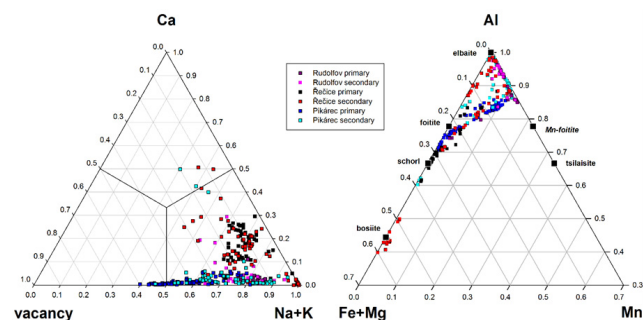


**Figure 1.** Evolution of tourmaline from selected elbaite-subtype pegmatites; a) X-site occupancy, b) Y+Z site occupancy.

### References

- [1] Jollif, et al. (1986) *Am. Mineral.* 71, 472–500.
- [2] Novák, Povondra (1995) *Mineral. Petrol.* 55, 159–176.
- [3] Novák, et al. (1999) *Eur. J. Mineral.* 11, 4, 669–678.

[4] Henry, et al. (2011) *Am. Mineral.* 96, 895–913.

[5] Flégr, et al. (2017) *Abstracts and Proceedings of the Geological Society of Norway*, 2, 29–33.

[6] Flégr, et al. (2017) *Tourmaline 2017 Book of Abstracts*, 35–38.

[7] Novotný, F., et al. (2019) *Bull. Mineral. Petrolog.* 27, 1, 38–45.

## Scientific Development and Digitization of the Gemological Collection from Abraham Gottlob Werner

Shijia Gao (presenting author)

Institute of Mineralogy, Freiberg University of Mining and Technology, Germany

Co-author(s): Gerhard Heide<sup>1</sup>, Andreas Massanek<sup>2</sup>

<sup>1</sup>Institute of Mineralogy, Freiberg University of Mining and Technology, Germany

<sup>2</sup>Geoscientific Collection, Freiberg University of Mining and Technology, Germany

Abraham Gottlob Werner was one of the most internationally famous personalities in the history of Freiberg University of Mining and Technology. He was the first scientist, who systematized geology to be a science subject, he provided an extremely important theoretical foundation for the modern nomenclature and classification of minerals, this was also crucial to the research and development of gemology [1–4].

In his unique geological collection, the most special is his gemological collection. The gemological collection was in Werner Museum from 1814 at today's Akademiestraße, now it's in its own prestigious rooms on the first floor of the new institute building at Brennhaugasse 14. According to the Taxation Protocol in 1814, this collection comprised 2,428 samples with a large part cut and some of them are with considerable quality. 1368 groups of samples for 22 kinds of minerals in this collection include diamond, zircon, garnet, chrysoberyl, peridot, spinel, corundum, topaz, beryl, tourmaline and another gemstones. But the gemological collection of Werner is not visible and available for general public.

Since Werner had written only a few of his samples labels and the gemstones were not signed in each piece, today it is no longer possible to determine which sample in the the systematic mineralogical collection comes from the Werner collection. Such work can probably never be considered completely. The collection is basically recorded in Access database (ca. 2005) and Zettelkartei (mid. 20<sup>th</sup> century), but the data are incomplete and some out of date. The documentation for the items is very heterogeneous and most of it is handwritten. The biggest challenge is the non-destructive analysis of the gemstones.

The concrete goal of this research achievement lies in the development and determination of the data, the digitization of the samples and documents, the updating of the gemstone and origin designations, the research to the history of samples, the literature to the samples, and the incorporation into the data base system AQUILA. The target audience is not only the specialist of gemology, mineralogy, geology and history, but also the general public.

During the work, the meta data, the physical properties and the chemical properties of selected samples were analyzed to update the samples according to the order of today's mineral name. After the collection of information and literature research with manuscript literature in the archive and library, the origin of samples are searched. Finally, the results are published in database.



**Figure 1.** Samples in the gemological collection of Abraham Gottlob Werner.

### References

- [1] Ospovat, A.M. (1980) *Ann. Sci.* 37, 433–440.
- [2] Ospovat, A.M. (1960) *Abraham Gottlob Werner and his Influence on Mineralogy and Geology*. The University of Oklahoma Press.
- [3] Seddon, G. (1973) *J. Geol. Soc. Aust.* 20, 381–395.
- [4] Eyles, V.A. (2015) *Hist. Sci.* 3, 102–115.

## A microXRF study of silicon and its behaviour in lung tissues with evidence of silicosis

**Andrea Giaccherini** (presenting author)

Department of Earth Sciences, University of Florence, Florence, Italy

Department of Industrial Engineering, University of Florence, Florence, Italy

Co-author(s): Francesco Di Benedetto<sup>1</sup>, Elena Belluso<sup>2,3,4</sup>, Silvana Capella<sup>2,3</sup>, Silvia Visona<sup>5</sup>, Matteo Moretti<sup>5</sup>, Antonio Osculati<sup>6</sup>, Antonella Buccianti<sup>1</sup>, Maurizio Romanelli<sup>1</sup>, Giordano Montegrossi<sup>1</sup>, Giulio Arcangeli<sup>6</sup>, Fabio Capacci<sup>7</sup>

<sup>1</sup>Department of Earth Sciences, University of Florence, Florence, Italy

<sup>2</sup>Department of Earth Sciences, University of Torino, Torino, Italy

<sup>3</sup>Interdepartmental Centre for Studies on Asbestos and Other Toxic Particulates G. Scansetti, University of Torino, Torino, Italy

<sup>4</sup>Institute of Geosciences and Earth Resources, CNR, Unit of Torino, Torino, Italy

<sup>5</sup>Department of Public Health, Experimental and Forensic Medicine, University of Pavia, Italy

<sup>6</sup>Department of clinical and experimental medicine, University of Florence, Florence, Italy

<sup>7</sup>Dipartimento di Prevenzione, PISLL, Health Agency of Tuscany (USL Toscana Centro), Florence, Italy

The study of the health issues (silicosis, lung cancer and also self-immune diseases) raised by occupational exposure to respirable crystalline silica (RCS) attracted the interest of a multidisciplinary scientific community for at least three decades. Still, many external variables limited the clarification of the relationship between the pathogenic factors and the occurrence of the illness in cases of low exposure doses. In this study we aimed at verifying the spatial distribution of Silicon (as a tracer of RCS) in relation to other potentially modulating agents as e.g. transition metal ions, in tissue where the occurrence and localisation of silicotic nodules has been diagnosed. Namely, selected samples of lymph nodes were considered. The investigation was carried out by means of synchrotron-radiation micro-X-ray Fluorescence (experiments were performed at the beamline ID21 of ESRF, Grenoble, France), a technique that can provide significant information especially on biologic samples, where the matrix effect is considerably low. X-ray element distribution maps were obtained for all the considered samples, and a preliminary study of the obtained chemical composition results has been undertaken by means of a properly designed robust statistical approach, which will allow to sort out internal laws of interaction between different elements in the obtained database.

## Spectroscopic analysis of nanocrystalline $\text{Cu}_3\text{SnS}_4$ : evidence of a low temperature transition

**Andrea Giaccherini** (presenting author)

Dipartimento di Scienze della Terra, Università degli Studi di Firenze, Firenze, Italy

Co-author(s): Giuseppe Cucinotta<sup>1</sup>, Stefano Martinuzzi<sup>1</sup>, Enrico Berretti<sup>2</sup>, Werner Oberhauser<sup>2</sup>, Alessandro Lavacchi<sup>2</sup>, Giovanni Orazio Lepore<sup>3</sup>, Giordano Montegrossi<sup>4</sup>, Maurizio Romanelli<sup>5</sup>, Antonio De Luca<sup>1</sup>, Massimo Innocenti<sup>1</sup>, Vanni Moggi Cecchi<sup>6</sup>, Matteo Mannini<sup>1</sup>, Antonella Buccianti<sup>5</sup>, Francesco Di Benedetto<sup>5</sup>

<sup>1</sup>Dipartimento di Chimica "U.Schiff", Università degli Studi di Firenze, Firenze, Italy

<sup>2</sup>CNR-ICCOM, Firenze, Italy

<sup>3</sup>CNR-OGG, c/o ESRF Grenoble, France

<sup>4</sup>CNR-IGG, Firenze, Italy

<sup>5</sup>Dipartimento di Scienze della Terra, Università degli Studi di Firenze, Firenze, Italy

<sup>6</sup>Sistema museale dell'Università Degli Studi di Firenze, Firenze, Italy

Energy and material depletion predicaments impose the highest possible cradle to grave full life cycle assessment, while requiring the reduction of the potential pollution and scarcity of the resources involved in the process. Nanocrystalline Cu-Sn-S materials (CTS) thin-films are promising candidates for overcoming the issues related to silicon-based devices (e.g. decommissioning, flexibility and high-energy cost of production). In this field, the solvothermal synthesis is one of the most successful in obtaining nanocrystalline CTS. Although, several works success in the synthesis of CTS, they often employ surfactant, high pressure or noxious solvents. In this paper, we show how to obtain nanocrystalline kuramite by means of a simpler, greener and scalable solvothermal synthesis. We exploited a multi-analytical characterization approach (XRD, EXAFS, FESEM, Raman spectroscopy and statistical analysis of EMPA) for the investigation of different samples. In this study, we confirmed the presence of structural defects due to a relevant antisite population. Moreover, the electrical transport proprieties confirmed the p-character of these ternary sulphides while recording a transition between two transport regimes at moderately low temperature (255 K). The structural and spectroscopic investigation at low temperature shows that a structural transition takes place in a temperature range closely related to the transition of the transport proprieties.

## Non-destructive Alpha spectroscopy as a tool for distinguishing equilibrium state on uranium minerals

Viktor Goliáš (presenting author)

Charles University, Faculty of Science, Department of geochemistry, mineralogy and mineral resources, Albertov 6, Prague 2, Czech Republic

Co-author(s): Petr Jarka<sup>1</sup>, Michal Fejgl<sup>2</sup>, Michal Rol<sup>3</sup>, Jakub Plášil<sup>4</sup>

<sup>1</sup>Police of the Czech Republic, Division of Forensic Science, Kongresová 1666/2, Prague 4, Czech Republic

<sup>2</sup>National Radiation Protection Institute, Bartoškova 28, Prague 4, Czech Republic

<sup>3</sup>Charles University, Faculty of Science, Department of geochemistry, mineralogy and mineral resources, Albertov 6, Prague 2, Czech Republic

<sup>4</sup>Institute of Physics, ASCR, v.v.i., Na Slovance 2, Prague 8, Czech Republic

Radionuclide dating is effectively used within the U-series. Different dating methods <sup>210</sup>Pb, <sup>230</sup>Th/<sup>234</sup>U, U/Pb are used for very different ages. For minerals, it is necessary to distinguish the deployment of appropriate one.

Alpha spectrometry offers the possibility of assessing the state of radioactive equilibrium without chemical separation. The method is not new. It was exhumed from [1, 2].

The method can only be used on water insoluble substances and homogeneous within the particle size (minerals, glass). "Infinitely" thin samples are necessary. The method of application from a drop of water suspension to a polished stainless steel disc was optimized [3]. The ideal weight is about 200 µg. Thus, even the most active samples have activity of about 1 Bq only. Samples are measured on a Canberra PIPS 450 mm<sup>2</sup> silicon semiconductor detector at low pressure (4 kPa). The measurement time is usually one day. The lower limit of determination is about 200 mg/kg U.

The big problem was the standard. The only commercial "in-equilibrium" uranium standard is CRM 6-A, „pitchblende ore" (NBL) (67.91% U3O8 certified). Unfortunately, we have found that it contains a soluble component (Mg-Co-Ni sulphate, approved by XRD, EM-EDA), which crystallizes in time of evaporation and is unusable for producing targets. We produced the new in-home standard PU-1 (Příbram uraninite) and determined the U content (71.47%) by vanadimetry [3]. The standard is available to a wide audience for further verification.

For the spectral processing, we have also tried some software, but the appropriate software is not currently available. It may be developed in the future. A robust calculation using stripping factors, where  $\alpha = f(\text{FWHM})$ , but also its limitations, has proven itself [4].

Qualitative differentiation of age at first glance, what radionuclides it contains. We have experienced many different situations. Our team has successfully used the method for a long time.

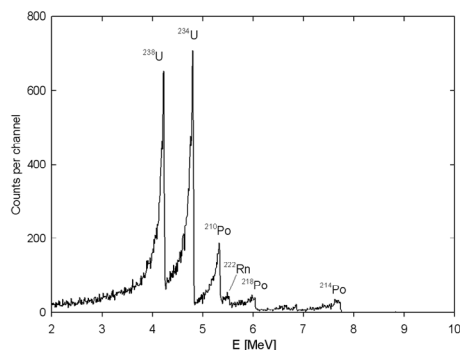


**Figure 1.** Alpha spectrum of the secondary uranium mineral from Jáchymov deposit. Present radionuclides speaks about strong radioactive disequilibrium of <sup>226</sup>Ra(<sup>214</sup>Po)/<sup>238</sup>U. Unsupported <sup>210</sup>Po activity (<sup>210</sup>Pb daughters) document what its very young (< 200 years).

### References

- [1] Moučka, V. (1968) Laboratory radiometric methods. In: Karous (Ed). Radiometry, textbook. UK univ. press, Prague. 29–47.
- [2] Killeen, P.G., Carmichael, C.M. (1976) Geol. Surv. Can. paper 1–17, 38–75.
- [3] Fejgl, M. (2003) MS, MSc Thesis, UK Prague, 44p.
- [4] Jarka, P. (2007) MS, MSc Thesis, UK Prague, 45p.

## Thermally induced solid-state transformations of Fe<sub>2</sub>O<sub>3</sub> polymorphs in reducing and inert atmospheres

Jana Havlíková (presenting author)

Regional Centre of Advanced Technologies and Materials, Palacký University in Olomouc, Czech Republic

Co-author(s): Jiří Tuček, Josef Kašík, Ondřej Malina, Ivo Medřík, Jan Filip, Radek Zbořil

Regional Centre of Advanced Technologies and Materials, Palacký University in Olomouc, Czech Republic

Ferric oxides (Fe<sub>2</sub>O<sub>3</sub>) belong to the most important nanomaterials because of their benefits to fundamental research, their broad application potential and close relation to occurrences of their natural counterparts [1]. Ferric oxides exhibit polymorphism – a feature manifested by an existence of various structural forms ( $\alpha$ -Fe<sub>2</sub>O<sub>3</sub>,  $\beta$ -Fe<sub>2</sub>O<sub>3</sub>,  $\gamma$ -Fe<sub>2</sub>O<sub>3</sub>,  $\epsilon$ -Fe<sub>2</sub>O<sub>3</sub>, and amorphous Fe<sub>2</sub>O<sub>3</sub>) differing in physical properties [2]. Moreover, upon exposing to increased temperature/pressure, ferric oxides undergo a polymorphic transformations, which can be of topotactic or non-topotactic nature. Therefore, these transformations provide a route to prepare different iron(III) oxide polymorphs with tailored physical properties tuned by a size, morphology and structural ordering [2]. Additionally, the course of a polymorphic transformation can be governed by atmosphere under which the transformation occurs while favouring emergence of rare and intermediate phases with interesting features. So far, phase transformations in oxidizing atmospheres have been well studied in the literature [2]. On the other hand, less attention has been devoted to the transformations in reducing or inert atmospheres [3].

Herein, we present a detailed experimental study of thermally induced transformations of three different ferric oxides (i.e.,  $\alpha$ -Fe<sub>2</sub>O<sub>3</sub>,  $\gamma$ -Fe<sub>2</sub>O<sub>3</sub>, and amorphous Fe<sub>2</sub>O<sub>3</sub>) under reducing/inert atmospheres (H<sub>2</sub>, CO, CO<sub>2</sub> and N<sub>2</sub>). The transformations were studied in situ by X-ray powder diffraction (XRD) in the temperature range from 25 to 900 °C. The transformation products were characterized by combination of <sup>57</sup>Fe Mössbauer spectroscopy, XRD, electron microscopy and magnetization measurements. Some rare intermediate phases, such as Haag's carbide or magnetite of different stoichiometries, were formed during the reduction of particular precursors. Under reducing conditions, metallic  $\alpha$ -Fe was identified as the final product. The presented experimental results open a journey to a more detailed knowledge on ferric oxide reduction pathways. Identification of intermediate phases provides an option to further study them with respect to search for optimal conditions for their stabilization, to characterize their physicochemical properties, to assess their application potential, and to understand more deeply their formation and role in natural environment. The authors gratefully acknowledge the support by Czech Science Foundation (grant No. 18-07585S) and Palacký University Olomouc (Project IGA\_PrF\_2019\_023).

## Electron microscopic study of burial diagenetic greigite and smythite in Gutingkeng Mudstone, SW Taiwan

Yu-Hsuan Cheng (presenting author)

Department of Earth Sciences National Cheng Kung University, 1 University Road, Tainan 70101, Taiwan

Co-author(s): Wei-Teh Jiang

Department of Earth Sciences National Cheng Kung University, 1 University Road, Tainan 70101, Taiwan

Confirmative identification and microstructural characterization of greigite and smythite can be of great importance to the discussion of diagenetic evolution and contradictory paleomagnetic records in sediments but have been limited in the literature. In this study, electron backscatter diffraction (EBSD) and high-resolution transmission electron microscopy (HRTEM) techniques were utilized to investigate microstructural properties of greigite and smythite in Gutingkeng Mudstone, SW Taiwan.

The Gutingkeng greigite occurred as a main constituent of millimeter- to centimeter-sized plant-fossil, ichnofossil, and semi-spherical iron-sulfide nodules but was not observed in the sediment matrix of all studied samples. These nodules contained early-formed aggregates of granular or <100>-elongated nanocrystals of greigite ( $\sim\text{Fe}_3\text{S}_4$ ) about 100 nm in size or width with the aggregates surrounded by and nodule cavities filled with coarser grained greigite crystals up to 1  $\mu\text{m}$  in size, locally intergrown with platy crystals with a composition of smythite ( $\sim\text{Fe}_9\text{S}_{11}$ ).

The greigite nanocrystals invariably exhibited a high density of {111} planar defects and intense diffraction streaks parallel to the greigite <111> directions, implying close packed layers irregularly interrupted by stacking mistakes and/or changes of iron occupancy. They could not produce EBSD Kikuchi bands with sufficient quality for a reliable phase identification. Such nanocrystals are microstructurally similar to early diagenetic greigite found in sediments offshore SW Taiwan. The coarser grained crystals of greigite were characterized by a defect-free domain epitaxially or topotaxially rimmed by areas showing layers with a 1.71-nm periodicity that might be hypothesized to include interstratified greigite-like 0.57 nm and smythite-like 1.14 nm units in the close packed layer sequence. Kikuchi bands consistent with the identification of greigite were obtained from such crystals. Electron diffraction patterns of the platy crystals exhibited a 1.14-nm periodicity along the  $c^*$  direction, consistent with the rhombohedral lattice of smythite with  $c = 3.42$  nm. Local interstratification of smythite with single or multiple greigite-like 0.57 nm layers was associated with diffuse odd-order and sharp even-order 00l reflections with  $l = 3n$  in electron diffraction patterns. The EBSD patterns of such crystals could be indexed as smythite.

The direct electron microscopic observations demonstrated two generations of greigite with distinct microstructures and late formation of smythite with complex transitional structures. The greigite-dominated nodules were largely modified by recrystallization of pre-existing early-diagenetic greigite and smythite neof ormation, which could have significantly influenced the paleomagnetic record of Gutingkeng Mudstone.

## Crystal chemistry of natural and synthetic oxalates of divalent cations

Alina Izatulina (presenting author)

St. Petersburg State University, St. Petersburg, Russian Federation

Co-author(s): O. V. Frank-Kamenetskaya, Vladislav V. Gurzhiy, M. A. Kuz'mina, M. S. Zelenskaya

St. Petersburg State University, St. Petersburg, Russian Federation

Oxalate minerals (salts of oxalic acid) represent a large group of organic minerals. Oxalate minerals contain various cations: alkaline, alkaline earth, transition and rare earth elements. A feature of this group of natural compounds is that, they combine an organic component (the radical of oxalic acid), along with the usual inorganic coordination complexes.  $\text{H}_2\text{O}$  molecules play an important role in the structure formation of these compounds. Oxalate minerals are often formed by the contact of rocks with groundwater containing dissolved guano of birds and bats. A number of lichens and bacteria that are directly in contact with rocks, may also produce an oxalic acid, which leads to the formation of oxalates. Nowadays, there are 18 known mineral species, which include oxalate ions. Within the framework of the current project, calcium oxalates (caoxite ( $\text{CaC}_2\text{O}_4 \cdot 3\text{H}_2\text{O}$ ), weddellite ( $\text{CaC}_2\text{O}_4 \cdot 2\text{H}_2\text{O}$ ) and whewellite ( $\text{CaC}_2\text{O}_4 \cdot \text{H}_2\text{O}$ )) were studied along with minerals from the humboldtine group ( $\text{M}^{2+}(\text{C}_2\text{O}_4) \cdot 2\text{H}_2\text{O}$  ( $\text{M} = \text{Fe}, \text{Mn}, \text{Mg}$ )). Calcium oxalate mineralization is of great interest for mineralogy, medicine and the protection of cultural heritage sites. Calcium oxalate mono- and dihydrate are the most common components of human renal stones (55% -75%, depending on the region). Caoxite is very rarely found within the renal stones, but according to some researchers it can serve as a precursor for the formation of whewellite and weddellite. Rather complex evolution of the structure and composition of the calcium oxalate crystalline phases was described in a wide temperature range using single-crystal and powder XRD techniques. The main trends of crystal chemical evolution can be characterized as follows: a decrease in the number of  $\text{H}_2\text{O}$  molecules in compounds increases the dimensionality of structural complexes (from dimers and chains to layered structures), and also increases the density of layered structures. As the result of research, it was found that whewellite should be considered as the most stable crystalline phase in atmospheric conditions of the environment among calcium oxalate hydrates. Weddellite and caoxite transform into whewellite as a result of dehydration with time and / or when heated. In a course of single crystal XRD studies at heating, two calcium oxalates were structurally characterized for the first time:  $\alpha\text{-CaC}_2\text{O}_4$  and a new modification of calcium oxalate monohydrate, the latter has also been obtained for the first time. Comparison of the TGA and XRD experiments results showed that the phase transition caused by dehydration occurs in a relatively large temperature range and strongly depends on the heating rates. The phase transition can take from several minutes (at the highest temperatures) or can last years at lower values (for example, at room temperature). Thus, the phase transitions of calcium oxalate hydrates can occur over time at the human body temperature, which can have a significant impact on human health. The results of investigation of the humboldtine mineral group members biomimetic analogs (humboldtine, glushenskite and lindbergite), which were obtained under the action of *Aspergillus niger* microscopic fungi on the surface of a number of rock-forming minerals (biotite, pyrrhotite, siderite, todorokite, kutnohorite and magnesite) showed that oxalate minerals can be considered as a solid solution with the general formula  $(\text{Fe}, \text{Mg}, \text{Mn})\text{C}_2\text{O}_4 \cdot 2\text{H}_2\text{O}$ . Variations in the composition slightly affect an alteration in the crystal chemical characteristics. Thus, for example, an increase in the Mn / Mg ratio leads to the compression of octahedral chains and, as a result, a decrease in the b unit-cell parameter. According to our research, the structure of biomimetic falottaite ( $\text{MnC}_2\text{O}_4 \cdot 3\text{H}_2\text{O}$ ) is identical to the previously investigated structure of manganese oxalate trihydrate, obtained by chemical method from an aqueous solution of  $\text{MnCO}_3$  and oxalic acid. The closeness of the falottaite and lindbergite crystal structures indicates the possibility of the formation of the latter by dehydration of the trihydrate phase. High temperature powder XRD analysis of manganese oxalate trihydrate, falottaite, showed that its transition into manganese oxalate dihydrate, lindbergite, occurs in a narrow temperature range between 80 and 100 °C. Then, the process of amorphization occurs at the temperature range of 100 - 110 °C. Lindbergite, is stable

up to 100 °C, afterwards  $\alpha$ - $\text{Mn}_2\text{O}_4$  diffraction peaks appear after 110 °C, which phase in turn disappear after 250 °C. Diffraction patterns of the falottaite and lindbergite samples after 450 °C contain only peaks of manganese oxide ( $\text{Mn}_2\text{O}_3$ , bixbyite), which persists up to 550 °C and also when the samples are cooled to room temperature. This work was supported by the Russian Science Foundation. (grant No. 19-17-00141). The XRD studies have been performed at the X-ray Diffraction Centre of St. Petersburg State University.

## Emission mechanism of the cathodoluminescence in a series of scheelite-powellite

**Ryou Kariya** (presenting author)

Department of Biosphere-Geosphere Science, Okayama University of Science, Japan

Co-author(s): Nobuhiro Kusano, Hirotsugu Nishido

Department of Biosphere-Geosphere Science, Okayama University of Science, Japan

A calcium tungstate (mineral scheelite) generally shows a remarkable blue luminescence under ultraviolet light, whereas a calcium molybdate (mineral powellite) shows an intense luminescence in a yellow region. The scheelite luminescence rapidly changes from blue to yellow when it is replaced by  $\text{CaMoO}_4$  of several mol% [1]. Still now, the luminescence mechanism in this process has been under discussion. In this study, we have investigated the cathodoluminescence (CL) of the scheelite with various powellite composition to clarify luminescence centers and CL emission mechanism.

Color CL images of the samples employed here shows a blue emission in most samples and a yellow emission in the samples including Mo at room temperature. CL spectral analysis of the CL emissions was performed after a total sensitivity correction of digital data obtained using a SEM-CL by a Gaussian peak-fitting method. Blue CL is attributed to the emission caused by the charge transfer transition between the 2p orbit of four oxygen ions  $\text{O}^{2-}$  arranged in the tetrahedron and the central metal W, which constitutes the  $\text{WO}_4^{2-}$  ion. In a few samples, a broad band emission in a yellow region was detected at around 500 nm with not so intense intensity.

The scheelite with yellow emission has a certain amount of Mo estimated by EPMA. According to fluorescence emission analyses [1], when  $\text{WO}_4$  is replaced with  $\text{MoO}_4$  up to around 10 mol%, the blue emission of the  $\text{WO}_4^{2-}$  changes to yellow emission assigned to  $\text{MoO}_4^{2-}$  center without any component of  $\text{WO}_4^{2-}$  center. The reason for this phenomenon has been interpreted as thermal quenching of  $\text{WO}_4^{2-}$  excitation more efficient than that in the case of  $\text{MoO}_4^{2-}$ , but not proved by the measurements. In this study, same behavior has been recognized in the CL of the scheelite with 10 mol% powellite. The CL spectra of the scheelite were obtained at various temperatures here. The results of the spectral analysis based on the Mott-Seitz model reveal that the end-membered scheelite shows almost no thermal quenching, whereas the scheelite with powellite composition of 10 mol% shows a significant temperature quenching above -70 °C. The facts are inconsistent with the conventional explanations. A peak energy in a yellow emission for partially Mo-replaced scheelite (10 mol %) is almost the same as the end-membered powellite. Therefore, two emission mechanisms might be presumed as follows. The energy transfer from  $\text{WO}_4^{2-}$  center to  $\text{WO}_4^{2-}$  center can rapidly undergo, because the transition energy for the radiation in  $\text{WO}_4^{2-}$  center is higher than that in  $\text{MoO}_4^{2-}$  center. The existence probability of  $\text{MoO}_4$  in nearest neighbor of  $\text{WO}_4$  rapidly increases above the powellite component of 10 mol %, resulting in energy transition easily from  $\text{WO}_4^{2-}$  center to  $\text{MoO}_4^{2-}$  center as drastically changed in color from blue to yellow in a series of scheelite-powellite.

### References

[1] Tyson, R.M., et al. (1988) American Mineralogist, 73, 1145–1154.

## Monazite and tourmaline from the Albian (Lower Cretaceous) sands from the Miechów Synclinorium (southern Poland) as a tool in provenance study

Jakub Kotowski (presenting author)  
University of Warsaw, Faculty of Geology, Poland

Co-author(s): Krzysztof Nejbert, Danuta Olszewska-Nejbert  
University of Warsaw, Faculty of Geology, Poland

The detrital monazite and tourmaline were analyzed from Albian quartz sands that occur in Miechów Synclinorium in southern Poland. The five sand pits: Korzkiew, Głanów-Stroniczki, Przychody, Lelów, Mokrzysz from the western skirt of the Miechów Synclinorium, one small pit in Bolmin (eastern skirt) and one from the Chełmo Mt. in northern margin of the Miechów Synclinorium were sampled for heavy mineral analyses. Alimentation areas for the Albian sands have not yet been precisely indicated. The Bohemian Massif (I), a hypothetical Holy Cross Mountain – Dobruja Land (SE from studied area) (II) and/or the crystalline rocks from Eastern European Platform (III) are considered as the most probable source area(s) for the Albian sands.

Tourmaline is the dominant mineral in the detrital heavy mineral assemblages of the studied samples. The preliminary study shows that the examined 520 tourmaline grains (EPMA data) are represented mainly by dravite and schorl with avg.  $X_{Mg}$  values  $>0.6$  [1]. The chemistry of the studied tourmalines [1] are similar to the composition of tourmalines from eastern part of the Bohemian Massif [2], though tourmaline mineral chemistry is not a precise indicator of the origin of detrital material.

The geochronological dating of detrital monazite were done to confirm the above mentioned interpretation. Monazite can be found in small quantities in every sample. CHIME method was chosen for determining age of detrital monazites [3]. Analysis were carried out using CAMECA SX Five electron microprobe at Faculty of Geology (University of Warsaw).

A total of 330 monazite grains from all samples were dated. Most monazite grains are unzoned and yield CHIME ages between 320 and 340 Ma. The monazite's age spectra are nearly identical for all examined localities. Obtained ages coincide with the final stage of the Variscan collision, well documented by metamorphic rocks from the eastern part of Bohemian Massif [4, 5].

The calculated Variscan ages of the detrital monazite support the hypothesis that Bohemian Massif [1] could have been the main alimentation area for Albian marine sands cropped out at the Miechów Synclinorium area.

This work was funded by University of Warsaw (grants no: DSM 118210; BOB-661-300/17 and BSt 185702).

### References

- [1] Kotowski, J., et al. (2018) 5<sup>th</sup> CEMC book of abstracts 54.
- [2] Čopáková, R., et al. (2009) *J. Geosci.* 54, 221–243.
- [3] Suzuki, K., Kato, T. (2008) *Gondwana Research* 14, 569–586.
- [4] Mazur, S., et al. (2006) *Geol. Quarterly* 50, 89–118.
- [5] Chopin, F., et al. (2012) *J. metamorphic Geol.* 30, 347–376.

## Mineralogy of silicified zones of the Southern Buh area silicate nickel deposits

Maryna Kutsevol (presenting author)  
National Technical University Dnipro Polytechnic, Ukraine

The usual focus of research of lateritic nickel deposits formed over ultramafic rocks is the study of Ni-bearing minerals and establishment of Ni and Co enrichment areas. We focus rather on mineral aggregates of silicified zones which can be both of mineralogical interest and useful as decorative stones.

There are a number of small massifs of Precambrian mafic-ultramafic rocks altered to serpentinite in the Southern Buh area of Ukraine. A lateritic weathering crust of Mesozoic age over them includes (upward): leached and carbonatized serpentinite, nontronite containing economic grades of nickel, and an ocher and ironstone zone. Free silica minerals exist throughout weathered rocks in zones of massive silicification as well as in veins and veinlets, incrustations and concretions.

Samples from silicified zones were studied using polarized light microscopy (including the immersion method to measure refractive indices), X-ray powder diffraction (XRD) and other methods. Three sets of results are presented as follows.

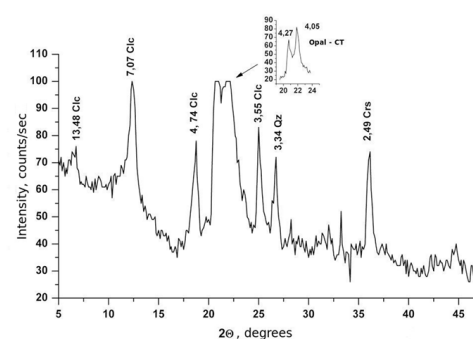


**Figure 1.** Diffractogram of silicified chlorite from a pocket in a plasma nodule showing opal-CT, cristobalite (Crs), clinochlore (Clc) and quartz (Qz) peaks (DRON-2 diffractometer, Cu-K $\alpha$  radiation).

1. Some of the veins and incrustations are composed of agate and jasper. The colors of the agate are white, gray or pink while the colors of the jasper are yellow or red. A few types of agate were described earlier by the author: banded, lace, pseudo-stalactitic and spotty. The main silica mineral of the agates is  $\alpha$ -quartz including length-fast chalcedony. Quartzine (length-slow chalcedony), opal-AG and  $\alpha$ -tridymite are present in much smaller amounts. Splitting of quartz crystals with formation of length-fast chalcedony was observed. Pseudo-stalactites were found to be composed of alternating chalcedony and quartzine micro-zones. Microcrystalline granular quartz clusters with inclusions of colorless clinochlore were registered in the host rock.

2. Another decorative stone, plasma, was recognized in some concretions which are dark green in the center and light green on the periphery. SiO<sub>2</sub> content variation, with a simultaneous change in the content of MgO, Al<sub>2</sub>O<sub>3</sub> and FeO, was detected in a study of a dark green sample using energy dispersive X-ray microanalysis; Ni and Cr impurities were also detected. Study of thin sections proved that coloration of the stone as well as the above-mentioned chemical composition changes are due to green chlorite inclusions in chalcedony. Vermicular aggregates of chlorite were noted in light green areas of nodules. XRD analysis showed that the main mineral of such areas is opal-CT and clinochlore is the subordinate one.

3. Manganese hydroxides, nontronite, goethite and hematite were identified in veins in association with free silica minerals. According to XRD patterns, manganese hydroxides are poorly crystallized. However, some diffraction peaks can be accounted for by vernadite and birnessite.

## Synthesis and crystallographic study of laflammeite (Pd<sub>3</sub>Pb<sub>2</sub>S<sub>2</sub>) and thalhammerite (Pd<sub>9</sub>Ag<sub>2</sub>Bi<sub>2</sub>S<sub>4</sub>)

František Laufek (presenting author)

Czech Geological Survey, Geologická 6, 152 00 Prague 5, Czech Republic

Co-author(s): Anna Vymazalová<sup>1</sup>, Sergei F. Sluzhenikin<sup>2</sup>, Vladimir V. Kozlov<sup>3</sup>, Jakub Plášil<sup>4</sup>, Mariana Klementová<sup>4</sup>

<sup>1</sup>Czech Geological Survey, Geologická 6, 152 00 Prague 5, Czech Republic

<sup>2</sup>Institute of Geology of Ore Deposits, Mineralogy, Petrography and Geochemistry RAS, Staromonetnyi per. 12, Moscow 119017, Russia

<sup>3</sup>Oxford Instruments (Moscow Office), 26, Denisovskii Pereulok, Moscow, 105005, Russia

<sup>4</sup>Institute of Physics, AS CR v.v.i. Na Slovance 2, 182 21, Prague 8, Czech Republic

Mineral laflammeite (Pd<sub>3</sub>Pb<sub>2</sub>S<sub>2</sub>) was firstly described by Barkov et al. (2002) [1] from the Kirakkajuppura platinum-deposit, Penikat layered complex, Finland. Barkov et al. (2002) provided chemical and physical characterisation of this mineral, however its detailed crystal structural analysis has been lacking. Thalhammerite (Pd<sub>9</sub>Ag<sub>2</sub>Bi<sub>2</sub>S<sub>4</sub>) was discovered in millerite-pyrite-chalcopyrite vein-disseminated ore from ore from the Komsomolsky mine in the Talnakh deposit, Russia [2]. Crystal structures of both minerals and relevant crystal-chemical implications will be presented.

Laflammeite occurs as subhedral platelets up to 150 μm, however the crystals are finely twinned and consequently unsuitable for a direct crystal structure study [1]. Thalhammerite occurs as tiny inclusions (from few μm up to about 40–50 μm) in sulphide ore where it forms intergrowths with other Pd-bearing minerals. Therefore, both minerals were synthesized by silica glass tube technique by heating from stoichiometric mixture of elements. The prepared synthetic analogues of laflammeite and thalhammerite were used for a structure study. The structural identity between natural and synthetic materials was subsequently confirmed by an electron-backscattered diffraction (EBSD) study.

Laflammeite, Pd<sub>3</sub>Pb<sub>2</sub>S<sub>2</sub>, crystallizes in Pmmn space group (a = 5.78, b = 8.18, c = 5.96 Å) and Z = 2. Its crystal structure shows many similarities with structures of shandite (Ni<sub>3</sub>Pb<sub>2</sub>S<sub>2</sub>, R3m), parkerite (Ni<sub>3</sub>Bi<sub>2</sub>S<sub>2</sub>, C2/m) and vymazalovaite (Pd<sub>3</sub>Bi<sub>2</sub>S<sub>2</sub>, I213). All these minerals show a common structure motive: a pseudocubic subcell of the CsCl-type composed of Bi(Pb) and S atoms. A half of available octahedral voids is occupied by Pd or Ni atoms. The distribution of Ni(Pd) atoms (i.e. the ordering scheme) determines the structure type [3]. This distribution is influenced by the different stereochemical behaviour of the 6s<sup>2</sup> lone electron pair on Bi or Pb atoms.

Thalhammerite, Pd<sub>9</sub>Ag<sub>2</sub>Bi<sub>2</sub>S<sub>4</sub> shows I4/mmm symmetry (a = 8.02, c = 9.15 Å) and Z = 2. Its unique crystal structure is based on a three-dimensional framework which consists of two types of blocks of polyhedra that interpenetrate and support each other. The first type consists of corner-sharing [PdS<sub>4</sub>] and [PdB<sub>2</sub>S<sub>2</sub>] squares. The second is formed by flattened tetrahedra [PdB<sub>2</sub>S<sub>2</sub>]. Ag atoms occupy channels running along the c direction. Thalhammerite crystal structure merges metallic building blocks with structure motives typical for polar sulphides.

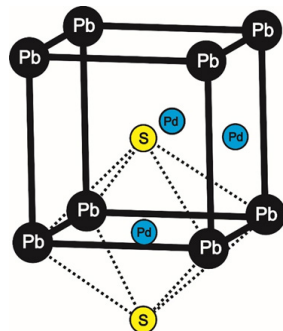


**Figure 1.** Main structural motive of the laflammeite structure: a pseudocubic subcell composed of Pb and S atoms. Distorted octahedral coordination of Pd is indicated.

### References

- [1] Barkov, Y.A., et al. (2002) *Can. Mineral.* 40, 671–678.
- [2] Sluzhenikin, S.F., Mokhov, A.V. (2015) *Mineralium Deposita* 50, 465–492.
- [3] Wehrich, R., et al. (2007) *Prog. Solid State Chem.* 35, 309–327.

## Raman spectroscopy and the K<sub>2</sub>O content of glauconites

Davide Lenaz (presenting author)

University of Trieste, Italy

Co-author(s): Danilo Bersani

University of Parma, Italy

Glauconite mineral is one of the most sensitive indicators of low sedimentation rate in marine environment. The time of residence of glauconites at the sea bottom before burial is reflected by their so-called maturity that is differentiated on the basis of their K<sub>2</sub>O content. Here we studied about 120 glauconites from the Belluno basin (N Italy) via electron microprobe. These glauconites show different K<sub>2</sub>O content (5.8–9.5 wt.%) suggesting a different maturity from slightly to highly evolved [1–5]. As Raman spectroscopy is a fast method of analyses we selected some glauconites with different K<sub>2</sub>O content in order to verify if any of the Raman peak could be related to the K<sub>2</sub>O content.

It is possible to see that resolvable peaks in the low frequency region can be discerned only, but not always, when the K<sub>2</sub>O content is higher than 8 wt. %. There are negative relations between the position of the peak at 260–280 cm<sup>-1</sup> and the K<sub>2</sub>O content and the position of the peak at 550 cm<sup>-1</sup> and the MgO content. Moreover, there is a weak relation between the width of the peak at 690–700 cm<sup>-1</sup> and the K<sub>2</sub>O content. There are two contrasting behaviour when considering the K<sub>2</sub>O content and the strong peak at 690–700 cm<sup>-1</sup>. There is a negative relation for those glauconites with MgO/Al<sub>2</sub>O<sub>3</sub> ratio in the range 0.9–1.1 and a positive one for the glauconites with MgO/Al<sub>2</sub>O<sub>3</sub> ratio lower than 0.9 and higher than 1.2. Considering these results, it seems that Raman spectroscopy cannot be used to determine the K<sub>2</sub>O content because the only present relation is rather weak.

### References

- [1] Giresse, P., et al. (1980) *Ocean. Acta* 3, 251–260.
- [2] Odin, G.S., Matter, A. (1981) *Sedimentology* 28, 611–641.
- [3] Odin, G.S., Fullagar, P.D. (1988) *Green Marine Clays*. Elsevier.
- [4] Amorosi, A. (1997) *Sed. Geol.* 109, 135–153.
- [5] Amorosi, A. et al. (2007) *Deep-Sea Res. II* 54, 1364–1374

## Non-destructive investigation of natural, treated, and synthetic amber by handheld XRF and ATR-FTIR spectroscopy

**Eugen Libowitzky** (presenting author)

Institut für Mineralogie und Kristallographie, Universität Wien, Althanstr. 14, A-1090 Wien, Austria

Co-author(s): Gerald Giester

Institut für Mineralogie und Kristallographie, Universität Wien, Althanstr. 14, A-1090 Wien, Austria

Amber is a natural fossil resin from ancient trees that occurs worldwide in a number of sedimentary deposits, the most famous ones being those from the shores of the Baltic region. The scarcity of excellent amber quality (in terms of color, clarity, and size) and the high prize of the resulting gems trigger a market that is diluted by synthetic polymer imitates and treated/enhanced varieties with and without correct labeling. It is the aim of the present investigation to distinguish between these stones by modern, non-destructive analytical techniques.

Infrared spectroscopy has been used for a long time to investigate amber from various occurrences [1, 2]. However, as precious gem objects must not be prepared routinely to KBr pellets or Nujol mulls, the stones (even round-tumbled) were pressed carefully on the diamond window of a HARRICK MPV2 ATR (attenuated total reflectance) accessory of a BRUKER Tensor27 FTIR (Fourier transform infrared) spectrometer. The acquired spectra in the wavenumber range 370–4000  $\text{cm}^{-1}$  are distinctive with the characteristic „Baltic shoulder“ at approximately 1250  $\text{cm}^{-1}$  and generally narrow bands of natural material, while broadened bands indicate heat-treatment of e.g. sunspark or red amber, and different other spectra result from a wide range of synthetic resins and polymers.

Handheld XRF (X-ray fluorescence) analysis is a modern and versatile tool to obtain the chemical composition of all sorts of objects, even those that are too big and heavy or too precious to be moved to a lab [3]. The battery-operated BRUKER Tracer IV-SD XRF employs an energy-dispersive detector to record the X-ray fluorescence emission after excitation by a rhodium X-ray source. While true Baltic amber contains only light elements such as H, C, O, and minor S, synthetic polymers reveal elevated metal contents such as Ti and Zn (their oxides acting as white pigments), Co (a curing accelerator in polyester resins), and halogens such as Cl and Br (the latter is a common constituent in flame retardants of various plastics).

The combination of both methods results in strong constraints on the type of material purchased as „amber“ in an unsafe gem market.

### References

- [1] Vavra, N., Vycudilik, W. (1976) Beitr. Paläont. Österr. 1, 121–135.
- [2] Gröhn, C. (2013) Alles über Bernstein. Wachholtz Verlag
- [3] Young, K.E., et al. (2016) Appl. Geochem. 72, 77–87.

## Sulfate assemblages from the Monte Arsiccio pyrite ore deposit (northern Tuscany, Italy): spectroscopic data on unusual mineral species

**Daniela Mauro** (presenting author)

Dipartimento di Scienze della Terra, Università di Pisa, Italy

Co-author(s): Cristian Biagioni, Marco Pasero

Dipartimento di Scienze della Terra, Università di Pisa, Italy

A complex sulfate assemblage related to the weathering of pyrite ores has been discovered at the Monte Arsiccio mine (Apuan Alps, northern Tuscany, Italy). Fifteen different sulfates have been identified using X-ray diffraction, electron microprobe analyses, and micro-Raman spectroscopy. Among them, three new mineral species have been characterized, i.e., giacovazzoite,  $\text{K}_5\text{Fe}^{3+}_3\text{O}(\text{SO}_4)_6 \cdot 10\text{H}_2\text{O}$ , magnanelliite,  $\text{K}_3\text{Fe}^{3+}_2(\text{SO}_4)_4(\text{OH}) \cdot 2\text{H}_2\text{O}$ , and scordariite,  $\text{K}_8(\text{Fe}^{3+}_{0.67}\square_{0.33})[\text{Fe}^{3+}_3\text{O}(\text{SO}_4)_6]_2 \cdot 14\text{H}_2\text{O}$ . These phases are associated with two other uncommon K-Fe sulfates, krausite,  $\text{KFe}^{3+}(\text{SO}_4)_2 \cdot \text{H}_2\text{O}$ , and goldichite,  $\text{KFe}^{3+}(\text{SO}_4)_2 \cdot 4\text{H}_2\text{O}$ . The origin of these phases is related to the action of acid solutions derived from the pyrite oxidation on K-rich host rocks.

Raman spectra of these K-Fe sulfates are characterized by the four fundamental modes of the  $\text{SO}_4$  group as well as by bending and stretching vibrations of O–H bonds. Bands related to the  $\text{SO}_4$  groups occur between 400 and 1300  $\text{cm}^{-1}$ . In agreement with Chio et al. [1], the most intense bands between 950 and 1300  $\text{cm}^{-1}$  are due to  $\nu_1$  and  $\nu_3$  modes, whereas the bands between 400 and 650  $\text{cm}^{-1}$  are related to  $\nu_2$  and  $\nu_4$  modes. The occurrence of multiple bands for the  $\text{SO}_4$  groups is related to the occurrence of structurally different  $\text{SO}_4$  groups, in agreement with structural data collected through single-crystal X-ray diffraction. Bands at wavenumbers lower than 300  $\text{cm}^{-1}$  are likely related to Me–O vibration modes or to lattice vibration modes. The stretching modes of O–H bonds, due to the presence of  $\text{H}_2\text{O}$  or OH groups, are usually represented by relatively weak and broad bands between 2800 and 3600  $\text{cm}^{-1}$ , whereas the bending modes occur in the range between 1550 and 1650  $\text{cm}^{-1}$ . The occurrence of several bands in the O–H stretching suggest the presence of different non-equivalent H-environments. This study shows that Raman spectroscopy can be a useful tool for the identification of the uncommon sulfates found at the Monte Arsiccio mine. Indeed, these K-Fe sulfates studied can be easily distinguished on the basis of their Raman spectra only.

### References

- [1] Chio, C.H., et al. (2005) Spectrochim. Acta A 61, 2428–2433.

## Synthesis, Characterization, and Application of Greigite, Pyrite, and Violarite Nanoparticles

**Elmira Mohammadi** (presenting author)

Regional Centre of Advanced Technologies and Materials, Palacký University in Olomouc, Šlechtitelů 27, 783 71 Olomouc, Czech Republic

Co-author(s): Juri Ugolotti<sup>1</sup>, Remi Coulon<sup>1</sup>, Jiří Šponer<sup>1</sup>, Judit Šponerová<sup>1,2</sup>, Radek Zbořil<sup>1</sup>, Michal Otyepka<sup>1</sup>

<sup>1</sup>Regional Centre of Advanced Technologies and Materials, Palacký University in Olomouc, Šlechtitelů 27, 783 71 Olomouc, Czech Republic

<sup>2</sup>Institute of Biophysics, Academy of Sciences of the Czech Republic, Královopolská 135, CZ-61265, Brno, Czech Republic

Iron sulfides such as greigite, pyrite, violarite, etc. are ubiquitous minerals in the lithosphere [1, 2]. Iron sulfides are present in various terrestrial natural environments such as hydrothermal and geothermal vents [3]. Moreover, nickel-containing iron sulfides have a range of important applications, including materials science [4], electrochemistry [5], CO<sub>2</sub> reduction [6], environmental science [7], etc. Intrinsic properties of nanocatalysts such as high catalytic activity, facile separation from the reaction mixture, and reusability have made them increasingly important in the field of heterogeneous catalysis. Herein, we report a straightforward synthetic approach for the preparation of these materials in nano-size in the range of 20–500 nm, using hydrothermal techniques. In this study, the as-synthesized greigite, pyrite, and violarite have been characterized by analytical techniques such as XRD, Mössbauer spectroscopy, TEM, and EDS. In a further step, these nanoparticles have been utilized as catalysts for the reduction of carbon dioxide to formate under prebiotic conditions.

### References

- [1] Vaughan, D.J., Corkhill, C.L. (2017) *Elements*, 13, 81–87.
- [2] Suib, S.L., et al. (2017) *J. Am. Chem. Soc.*, 139, 13604–13607.
- [3] Findlay, A.J., et al. (2019) *Nature Commun.* 10, 1597.
- [4] Kavalenko, M.V. (2015) *Nanoscale*, 7, 9158–9163.
- [5] Heift, D. (2019) *Inorganics*, 7, 75.
- [6] de Leeuw, N.H. (2015) *Chem. Commun.*, 51, 7501–7504.
- [7] His, H.-C., et al. (2019) *Sustainability*, 11, 1747.

## A preliminary investigation of Fe speciation in minerals by Fe K-edge XANES using a laboratory based spectrometer

**Lucy M Mottram** (presenting author)

Immobilisation Science Laboratory, Department of Materials Science and Engineering, University of Sheffield, UK

Co-author(s): Samuel Cafferkey, Martin C. Stennett, Daniel J. Bailey, Neil C. Hyatt

Immobilisation Science Laboratory, Department of Materials Science and Engineering, University of Sheffield, UK

Determinations of Fe speciation is of fundamental importance to problems in earth science, in which the oxidation state and co-ordination environment serve to constrain the thermodynamic and kinetic conditions of mineral formation and alteration. Both <sup>57</sup>Fe Mossbauer Spectroscopy and Fe K-edge X-ray Absorption Spectroscopy have proven essential, effective, and complementary tools for investigation of Fe speciation in minerals and materials. However, Mossbauer spectroscopy can prove challenging for application to dilute Fe concentrations and Fe K-edge XANES has, hitherto, required access to a synchrotron radiation source, which is a barrier to routine and high throughput analysis. In this contribution we present the first results of our investigation of Fe speciation in a suite of reference minerals, by Fe K-edge XANES using a commercially available laboratory X-ray absorption / emission spectrometer. This instrument is a development of the Seidler laboratory hard X-ray spectrometer, which utilises a spherically bent crystal monochromator, a low power X-ray tube (bremsstrahlung) source, and an energy resolving detector, in Rowland circle geometry [1, 2]. Using a Ge (6 2 0) monochromator, and 100 W Pd source, analysable Fe K-edge XANES data can be acquired in less than an hour for concentrated absorbers such as vivianite FePO<sub>4</sub>·8H<sub>2</sub>O, or several hours for more dilute absorbers such as staurolite - Fe<sub>2</sub>Al<sub>9</sub>O<sub>6</sub>(SiO<sub>4</sub>)<sub>4</sub>(OH)<sub>2</sub>. Using well established methodology we fit the pre-edge feature in Fe K-edge XANES, associated with 1s – 3d quadrupolar transition, which has been shown to be sensitive to Fe oxidation state and local environment [3–5]. We show excellent quantitative agreement between laboratory and synchrotron data, in terms of integrated intensity and centroid energy of pre-edge features in XANES spectra acquired from the same suite of mineral and synthetic reference compounds, even for relatively dilute minerals such as staurolite, see Figure 1. Thus, our preliminary data provide confidence that laboratory Fe K-edge XANES data are shown to enable robust and routine determination of Fe speciation from analysis of the pre-edge feature, which should find wide spread application in earth and materials science.

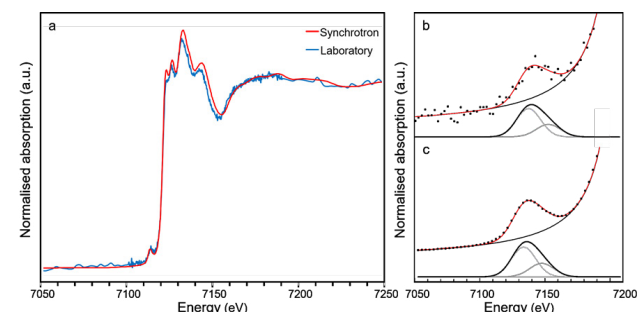


Figure 1: a) Fe K-edge XANES from staurolite with synchrotron (red) and laboratory (blue) spectrometer and extracted pre-edge features showing background subtraction (thin black line) and fitted Gaussians (thin grey line) for b) laboratory and c) synchrotron data.

### References

- [1] Seidler, G.T., et al. (2014) *Rev. Sci. Instrum.* 85, 113906.
- [2] Jahrman, E.P., et al. (2019) *Rev. Sci. Instrum.* 90, 024106.
- [3] Wilke, M., et al. (2001) *Am. Miner.* 86, 714–730.
- [4] Waychunas, G.A. (1983) *J. Mat. Sci.* 18, 195–207.
- [5] Galois, L., et al. (2001) *Chem. Geol.* 174, 307–319.

## The complexity behind the simple Ti oxide structure

**Kira Musiyachenko** (presenting author)

Università degli Studi di Pavia, Italy

Co-author(s): Mara Murri<sup>1</sup>, Mauro Prencipe<sup>2</sup>, Matteo Alvaro<sup>1</sup>

<sup>1</sup>Dipartimento di Scienze della Terra e dell'Ambiente, Università degli Studi di Pavia, via Ferrata 1, Pavia, Italy

<sup>2</sup>Dipartimento di Scienze della Terra, Università degli Studi di Torino, via Valperga Caluso 35, Torino, Italy

Rutile (TiO<sub>2</sub>) is a large used material in a variety of technological and industrial applications (e.g. pigments, battery electrolytes, catalysis, etc.). Therefore, its properties have been the subject of numerous experimental and theoretical studies. For example, Montanari and Harrison [3, 4] focused on the ferroelectric transverse-optical TO A<sub>2u</sub> mode in order to characterize the behavior of TiO<sub>2</sub> as a function of the applied strains along different crystallographic directions (i.e. axial deformation). They observed a softening of this mode when the structure is expanded and they predicted a decreasing of its frequency for this TO A<sub>2u</sub> mode towards zero under a 3% expansive strain along the [0 0 1] direction. Moreover, recent studies revealed an additional complexity of the phonon behavior in the TiO<sub>2</sub> structure. For example a softening of the TA A<sub>2u</sub> acoustic mode around  $q = \frac{1}{2} \frac{1}{2} \frac{1}{4}$  that also decreases to zero under specific strain conditions has been observed by Mitev et al. [2]. Whereas Lan et al. [1] found that this acoustic mode increases in frequency as a function of temperature stabilizing the rutile structure.

In the present study we investigated the ferroelectric behavior of rutile using ab initio methods. We calculated the elastic and vibrational properties of rutile using hybrid Hartree-Fock/Density Functional Theory (HF/DFT) simulations under different strain conditions. Furthermore, to resolve the ambiguity related to the behavior of the acoustic A<sub>2u</sub> phonon mode, we adopted a supercell approach in the framework of the HF/DFT to study this acoustic mode beyond the center of the Brillouin zone.

This project has received funding from the European Research Council under the H2020 research and innovation program (N. 714936 TRUE DEPTHS to M. Alvaro).

### References

[1] Lan T., et al. (2015) Phys. Rev. B 92, 5, 054304.

[2] Mitev, P.D. (2010) Phys. Rev. B, 81, 13, 134303.

[3] Montanari, B. (2002) Chem. Phys. Lett. 364, 5-6, 528–534.

[4] Montanari, B. (2004) J. Phys: Condens Matter. 16, 3, 273.

## Petrographic, Geochemical and mineralogical investigations of Koga and Jambil carbonatites from Peshawar Plain Alkaline Igneous Province (PPAIP), Pakistan

**Adil Nawaz** (presenting author)

AGH University of Science and Technology Krakow, Poland

Co-author(s): Jaroslav Presk

AGH University of Science and Technology, Krakow, Poland

Carbonatites are the intrusive and extrusive igneous rocks having more than 50% carbonate minerals (Calcite, Ankerite, and Dolomite) and less than 10% SiO<sub>2</sub>. It is believed that these are derived from the mantle and are the most complex and unusual type of magma/lava (Woolley and Kempe, 1989). Carbonatites generally occur in association with alkali-rich silicate intrusions. Intrusive carbonatites have been found on all continents, while, the extrusive carbonatites are only limited to a few continental rift zones (Hoemle et al., 2002). Carbonatites are found in 522 localities globally and can occur in various forms i.e. dykes, plugs, cone-sheets, sills, volcanic necks and complexes or intrusive bodies and sizes i.e. from meters up to several kilometers (Woolley and Kempe, 1989). Carbonatites are important because they are the source of rare earth elements (REEs). Concentrated and economically mineable deposits of REEs are unusual. Rare earth elements have diverse applications in various industries i.e. glass industry, automotive, petroleum refinery, anodes in batteries and alloys. Peshawar plain alkaline igneous province (PPAIP) is a series of alkaline-per alkaline magmatism intruded in Swat-Buner schistose group and Swabi-Chamla sedimentary groups (Kempe, 1973). This province extends from Tarbela in the east to Pak-Afghan border in the west (Kempe, 1973). The major complexes of PPAIP are i.e. Mansehra granite, Malakand granite, Shewa-Shahbazgarhi complex, Koga syenites, Ambela granitic complex, and Warsak igneous complex. The carbonatites are reported from Ambela granitic complex, Koga syenites, Malakand granite, and Warsak igneous province. The main aim of the present research work is to classify the Koga and Jambil carbonatites and their associated rocks and also their economic importance. Research Objectives is to follow detailed fieldwork to note the important geological features as well as to collect samples for laboratory studies. Petrography of the selected samples both under the polarizing microscope as well as electron microscope, Geochemical analysis for the characterization as well as the petrogenesis of carbonatites by using the XRF and EDX techniques. The complete understanding of the petrology and petrogenesis of carbonatites and their associated alkaline rocks is essential in unraveling the complexities of REEs present in these deposits. These carbonatites are enriched in lighter REEs, particularly cerium, lanthanum, and neodymium. This study will not only give a detailed account of the REEs present in the Koga and Jambil carbonatites but also a petrogenetic model will be drawn for these carbonatites.

## Geochemical signatures and scandium mineralization potential of NYF member of the Julianna Pegmatite System, Sudetes

Krzysztof Nejbert (presenting author)

University of Warsaw, Faculty of Geology, al. Żwirki i Wigury 93, 02-089 Warszawa, Poland

Co-author(s): Adam Pieczka<sup>1</sup>, Sławomir Ilnicki<sup>2</sup>, Elżbieta Szeleg<sup>3</sup>, Adam Szuszkiewicz<sup>4</sup>, Krzysztof Turniak<sup>4</sup>

<sup>1</sup>AGH University of Science and Technology, Department of Mineralogy, Petrography and Geochemistry, Mickiewicza 30, 30-059 Kraków, Poland

<sup>2</sup>University of Warsaw, Faculty of Geology, Al. Żwirki i Wigury 93, 02-089 Warszawa, Poland

<sup>3</sup>University of Silesia, Faculty of Earth Sciences, Department of Geochemistry, Mineralogy and Petrography, Będzińska 60, 41-200 Sosnowiec, Poland

<sup>4</sup>University of Wrocław, Institute of Geological Sciences, Cybulskiego 30, 50-205 Wrocław, Poland

The Julianna Pegmatite System, that represents mixed NYF+LCT anatectic pegmatite system, consist of numerous anatectic pegmatite bodies with a thickness range from ca. 0.2 m up to 6 m. The thickest pegmatites show well developed zoning, represented from contact with the host rock by granitic border zone (I), graphic intermediate zone (II), blocky feldspar intermediate zone (III), and quartz core (IV). Examined pegmatite dykes occur within gneisses, migmatites, amphibolites, and retrogressed eclogites at Piława Górna (Góry Sowie Block). The origin of pegmatite bodies is related with tectonic exhumation of the Góry Sowie Block, ca. 370–385 Ma, under amphibolite facies metamorphism.

The Sc mineralization were discovered only in one pegmatite dyke with rose quartz in the core. The main scandium mineral in the mineral association is thortveitite, which co-occur with garnets that show enhanced concentration of Y<sub>2</sub>O<sub>3</sub> (up to 1.11 wt.%) and Sc<sub>2</sub>O<sub>3</sub> up to 0.23 wt%). The Sc/Y ratio in the thortveitite range from 0.85 to 1.32. The Yb<sub>2</sub>O<sub>3</sub> amount in thortveitite fill narrow range from 5 to 5.86 wt.% which is an equivalent of 0.08–0.10 apfu. Earlier results of NYF pegmatite studies from Piława Górna indicate that scandium usually occurs as a permanent admixture in Nb-Ta accessory minerals. Increased Sc concentrations were documented in columbite (0.03–0.27 wt.%), ixiolite (0.06–1.0 wt.%), ferrowodginite (0.09–0.19 wt.%), and samarskite (0.02–1.24 wt.%) [1, 2]. In euxenite-group minerals low concentration of Sc were documented (range from 0.03 to 0.08 wt %) [3].

The amount of Sc in pegmatite samples from Piława Górna (whole-rock geochemical data) is generally low and varies from <1 ppm to 23 ppm. Pegmatite samples with Sc-bearing minerals contain slightly elevated Sc (2–8 ppm) and are geochemically similar to NYF pegmatites referred to as TRIO and SubTrio [1–3], where maximum concentrations of Sc have been found up to 23 ppm. Relations between individual pegmatite dykes are difficult to trace, mainly due to a sudden change in the thickness of pegmatite bodies or lack of visible contacts between them. The crystallization of pegmatites with Sc-bearing minerals is probably the result of crystallization of pegmatite melts under conditions of strong tectonic activity, which results in partial displacement of pegmatite melts, with different degree of fractionation, into newly opened spaces. The adoption of such a model can explain the diverse mineralogical characteristics of the Julianna pegmatite system.

The NCN grant No 2015/19/B/ST10/01809 supported the study.

### References

- [1] Pieczka, A., et al. (2013) Journal of Geosciences 58, 91–112.
- [2] Pieczka, A., et al. (2014) Can. Mineral. 52, 303–319.
- [3] Szuszkiewicz, A., et al. (2016) Can. Mineral. 54, 879–898.

## Provenance study of eolian sediments by cathodoluminescence spectral analysis of quartz grains for a stratigraphic interpretation in the Gobi desert

Hirotsugu Nishido (presenting author)

Okayama University of Science, Japan

Co-author(s): Risa Masuda<sup>1</sup>, Mototaka Saneyoshi<sup>1</sup>, Shin Toyoda<sup>1</sup>, Khishigjav Tsogtbaatar<sup>2</sup>

<sup>1</sup>Okayama University of Science, Japan

<sup>2</sup>Mongolian Academy of Sciences, Mongolia

The Gobi desert in Mongolia is one of the most important occurrences of dinosaur fossils in the world. In this area, a stratigraphic assignment of the eolian sediments should be acquired for paleontological investigations on the evolution of the dinosaurs as well as geological study, because any of tephra and micro-fossil for geochronological examination has not been identified. We focus on the variation in cathodoluminescence (CL) features of quartz grains extensively occurred in the eolian sediments. CL spectra of quartz have been demonstrated to show different patterns between the quartz from hydrothermal, plutonic, volcanic and metamorphic origins [1, 2], suggesting the spectra reflect the condition of the quartz formation and the local environment. Therefore, we have conducted to clarify the CL properties of quartz in the sediments including dinosaur localities in central Gobi desert, and statistically analyze the provenance of the sediments for a stratigraphic interpretation.

A SEM-CL analysis was conducted using a SEM combined with a grating monochromator to measure CL spectra ranging from 300 to 800 nm in 1 nm steps. The CL spectra were excited using a continuous electron beam with accelerating voltage of 15 keV and probe current of 2.0 nA in a scanning mode. All CL spectra obtained by a photon counting method were corrected for total instrumental response and converted in energy units (eV).

All samples exhibit two broad bands at 400 nm in a blue region and at 600–650 nm in a red region. For the quantitative evaluation of the CL spectra, we first separated the original CL spectra into several Gaussian distributions determined based on the CL emission centers proposed by Stevens-Kalceff [3]. The deconvoluted components by a Gaussian curve fitting can be assigned to the emissions derived from structural defects related to Fe<sup>3+</sup> at 1.65 eV, Non-bridging oxygen hole center (NBOHC) at 1.89 eV, Ti<sup>4+</sup> at 2.75 eV and Al<sup>3+</sup> at 3.19 eV. The relative intensity of each component was calculated using the fractional area of each Gaussian curve. Correlation analysis among emission components of quartz CL reveals that an intensity of Al<sup>3+</sup> defect center be negatively correlated with those of Fe<sup>3+</sup> center and NBOHC, resulting in the discrimination as two groups of the quartz grains by a cluster analysis. Furthermore, a statistical examination using analysis of variance (ANOVA) for the intensities of four components indicates a characterized factor of Al<sup>3+</sup> center against Fe<sup>3+</sup> center and NBOHC, whereas Ti<sup>4+</sup> centers is independent on other emission centers. Therefore, quantitative ratios of each emission component in their CL spectra by the deconvolution method could be employed for as an indicator to characterize the eolian sediments in this area.

### References

- [1] Zinkernagel, U. (1978) Contributions to Sedimentology 8, 69.
- [2] Götze, J., et al. (2001) Mineralogy and Petrology 71, 225–250.
- [3] Stevens-Kalceff, M.A. (2009) Mineralogical Magazine 73, 585–605.

## Cation site preference in apatite estimated by cathodoluminescence spectroscopy for U-Pb dating

Hirotsugu Nishido (presenting author)  
Okayama University of Science, Japan

Co-author(s): Takuya Yoshimura, Kazumasa Aoki, Shogo Aoki  
Okayama University of Science, Japan

Cathodoluminescence (CL) has the advantage that it can reveal mineralogical features depending on various intervening factors; impurities of trace elements, lattice defects and sample temperature. Apatite is a common and widespread accessory mineral with a variety of occurrences in geological environments, suggesting a geochronological application added to zircon U-Pb dating. Therefore, CL imaging of apatite can discriminate various textures during crystal growth and metamorphic process for LA-ICP-MS analysis as similarly used in zircon. Apatite shows many color-CL emissions derived from impurity centers of transition metal elements and REE, and possibly from structural defect centers [1]. Recently, matrix effects in U-Pb measurements have been recognized in crystal chemical characteristics of apatite to be an important factor related to elemental differentiation during the ablation [2]. In this study, we have conducted to clarify the luminescent centers in apatite by a CL spectral analysis for U-Pb dating.

Forty-five samples of natural as well as synthetic apatite were employed for CL measurements. CL spectra were obtained employing a SEM-CL, which comprises a SEM combined with an integral grating monochromator (Mono CL2) in the range of 300 nm to 800 nm. The measurement condition was set at accelerating voltage of 15 keV, probe current of 2.0 nA at room temperature. All CL spectra were corrected for the total instrumental response. Major and trace element composition of apatite were determined by using EPMA (JEOL; JXA8230) and LA-ICP-MS (Thermo Fisher Scientific; iCAP-Q).

Lilac to violet color, yellow color and red color CL were observed in apatite with homogeneous, domain and oscillatory zoning textures. Lilac to violet color is attributed to predominant  $Ce^{3+}$  and trivalent REE, while yellow and red colors are derived from  $Mn^{2+}$  activator with different sites. The Ca ions occupy two sites in apatite structure; M1 site coordinated by 9 oxygens and M2 site by 6 oxygens and one F (Cl, OH). The emissions in a blue region are divided into two components of the impurity center related to  $Ce^{2+}$  ion and possibly defect center induced by Th and U by spectral analysis in energy units. Yellow and red emissions might be assigned to  $Mn^{2+}$  impurity centers in M1 and M2 sites, respectively, of which latter might be ascribed to yellow emission at around 2.2 eV due to the change of the emission peak depending on the composition in the X site (F, Cl, OH). U can replace Ca ion in M2 site as quadrivalent ion in preference to Ca ion in M1 site judging from ion radius and ion charge. If U ions occupy the M2 site coordinated with Cl and OH in apatite, the U ions might be able to move and ablate easier than those in the M1 site as an elemental differentiation during the LA-ICP-MS measurements.

### References

- [1] Kempe, U., Götze, J. (2002) Mineralogical Magazine 66, 151–172.  
[2] Thompson, J., et al. (2016) Journal of Analytical Atomic Spectrometry 31, 1206–1215.

## Magmatic-hydrothermal evolution of tourmaline from the elbaite pegmatite Dolní Rožínka, Czech Republic

František Novotný (presenting author)  
Department of Geological Sciences, Faculty of Science, Masaryk University, Kotlářská 267/2, 611 37, Brno, Czech Republic

Co-author(s): Jan Cempírek  
Department of Geological Sciences, Faculty of Science, Masaryk University, Kotlářská 267/2, 611 37, Brno, Czech Republic

Chemical composition of tourmaline is well known tool for characterization of evolution of magmatic and metamorphic systems. The elbaite-subtype granitic pegmatite at Dolní Rožínka shows complex magmatic and metasomatic/hydrothermal history of crystallization from two types of pegmatitic melt followed by hydrothermal overprint, well recorded by tourmaline compositional and textural evolution. The pegmatite minerals include dominant quartz, K-feldspar and albite (in center as cleavelandite with pockets), with common tourmaline and garnet (up to 0.5 wt.%  $P_2O_5$ ); accessory minerals include polyolithionite, beryl, apatite, zircon (up to 3 wt.%  $HfO_2$ ), manganocolumbite, ixiolite. Tourmalines are usually black in less evolved units, whereas near pockets they are pink or purple, rarely blue.

Tourmaline occurs in six textural-paragenetic types including metasomatic tourmaline after biotite, tourmaline + quartz intergrowths, zoned tourmaline from pocket, acicular tourmaline overgrowths on the top of the zoned crystal from pocket, and metasomatic/hydrothermal aggregates and veinlets of Li-tourmaline + quartz was studied. The tourmaline after biotite is Al-deficient Mg-enriched schorl whereas tourmaline intergrown with quartz is schorl with slightly higher Mg contents and vacancies at the X-site. Cores of tourmalines from pockets are formed by Li-rich schorl whereas rims by Mn-rich elbaite. The zoned crystals from pockets are sometimes overgrown by acicular tourmaline with heterogeneous composition corresponding to elbaite, locally with elevated amounts of Ca and F. Metasomatic tourmaline has very heterogeneous chemical composition enriched in F, Ca, Mn, and Mg, corresponding to fluor-schorl, fluor-elbaite and fluor-liddicoatite.

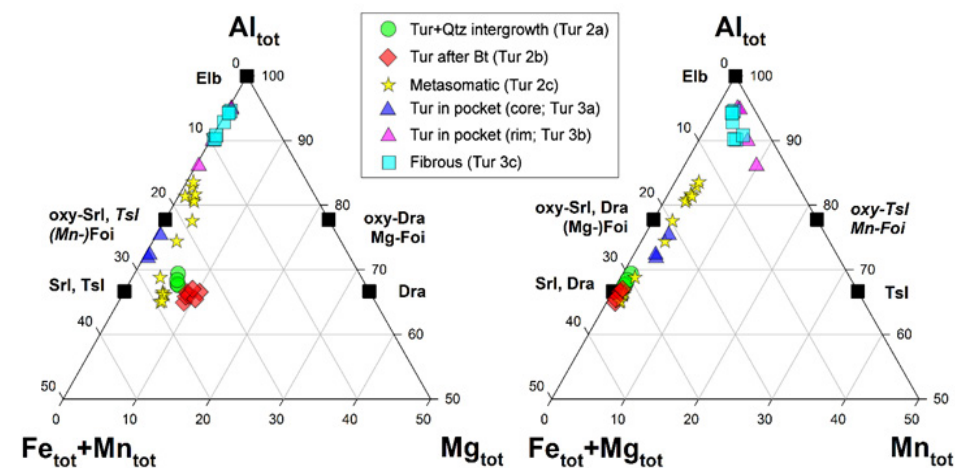


Figure 1. Composition of Y and Z sites occupancy.

Primary magmatic tourmaline shows a gradual enrichment in Al+Li and Mn and decrease of Fe+Mg (Figure 1); transition to hydrothermal stage caused change of habitus to fibrous only. Hydrothermal fluids that metasomatically reacted with early minerals are strongly enriched in Ca and F. We interpret the Ca,F-enrichment as combination of fractionation of late P,F-rich sodic melts and exsolution of hydrothermal fluids.

## Effect of electron irradiation on pseudogap in $\text{YBa}_2\text{Cu}_3\text{O}_{7-\delta}$ single crystals

**Liudmyla Omelchenko** (presenting author)

*B.Verkin Institute for Low Temperature Physics and Engineering of the National Academy of Sciences of Ukraine, Ukraine*

Co-author(s): A. L. Solovjov, E. V. Petrenko, R. V. Vovk

*B.Verkin Institute for Low Temperature Physics and Engineering of the National Academy of Sciences of Ukraine, Ukraine*

The effect of electron irradiation on the properties of the superconducting  $\text{YBa}_2\text{Cu}_3\text{O}_{7-\delta}$  in the normal and superconducting states is the subject of long-term research and an urgent task of modern solid-state physics. Of particular interest is the elucidation of the mechanism of influence of irradiation on a number of unusual phenomena observed in high-temperature superconductors (HTSCs), such as fluctuation conductivity,  $\sigma'(T)$ , and pseudogap (PG),  $\Delta^*$ , [1]. Despite a more than thirty-year history of intensive experimental and theoretical studies these phenomena, which can be the key to understanding the microscopic nature of HTSCs, still remain controversial [1-3].

The effects of electron irradiation on the temperature dependences of the resistivity  $\rho(T)$  of the optimally doped  $\text{YBa}_2\text{Cu}_3\text{O}_{7-\delta}$  single crystals were studied. Finally, in the model of local pairs, the temperature dependences of the excess conductivity  $\sigma'(T)$  and PG,  $\Delta^*(T)$  were calculated. Electron irradiation was done with electrons at energies in the range 0.5 – 2.5 MeV in a cryostat at  $T \approx 10\text{K}$ . The cumulative dose  $10^{18}\text{cm}^{-2}$  at an electron energy of 2.5 MeV produces a concentration of  $10^{-4}$  displacements per atom, averaged over all sublattices.

It is shown that the effect of irradiation on  $T_c$  and  $\rho(T)$  in YBCO is different. Under irradiation,  $T_c$  decreases (due to the displacement of oxygen and copper in the  $\text{CuO}_2$  planes), whereas  $\rho(T)$  increases. Regardless of the irradiation dose, in the temperature range from  $T_c$  to  $T_{01}$ ,  $\sigma'(T)$  is well described by the Aslamazov – Larkin (AL-3D) and Maki-Thompson (MT-2D) fluctuation theory, showing a 3D-2D crossover with increasing temperature. Accordingly,  $\sigma'(T)$  is called FLC near  $T_c$ . Found crossover temperature  $T_0$  allows us to determine the coherence length along the c axis,  $\xi_c(0)$ , which increases under irradiation as  $\xi_c(0) = (0.37-0.96)\text{Å}$  [2]. For the first time it was found that the maximum on the  $\Delta^*(T)$  of an optimally doped  $\text{YBa}_2\text{Cu}_3\text{O}_{7-\delta}$  single crystal, when irradiated with electrons with energies up to 2.5 MeV, increases and shifts to higher temperatures.

### References

- [1] Solovjov, A.L., et al. (2007) *Low Temp. Phys.* 32, 6, 576.  
 [2] Solovjov, A.L., et al. (2016) *Physica B.* 493, 58–67.  
 [3] Vovk, R.V., et al. (2019) *Low Temp. Phys.* 45, 155–158.

## Statistical analysis of temperature-dependent Raman spectra of minerals

**Elizaveta A. Pankrushina** (presenting author)

*Zavaritsky Institute of Geology and Geochemistry of UB of the RAS, Russia*

Co-author(s): Aleksandr S. Kobuzov, Yulia V. Shchapova, Sergei L. Votyakov

*Zavaritsky Institute of Geology and Geochemistry of UB of the RAS*

The implementation of statistical methods in temperature-dependent Raman spectroscopy is motivated by the necessity of analysis of complex spectra arrays  $I(\nu, T)$ , that sometimes are poorly resolved for low-symmetry minerals with large unit cell, and for crystals with structural and chemical disordering, as well as when studying spectra with a low signal-to-noise ratio. In this study several statistical methods have been proposed and tested for Raman data processing: the Pearson r-coefficient, the covariation function, the method of moments (skewness and kurtosis of the spectral data distribution) as well as autocorrelation function suggested elsewhere [1]. Both synthetic spectra and experimental temperature-dependent Raman spectra of zircon, quartz, and titanite are analyzed. The Pearson r-coefficient in the frontal analysis of neighboring spectra has been shown to be effective for quantifying the differences in T-behavior of modes in spectral ranges. The skewness and kurtosis of the spectrum intensity distribution provide information about the spectrum shape and allow quick quantification critical temperatures in the case of complex spectra. The covariance function analysis within the flank approach is a convenient tool to identify the most temperature-sensitive spectral ranges. High efficiency of the previously proposed [1] autocorrelation function algorithm for characterizing the width of vibration modes and phase transitions has been confirmed. The possibility of distinguishing changes associated with thermal expansion and anharmonic lattice vibrations on the one hand, and solid phase transformations on the other hand, has been shown. The prospects for the application of the statistical methods to unambiguously determine the temperature of thermo-induced transformations of complex spectra is demonstrated. It should be noted that virtually any statistical parameter somehow reflects changes in spectral parameters caused by an external factor  $\chi$ . Each of the algorithms has its limitations, therefore in particular cases, a specific types of algorithms and/or combination of algorithms should be used to reliably detect thermal-induced phenomena. Furthermore, the construction of algorithmic chains seems promising, which will be the subject of further research. The work was carried out at the UB RAS „Geoanalitik“ Center for Collective Use with the financial support by RSF grant No.16-17-10283.

### References

- [1] Salje, E.K.H., et al. (2000) *Eur. J. Mineral.* 2, 3, 503–519.

## Trace element chemistry of mica and quartz during magmatic-hydrothermal transition in the evolved granitic system of the eastern Krušné hory/Erzgebirge

**Tereza Peterková** (presenting author)

Czech Geological Survey, CZ-118 21 Prague, Czech Republic

Institute of Petrology and Structural Geology, Charles University in Prague, Prague, Czech Republic

Co-author(s): David Dolejš

Institute of Earth and Environmental Sciences, University of Freiburg, Freiburg i.Br., Germany

Magmatic-hydrothermal transition of highly evolved granitic melts play a major role in element transport, decoupling and deposition as well as formation of economic ore accumulations such as greisen or porphyry-style deposits. Trace element composition of minerals record the evolution of the system and can be used to distinguish rocks of different origin or hydrothermal recrystallization and to ascertain PT conditions of their formation. The geochemistry of minerals is determined by a complicated interplay of variables: the abundance of elements in the melt/fluid, coexistence of other mineral phases, partition coefficients between the mineral and its crystallization environment, relationships between the elements available (e.g. charge-compensation), crystallization temperature and pressure, growth rate and disequilibrium crystallization effects. We analyzed composition of quartz and mica by LA ICP-MS in representative samples of Li-F-rich granites, pegmatites, greisens and quartz veins in a highly evolved composite stock at Knöttel in the Krupka Sn-W-Mo ore district (eastern Krušné hory/Erzgebirge mountain range) [1]. Zoning of quartz was imaged with panchromatic cathodoluminescence, for mica was used back-scattered electrons mode. Comparison of EPMA (electron probe micro-analyser) and LA ICP-MS (laser ablation inductively coupled plasma mass spectrometry) methods was made via major composition of mica. The majority of micas in the system belong to zinnwaldite series (trioctahedral micas close to siderophyllite-polyolithionite join), part of the micas in greisenized rocks belong to phengite series (dioctahedral micas close to muscovite-aluminoceladonite join). In comparison with minerals from the surrounding gneiss, hydrothermal veins and greisenized rocks, the magmatic minerals are enriched in incompatible elements, mainly Li, Be, in the case of micas also F, Nb, Ta and their Fe/(Fe+Mg) is close to 1. During hydrothermal alteration and recrystallization (greisenization) Li, Be, Nb and Ta are decreasing in micas. Minerals in the surrounding gneiss are enriched in Mg, the mica also in Ba, Ti and V in comparison with other rocks from the study. The evolution of the system was going on in a magmatic trend, hydrosilicate liquid trend and hydrothermal trend, which partly overlapped in time. The hydrosilicate liquid [2] is something in between silicate melt and hydrothermal fluid with low density and viscosity and high diffusivity, mobility and reactivity, containing a lot of volatile and incompatible elements. It was probably formed as a disequilibrium boundary layer melt in front of quickly propagating solidification front during final stages of magmatic evolution due to the high degree of evolution of the whole system. The exsolution of hydrothermal fluids from the solidifying system was multi-phase and caused greisenization, silicification and crystallization of several types of discrete hydrothermal veins.

### References

- [1] Eisenreich, M., Breiter, K. (1993) Bulletin of the Czech Geological Survey 68, 3, 15–22.
- [2] Thomas, V.G., et al. (2014) Petrology 22, 293–309.

## High-temperature crystal chemistry of szenicsite $\text{Cu}_3(\text{MoO}_4)(\text{OH})_4$ , lindgrenite $\text{Cu}_3(\text{MoO}_4)_2(\text{OH})_2$ , cupromolybdate $\text{Cu}_3\text{O}(\text{MoO}_4)_2$ and copper trimolybdate $\text{CuMo}_3\text{O}_{10}\times\text{H}_2\text{O}$

**Rezeda M. Ismagilova** (presenting author)

Saint Petersburg State University, Saint Petersburg, Russia

Co-author(s): Elena S. Zhitova<sup>1,2</sup>, Andrey A. Zolotarev<sup>1</sup>, Sergey V. Krivovichev<sup>1,3</sup>

<sup>1</sup>Saint Petersburg State University, Saint Petersburg, Russia

<sup>2</sup>Institute of Volcanology and Seismology, Russian Academy of Sciences, Petropavlovsk-Kamchatsky, Russia

<sup>3</sup>Nanomaterials Research Center, Kola Science Center, Russian Academy of Sciences, Apatity, Russia

This work is devoted to the high-temperature crystal chemical study of three copper molybdates: szenicsite,  $\text{Cu}_3(\text{MoO}_4)(\text{OH})_4$ , lindgrenite,  $\text{Cu}_3(\text{MoO}_4)_2(\text{OH})_2$ , cupromolybdate,  $\text{Cu}_3\text{O}(\text{MoO}_4)_2$  and copper trimolybdate,  $\text{CuMo}_3\text{O}_{10}\times\text{H}_2\text{O}$ . The specific crystal chemical feature of studied Cu-Mo compounds is that Cu polyhedra are distorted due to the Jahn–Teller effect [1]. The trimolybdate compound is different from studied molybdates because Mo prevails over Cu and Mo is 6-fold coordinated in contrast to lindgrenite, szenicsite and cupromolybdate where Mo is tetrahedrally coordinated [2]. The dehydration of lindgrenite with phase transformation to cupromolybdate was observed at  $T > 325$  °C, while szenicsite transformed to cupromolybdate and tenorite at  $T > 350$  °C. The copper trimolybdate decomposed to  $\text{MoO}_3$  and  $\alpha\text{-CuMoO}_4$  at  $T > 300$  °C due to dehydration.

The thermal expansion of these compounds is strongly anisotropic. The values of  $\alpha_{\text{max}}/\alpha_{\text{min}}$  reached 5.6 for lindgrenite, 11.0 for szenicsite, 4.3 for cupromolybdate and 2.5 for copper trimolybdate. For all Cu molybdates, there are more or less aligned orientations of Jahn–Teller-distorted ( $\text{CuO}_6$ ) octahedra, which allowed us calculate the average  $\langle\text{Cu–O}\rangle$  bond lengths along particular crystallographic directions. Obtained  $\langle\text{Cu–O}\rangle$  values were in a good correlation with the observed anisotropy of thermal expansion. The anisotropy of thermal expansion of lindgrenite, szenicsite and cupromolybdate is determined by the relative arrangement of long and short  $\langle\text{Cu–O}\rangle$  bonds in the three-dimensional structure. In the case of szenicsite, all long  $\langle\text{Cu–O}\rangle$  bonds were located in one direction, due to which the mineral has strongly pronounced anisotropy of thermal behavior [3]. In the case of copper trimolybdate compound direct correlation of long and short  $\langle\text{Cu–O}\rangle$  bonds and the anisotropy of thermal expansion is not observed. The anisotropy of thermal expansion of the copper trimolybdate is determined by the changes of the interatomic angles in the  $\text{CuO}_6$  octahedra, while the  $\text{MoO}_6$  octahedra represent rigid structural units.

Thus, in all the Cu-Mo compounds, studied in this work, the copper polyhedra are most affected by increasing temperature and changes in their geometry determine the anisotropy of the thermal expansion/contraction.

The research was performed at the «Centre for X-ray Diffraction Studies» of Research park of St.Petersburg State University. The part of the research was supported by the President of Russian Federation grant for leading scientific schools (No NSH-3079.2018.5).

### References

- [1] Jahn, H.A., Teller, E. (1937) Proc. R. Soc. A. 161, 220–235.
- [2] Tian, C., et al. (2004) Solid State Chem. 177, 839–843.
- [3] Ismagilova, R.M., et al. (2019) Phys Chem Miner. 46, 5, 437–447

## Micro-Raman spectroscopy, technique allowing in depth identification/ characterization of asbestiform minerals

**Caterina Rinaudo** (presenting author)

Department of Science and Technological Innovation, University of Eastern Piedmont, Alessandria, Italy

Co-author(s): Alessandro Croce

Department of Science and Technological Innovation, University of Eastern Piedmont, Alessandria, Italy

Micro-Raman spectroscopy has been proved to be technique allowing a quick and sure identification of the asbestos fibers. In fact, Raman spectra representing a “fingerprint” of each mineral phase, in the spectral range 100–1200  $\text{cm}^{-1}$ , where lie the vibrational modes of the crystals, an easy discrimination among tremolite asbestos, actinolite asbestos, antophyllite asbestos, amosite, crocidolite, and chrysotile can be achieved [1, 2].

Moreover, micro-Raman spectroscopy is characterized by two main useful peculiarities: it does not need sample manipulation/preparation and it allows selecting, by means of the Optical Microscope (O.M.) annexed to the instrument, the analysis area.

Considering these peculiarities, different mineral fibers have been studied: erionite from Rome, Oregon, USA, and from Karlik, Cappadocia, Turkey, a non regulated fibrous phase and raw standard fibers of regulated “asbestos”-chrysotile, crocidolite, and amosite, the three most manufactured asbestos. In both cases, particular attention has been addressed to the particles lying on the crystal surfaces. In fact, under the O.M., it was possible to highlight different grains, micrometric in size, on the fiber surface.

As it concerns erionite, the recorded Raman spectra identified iron phases- hematite, goethite and jarosite- as mineral phases associated to the particles observed under O.M. This means that iron, normally ascribed as impurity to erionite chemical composition in literature data, is really associated to specific mineral phases lying on the fibers [3].

On the raw standard materials of regulated “asbestos”- chrysotile from Canada, crocidolite and amosite from South-Africa- in the spectral range 1200–4000  $\text{cm}^{-1}$ , Raman bands ascribable to Carbonaceous Materials (CMs) were detected. These carbonaceous particles, on the basis of the Raman band features, appeared characterized by different order/disorder degree [4].

The described results show the usefulness of the micro-Raman spectroscopy in the identification of the mineral fibers and of the associated phases.

### References

- [1] Rinaudo, C., et al. (2003) *Can. Mineral.* 41, 883–890.
- [2] Rinaudo, C., et al. (2004) *Mineral. Mag.* 68, 455–465.
- [3] Croce, A., et al. (2015) *Microsc. Microanal.* 21, 1341–1347.
- [4] Croce, A., et al. (2018) *Minerals* 8, 249.

## Origin of secondary uranyl-carbonate minerals at Giftkies mine, Jáchymov, Czechia: possible climate implications?

**Michal Roll** (presenting author)

Institute of Geochemistry, Mineralogy and Mineral Resources, Faculty of Science, Charles University in Prague, Albertov 6, CZ–128 43, Prague, Czech Republic

Co-author(s): Viktor Golíďš<sup>1</sup>, Jiří Zachariáďš<sup>2</sup>, Jakub Pláďil<sup>2</sup>

<sup>1</sup>Institute of Geochemistry, Mineralogy and Mineral Resources, Faculty of Science, Charles University in Prague, Albertov 6, CZ–128 43, Prague 2, Czech Republic

<sup>2</sup>Institute of Physics ASCR, v.v.i., Na Slovance 1999/2, Prague 8, 182 21, Czech Republic

Carbonate minerals that contain hexavalent U, as uranyl ion ( $\text{UO}_2^{2+}$ ), are common alteration products of uraninite weathering under oxidizing conditions [1]. Uranyl carbonates are usually relatively soluble in aqueous solutions; aqueous uranyl-carbonate complexes are thermodynamically stable and they are responsible for migration of uranium in the environment on a large scale [2]. In this work, we have investigated uranyl carbonate minerals: rutherfordine,  $\text{UO}_2(\text{CO}_3)$ , agricolaite  $\text{K}_4(\text{UO}_2)(\text{CO}_3)_3$  and liebigite  $\text{Ca}_2(\text{UO}_2)(\text{CO}_3)_3 \cdot 11\text{H}_2\text{O}$ , all of them collected in former arsenic mine Giftkies, located near Jáchymov ore district s.s., approximately 2 km NE direction from Northern fault. At the Giftkies mine are sharply developed vertical bodies of mica shist, intensively mineralized by arsenopyrite and less by chalcopyrite and tennantite. These minerals were a subject of the historical mining, besides As-mineralization there is a system of younger hydrothermal veins, cutting the rock bodies, mineralized by uraninite; gangue is dominantly represented by quartz, carbonate is lacking in fact. Rutherfordine forms rather inconspicuous aggregates of pale yellow color, only seldom of the bright yellow color that are more apparent. Nevertheless, these aggregates may cover large areas of the quartz fissures and thin veinlets, up to dozens of  $\text{cm}^2$ . Agricolaite is an extremely rare mineral, first described from this site [3]. Forms bright yellow to yellow-greenish, from isometric to elongated crystals. Liebigite forms well-developed euhedral crystals of the yellow-greenish color and their aggregates that cover larger areas up to first tens of  $\text{cm}^2$ . Minerals were identified by powder X-ray diffraction, using PANalytical Empyrean diffractometer, with CuK $\alpha$  radiation in the range from 3 °2 $\theta$  to 70 ° 2 $\theta$  at room temperature. For further interpretation more data were obtained. First we used non-destructive alpha spectrometry for radionuclides content and type of radioactive disequilibrium. Agricolaite and liebigite indicates very young ages and only rutherfordine was dated by  $^{230}\text{Th}/^{234}\text{U}$ , giving us following ages:  $3\,725 \pm 845$  years and  $3\,470 \pm 900$  years. Second carbon and oxygen stable isotopes measurements were carried out. Third hydrochemistry of the studied site. From these data we suggest three main hypothesis of origin:

Precipitation due to cold and dry event during epiatlantic period. Crystallization caused by mixing of meteoric waters and waters derivate from metamorphic basement. Crystallization from subglacial waters from melting firn cover or glacial relict.

### References

- [1] Krivovichev, S.V., Pláďil, J. (2013) *Mineralogy and crystallography of uranium*, Mineralogical Association of Canada, Short Courses 43, 15–119.
- [2] Clark, D.L., et al. (1995) *Chem. Rev.* 95, 25–48.
- [3] Skála, R., et al. (2011) *Mineral. Petrol.* 103, 169–175.

## A combined XRD and micro-Raman study of biogenic phosphates of fossil and subfossil animal bones

Anastasiya Ryanskaya (presenting author)

Institute of Geology and Geochemistry, Ural Branch of Russian Academy of Sciences, Ekaterinburg, Russia

Co-author(s): Daria Kiseleva<sup>1</sup>, Elizaveta Pankrushina<sup>1</sup>, Sergei Votyakov<sup>1</sup>, Pavel Kosintsev<sup>2</sup>

<sup>1</sup>Institute of Geology and Geochemistry, Ural Branch of Russian Academy of Sciences, Ekaterinburg, Russia

<sup>2</sup>Institute of Animal and Plant Ecology, Ural Branch of Russian Academy of Sciences, Ekaterinburg, Russia

The major constituent of vertebrate bones and teeth is a calcium phosphate mineral similar in composition and structure to the minerals of the apatite group. It is characterized by a unique combination of compositional and structural parameters, and is able to incorporate half of the elements in the periodic chart in its atomic structure [1]. For example, CO<sub>3</sub><sup>2-</sup> predominantly replaces PO<sub>4</sub><sup>3-</sup> in biological apatite [2]. This B-type carbonate substitution causes changes in various physical properties of hydroxylapatite, such as decrease in the a-axial length, the crystallite size, and increase in the c-axial length and the amount of crystallographic microstrain [1].

Ionic substitutions and a crystallite size both impose some level of disorder on the mineral phase of bone. The degree of this disorder can be monitored (e.g., through increased peak widths) with various spectroscopic techniques, such as X-ray diffraction (XRD) and Raman spectroscopy [1]. Vibrational spectroscopy (i.e., infrared and Raman) provides sensitive monitors of molecular structural differences among phases, but the determination of the structural mechanism behind those differences may require additional types of analyses, such as Rietveld refinement of XRD analyses [1]. In the present work, the structural features of a number of bone materials characterized by different age, degree of preservation and trace element accumulation (fossil, subfossil and modern) were studied using XRD and Raman spectroscopy.

Powdered samples were analyzed by XRD (Shimadzu XRD-7000) with Cu K $\alpha$  radiation ( $\lambda=1.5406$  Å) operating at 40 kV and 30.0 mA. XRD patterns were collected across the angular range of 20–70°. The preliminary qualitative phase analysis of the bones was conducted using the ICDD PDF-2 database. To perform the quantitative full profile analysis and unit cell lattice parameters determination, the digitized XRD patterns were analyzed by the Rietveld method using the Sietronics SiroQuant software. Raman microspectroscopy was performed using Horiba Jobin Yvon LabRam-HR Evolution based on a confocal Raman microscope, with 632.8 nm He–Ne laser excitation.

XRD crystallinity index (CI) was determined as the full width at half maximum (FWHM) of the apatite 002 reflection in degrees 2 $\theta$ . The average size of coherently diffracting domains (otherwise referred to as crystallites) was determined using Scherrer equation: the length by the 002 reflection, and the width by the 300 reflection. FWHMs of 002 and 300 principal reflections corresponding to apatite crystallites were measured after background subtraction and correction for the instrument function. Obtained crystallite dimensions and crystallinity indices are in a good agreement with the published values.

The work was carried out at the Geoanalyst Center for Collective Use and supported by RSF grant No. 16-17-10283.

### References

[1] Wopenka, B., Pasteris, J.D. (2005), *Mater. Sci. Eng. C*, 25, 131–143.

[2] Elliott, J.C. (2002), *RIMG*, 48, 427–454.

## Three natural As modifications from the Příbram uranium and base-metal district, Czech Republic

Jiří Sejkora (presenting author)

Department of Mineralogy and Petrology, National Museum, Prague, Czech Republic

Co-author(s): Pavel Škácha

Department of Mineralogy and Petrology, National Museum, Prague, Czech Republic

In the Příbram uranium and base-metal district (Czech Republic), all three known naturally occurring allotropic modifications of arsenic were found. The most abundant trigonal native arsenic (R-3m) occurs as hemispherical aggregates up to tens cm in size or small well development crystals up to 3 mm large. Native arsenic is one of the main components of the bonanza-type Ag-Sb-As ores of this ore district. The studied sample came from the shaft No. 16 - Hájce in central part of the ore district. Native arsenic forms spherical aggregates in calcite gangue in association with arsenolamprite and clausthalite. Its chemical composition is simple, beside As, only minority contents of Sb (0.76–4.23 wt%) were found. Orthorhombic arsenolamprite (Bmab, a 3.636(4), b 4.46(1), c 10.97(2) Å, V 177.9(3) Å<sup>3</sup>) was found on the mine dump of the shaft No. 16 - Hájce [1]. It occurs as well-formed thin tabular crystals up to 0.3 mm in length or their globular aggregates in calcite gangue, associated with native arsenic and clausthalite. It contains, beside As, traces of Sb (0.22–0.27 wt%), Cu (0.15–0.49 wt%) and S (0.06–0.15 wt%). Pararsenolamprite (orthorhombic, Pnm2<sub>1</sub>, a 10.130(4), b 3.646(4), c 10.340(3) Å, V 381.9(4) Å<sup>3</sup>) has been found in specimen from the T1 vein, 1<sup>st</sup> level, shaft No. 7 - Třebesko in the southern part of the district. It forms radial aggregates composed of very thin needles with diameter up to 2 mm in association with native arsenic, miargyrite, Ag-rich tetrahedrite, pyrargyrite, semseyite and andorite. Its chemical composition (beside As, Sb 7.64 wt% and S 0.45 wt%) match very well with published data from type locality (Sb 7.25 and S 0.48 wt%) [2]. All three samples were studied by Raman microscopy (DXR dispersive Raman Spectrometer Thermo Scientific mounted on a confocal Olympus microscope, an unpolarised 633 nm He-laser, CCD detector, objective 100x, exposure time 10 s, 100 exposures, 2 mW laser power level). The observed bands in experimental spectra (Figure 1) of arsenic and arsenolamprite is possible to attribute to the out-of-plane A<sub>g</sub><sup>1</sup> and in-plane A<sub>g</sub><sup>2</sup> and A<sub>g</sub><sup>2</sup> modes, respectively [3]. The spectrum of pararsenolamprite is significantly more complex (Figure 1) and does not correspond to simple combination of regularly arranged arsenic and arsenolamprite structural units determined in the crystal structure of pararsenolamprite [4]. The results demonstrate possible application of Raman spectroscopy for micro-identification of natural allotropic modifications of elements.

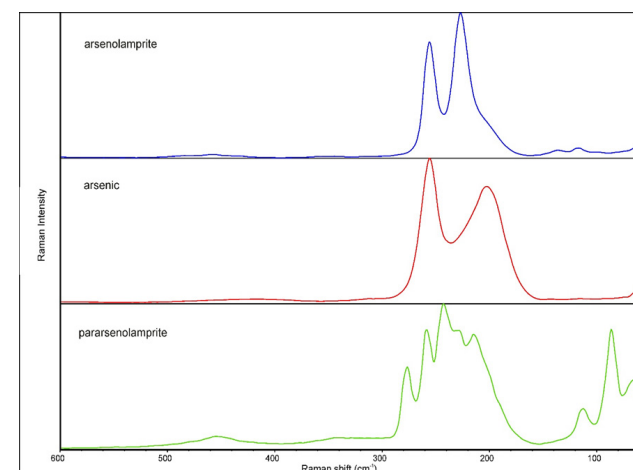


**Figure 1.** Raman spectra of three natural As modifications from Příbram

This study was financially supported by Czech Science Foundation (project GAČR 19-16218S).

### References

[1] Škácha, P., Sejkora, J. (2007) *Bull. mineral.-petrolog. Odd. Nár. Muz. (Praha)* 14-15, 131–133.

[2] Matsubara, S., et al. (2001) *Miner. Mag.* 65, 807–812.

[3] Chen, Y., et al. (2018) *Advanced Materials* 30, 1800754.

[4] Yoshiasa, A., et al. (2019) *Scientific reports* 9, 6275.

## Lattice dynamics of crystalline and radiation-damaged zircon by the data of low-temperature Raman spectroscopy

**Yuliya V. Shchapova** (presenting author)

*Institute of Geology and Geochemistry, Ural Branch of the Russian Academy of Sciences, Russia*

Co-author(s): Aleksander S. Krylov<sup>2</sup>, Dmitrii A. Zamyatin<sup>1</sup>, Sergey L. Votyakov<sup>1</sup>

<sup>1</sup>Institute of Geology and Geochemistry, Ural Branch of the Russian Academy of Sciences

<sup>2</sup>Kirensky Institute of Physics, Federal Research Center KSC, Siberian Branch of the Russian Academy of Sciences

Natural zircon  $\text{ZrSiO}_4$  (tetragonal, space group  $I4_1/amd$ ) generally incorporates trace amounts of U and Th. Alpha-decay events cause self-irradiation with high-energy alpha particles and heavy recoil nuclei over geologic periods of time, causing transition of the crystalline to a radiation-damaged state. The heavily radiation-damaged state exhibits a nano-heterogeneous structure that consists of crystalline remnants in an amorphous matrix. It results in specific zircon behavior in secondary alteration processes. To reveal the peculiarities of an atomic-level response of perfect and disordered structures to external influences (e.g. T, P), the lattice dynamics of crystalline and radiation-damaged zircon was investigated by low-temperature Raman spectroscopy. Two natural U, Th-bearing zircon samples were used: (1) the crystalline specimen from the Mud Tank carbonatite, Australia and (2) the museum specimen of radiation-damaged zircon from Sri Lanka. The accumulated  $\alpha$ -dose values ( $D_\alpha$ ), estimated in accordance with [1] on the basis of the width of  $\nu_3(\text{SiO}_4)$  Raman band at 300K, were  $D_\alpha < 0.01$  a/g (FWHM =  $2.2 \text{ cm}^{-1}$ ) and  $\sim 0.4 \cdot 10^{18}$  a/g (FWHM =  $7.9 \text{ cm}^{-1}$ ), for (1) and (2) samples, respectively. The T-dependences of positions and widths of all Raman lines were determined at  $T=8\text{--}300\text{K}$ . The effect of temperature on Raman shift (related to lattice thermal expansion and phonon interaction) is comparable in magnitude with that of radiation damage (related to structural strain in the crystalline remnants). In contrast, the effect of temperature on Raman band broadening (associated with phonon interaction) is much smaller than radiation damage induced broadening (associated presumably with phonon confinement, crystallite size distribution, point defects). The T-dependences of Raman parameters are non-linear and display anharmonic behavior. Most of the Raman bands of crystalline zircon show a normal softening trend with an increase in T, except for low-energy external modes. The latter bands are only slightly dependent on temperature and display a weak hardening with an increase in T at  $T < 170\text{K}$ . For radiation-damaged zircon, the unusual hardening trend of the internal stretching  $\nu_3(\text{SiO}_4)$  mode accompanied by non-monotonous broadening behavior was found at  $T < 70\text{K}$ . It was suggested that the temperature behavior of  $\nu_3(\text{SiO}_4)$  mode is related to T-dependent thermal expansion and structural strain in the crystalline remnants in an amorphous matrix. The mechanisms of optical-phonon decay were analyzed in crystalline and radiation-damaged zircon. The work was carried out in the „Geoanalitik“ Center with the financial support by RSF grant No.16-17-10283.

### References

[1] Vaczi, T., Nasdala, L. (2016) Phys. Chem. Mineral. 44, 6, 389–401.

## Elastic properties of monoclinic alkalifeldspars

**Jürgen Schreuer** (presenting author)

*Ruhr-University Bochum, Germany*

Co-author(s): Jessica Wierbik

*Ruhr-University Bochum, Germany*

Feldspars are among the most important minerals constituting the Earth's crust, and have been therefore in the focus of scientific research for decades. Particular challenges arise from structural instabilities caused by different sizes of cations and their specific distribution on certain lattice sites. On the one hand, many properties are sensitive to these instabilities, and on the other, reaching equilibrium at ambient conditions on the laboratory time scale is impossible due to the slow kinetics of most of the underlying processes.

Elasticity provides an excellent probe for structure-property relationships of a single crystal because the elastic properties exclusively arise from interactions between its constituents. In order to shed light onto the atomistic processes responsible for the structural instabilities or anomalies like the rapid irreversible changes of optical properties of sanidine megacrystals from the Eifel, Germany, we studied the elastic behavior of a variety of monoclinic alkalifeldspars between 100 K and 1370 K with the aid of resonant ultrasound spectroscopy. Additionally, the structural states of the crystals were thoroughly characterized employing a combination of X-ray and neutron diffraction techniques with UV/VIS/IR- and NMR-spectroscopy.

The composition,  $\text{K}_{1-x}\text{Na}_x\text{AlSi}_3\text{O}_8$ , of the investigated crystals ranges from  $x \approx 0.04$  to  $x \approx 0.37$  with minor amounts of  $\text{Ba}^{2+}$  and  $\text{Fe}^{3+}$ , and almost no  $\text{Ca}^{2+}$ . The state of Al/Si ordering as indicated by the occupation of the tetrahedral T<sub>1</sub> site by aluminum varies between highly disordered ( $2t_1 \approx 0.55$ ) and highly ordered ( $2t_1 \approx 0.85$ ). In contrast to earlier results reported in literature [1, 2], the elastic constants  $c_{ij}$  of our alkalifeldspars depend clearly on their chemical composition, in particular on the K/Na ratio. Most sensitive, however, is the shear resistance  $c_{44}$  which is closely related to the structural instability that drives the ferroelastic phase transition. With increasing albite component the transition temperature increases causing a softening of  $c_{44}$  at room temperature and an increase of  $\partial c_{44}/\partial T$ . At temperatures above about 1000 K distinct ultrasound dissipation effects occur in all samples. However, these effects are most pronounced in Eifel sanidines. A more ordered Al/Si distribution leads to a significant elastic stiffening which, however, is less pronounced than expected from Landau theory [3].

### References

[1] Crystallogr. Rep. 38 (1993) 698–709.

[2] Haussühl, S. (1993) Z. Kristallogr. 204, 67–76.

[3] Redfern, S.A.T., Harrison, R.J. (2000) Ferroelectrics 236, 293–303.

## Tourmaline OH contents studied by FTIR spectroscopy and proton-proton scattering analysis

Henrik Skogby (presenting author)

Department of Geosciences, Swedish Museum of Natural History, 104 05 Stockholm, Sweden

Co-author(s): Patrick Reichart<sup>1</sup>, Franz Weis<sup>2</sup>, Ferdinando Bosì<sup>3</sup>, Günther Dollinger<sup>1</sup>

<sup>1</sup>Institut für Angewandte Physik und Messtechnik LRT2, Universität der Bundeswehr München, WernerHeisenbergWeg 39, 85577 Neubiberg, Germany

<sup>2</sup>Department of Earth Sciences, Section for Mineralogy, Petrology and Tectonics, Uppsala University, 752 36 Uppsala, Sweden

<sup>3</sup>Dipartimento di Scienze della Terra, Sapienza Università di Roma, Piazzale Aldo Moro 5, I-00185 Roma, Italy

Tourmaline has in recent years attracted an increasing interest as a petrogenetic indicator since it occurs in a wide range of crustal rocks and is able to constrain physical-chemical conditions as temperature, composition and oxidation state. Tourmaline supergroup minerals are among the hydrous minerals that frequently show a variation in their (OH) contents, which should also relate to their crystallization conditions. However, the actual (OH) contents are difficult to analyze by direct methods. In this study, we have analyzed a set of tourmaline crystals, mostly elbaite  $[\text{Na}(\text{Li}_{1.5}\text{Al}_{1.5})\text{Al}_6(\text{Si}_6\text{O}_{18})(\text{BO}_3)_3(\text{OH})_3(\text{OH})]$  and dravite  $[\text{NaMg}_3\text{Al}_6(\text{Si}_6\text{O}_{18})(\text{BO}_3)_3(\text{OH})_3(\text{OH})]$ , with varying (OH) contents by FTIR spectroscopy and proton-proton scattering analyses in an attempt to calibrate the absorbance intensity of the (OH)-bands.

Ten different tourmaline crystals were oriented and polished to thicknesses around 100  $\mu\text{m}$ . Polarized FTIR spectra were measured both parallel and perpendicular to the c-axis direction. As typically observed for tourmaline spectra, the main (OH)-band is off-scale for the  $E_{\parallel c}$  direction due to excessive absorption, and it was not possible to get this band on scale by sample thinning. Instead, we focused on the first overtone region of the (OH)-bands around 6500–7500  $\text{cm}^{-1}$  where the bands are considerably weaker and on scale, and also on spectra polarized along the  $E_{\perp c}$  direction.

To determine the (OH) contents by an independent method, proton-proton scattering experiments were performed using the microprobe SNAKE (Superconducting Nanoscope for Applied Nuclear (Kern) physics Experiments) at the Maier-Leibnitz Laboratory (MLL) in Munich. The same samples as used for the FTIR studies were analyzed under a scan area of 100  $\mu\text{m} \times 100 \mu\text{m}$  with a focused beam. For this, a 20 MeV proton beam was focused to a spot size of about 2  $\mu\text{m} \times 2 \mu\text{m}$  perpendicular to the crystal surface.

The (OH) contents were derived from the atomic H content measured by proton-proton scattering experiments assuming all H is bound in (OH) groups. They show a marked correlation with the contents calculated from sample composition and stoichiometry. However, a general correlation of (OH) contents derived from p-p scattering with the intensity of absorption bands from the overtone region is not observed. On the other hand, for samples that have relatively similar composition and (OH)-band positions, a correlation is observed for the intensity of the main bands in spectra measured  $E_{\perp c}$ . This observation indicates that absorption coefficients for tourmalines may be dependent on the tourmaline species, or wavenumber-dependent, similar to what has been observed for principal (OH)-bands for several nominally anhydrous mineral groups [1].

### References

[1] Libowitzky, E., Rossman, G.R. (1997) Am. Mineral. 82, 1111–1115.

## Role of dissolution-precipitation in deciphering mineral evolution trends in lepidolite-subtype pegmatites

Lenka Skřápková (presenting author)

Department of Geological Sciences, Faculty of Science, Masaryk University, Kotlářská 2, 611 37 Brno, Czech Republic

Co-author(s): Jan Cempírek

Department of Geological Sciences, Faculty of Science, Masaryk University, Kotlářská 2, 611 37 Brno, Czech Republic

The lepidolite-subtype pegmatite at Lhenice is a member of the South-Bohemian pegmatite field, in the southern part of the Bohemian Massif. The Lhenice pegmatite forms flat-laying tabular body ca. 4 m thick and 20 m long in its most fractionated part. The dike has concentric zoning (from border to center): graphic zone, granitic zone, Qtz-Ms-Ab zone and Ab-Lpd zone. We present results of textural and mineralogical analysis combined with data acquired using electron microprobe and LA-ICP-MS.

The tourmaline evolved in several generations through the pegmatite. The crystallization sequence of primary (magmatic) tourmaline from the graphic zone to the Qtz-Ms-Ab zone is: Mg-bearing foitite to Al-rich schorl  $\rightarrow$  foitite to schorl  $\rightarrow$  F-rich schorl. These three zones represent outer part of the pegmatite that crystallized from the original potassic-sodic pegmatitic melt. The final stage of the primary crystallization took place in the inner, most fractionated Ab-Lpd zone, from a residual Li-rich albitic melt. The primary tourmaline slightly changed its composition during the crystallization from its core to rims: Ca-bearing fluor-elbaite  $\rightarrow$  Mn-bearing darrellhenryite  $\rightarrow$  fluor-elbaite.

Metasomatic tourmaline partly replaced the primary generations in all pegmatite zones mainly at the rims and along fractures, and in some cases replaced it completely. Its composition is quite similar in all zones: Li-rich schorl  $\rightarrow$  fluor-elbaite  $\rightarrow$  fluor-elbaite  $\rightarrow$  Fe-bearing fluor-elbaite. The metasomatic tourmaline formed from a Li,F-rich sodic melt that reacted with early tourmaline generations and other minerals (e.g. montebasite, garnet).

During pegmatite crystallization, micas evolved from biotite in the graphic zone, through muscovite in the Qtz-Ab-Ms and Ab-Lpd zones to lepidolite (trilithionite, locally up to 60 mol.% of the polyolithionite component) which is dominant mica in the Ab-Lpd zone. Lepidolite zone most likely crystallized from an immiscible Li,F-rich fluid that caused late-stage hydrothermal alteration of early minerals, e.g. muscovite overgrowth by lepidolite, and in the granitic zone garnet ( $\text{Sps}_{53}\text{Alm}_{46.7}\text{Grs}_{0.3}\text{Prp}_{0.1}$ ) replacement by zinnwaldite.

Compositions of columbite (primary and secondary manganocolumbite, locally secondary manganotantalite), cassiterite (primary generation enriched in Ta, Nb, Fe, and recrystallized generation with columbite-tantalite inclusions) and montebasite ( $x_{\text{F}} \sim 0.44$ ) indicate a moderate degree of fractionation and common post-magmatic dissolution-precipitation and alteration.

Textural analysis and mineralogy of the pegmatite indicate a complex crystallization history, with initial potassic melt followed by (auto)metasomatism by Li,B,F-rich sodic melt and final alteration by Li,F-rich immiscible liquid phase. The new results show that the evolution trend in this type of pegmatites can be distorted by common dissolution or recrystallization of early minerals by later events.

## The clay minerals/phosphogypsum-based ceramic composite as a useful adsorbent for the uranium uptake

**Marcin Syczewski** (presenting author)

Faculty of Geology, University of Warsaw, Żwirki i Wigury 93, 02-089 Warsaw, Poland

Co-author(s): Andrzej Borkowski<sup>1,2</sup>, Igor Grądziel<sup>1</sup>, Magdalena Krzesicka<sup>1</sup>, Katarzyna Mordak<sup>1</sup>, Jan Raczko<sup>1</sup>, Rafał Siuda<sup>1</sup>, Maciej Kałaska<sup>1</sup>, Arkadiusz Gąsiński<sup>3</sup>

<sup>1</sup>Faculty of Geology, University of Warsaw, Żwirki i Wigury 93, 02-089 Warsaw, Poland

<sup>2</sup>Faculty of Geology, Geophysics and Environmental Protection, AGH University of Science and Technology, Al. Mickiewicza 30, 30-059 Krakow, Poland

<sup>3</sup>Institute of Ceramics and Building Materials, Postępu 9, 02-676 Warsaw, Poland

The research concerns a sorption capacity of the phosphogypsum and clay minerals-based ceramic composites. The phosphogypsum is a waste by-product generating during the phosphoric acid production from apatite. On one hand, the chemical composition of the phosphogypsum is a serious problem due to the acidic properties. On the other hand, the phosphogypsum might be excellent sorbent for the cations that might create insoluble phosphoric mineral phases. The composites with the different phosphogypsum content were prepared in order to determine changes in mechanical properties. Isotherms of adsorption of the uranyl ions on the composite surface were then examined and kinetic parameters have been determined. The research was carried out under static and dynamic conditions. In addition, diffraction studies and chemical composition analyses were conducted using the scanning electron microscope with energy dispersive spectrometry and the wavelength-dispersive X-ray spectrometry. The results indicated an efficient process of the uranyl ions chemisorption on the obtained composites. The occurrence of phases corresponding to the composition of the minerals of the autunite group has been revealed.

Our studies suggest that obtained composites may be potentially implemented in both water treatment technologies and protection of the hazardous waste landfills.

## Pigments characterization by spectroscopic methods of three Apulian precious parchments (Privilegium XV-XVII) from State Archives of Bari

**Gioacchino Tempesta** (presenting author)

Dipartimento di Scienze della Terra e Geoambientali, Università degli Studi di Bari Aldo Moro, Bari, Italy

Co-author(s): Alessandro Monno

Dipartimento di Scienze della Terra e Geoambientali, Università degli Studi di Bari Aldo Moro, Bari, Italy

The parchments “Le pergamene di Chigago” were recovered from the national heritage, on 4 July 2017, following the seizure and recovery of cultural property illegally exported abroad. The operation was a conclusion of a complexity FBI collaboration with the Carabinieri Unit for the Protection of Cultural Heritage of Bari. In order to evaluate the authenticity and to characterize the pictorial materials of the illuminated parchments, a microscopic detailed observation of the parchments was made and diagnostic measures by non-destructive and non-invasive spectroscopic analyses were performed by complementary use of micro-Raman, X-Ray Fluorescence and VIS Reflectance spectroscopy in situ. This multi-methodological approach for the pigments characterization of parchments were established as an appropriate methodology for the complete characterization of the pigments [1-4]. The study allowed the complete characterization of the pictorial palette and red ink. The analysis and identification of pigments were made not only for dating but also for conservative and restorative purposes. The mineral and organic pigments used in each illuminated manuscript were peculiar of the historical period of production (reported in the text or into the sign below). In particular, the following pigments have been identified: blue indigo (isatis tinctoria), smalt, malachite, minium and cinnabar. Precious decorations made by gold and silver were also identified by XRF only in one parchment, underlining the importance of this Degree or “doctoratus privilegium” given to Vito Lorenzo Gonnella in 1663. Uncommon mixing of red pigments in all the coat of arms in all the parchments suggests a possible restoration made in the past by inexperienced craftsperson that didn’t know the cinnabar’s incompatibility with other metal-sulfide pigments. Two parchment those signed by Frederick III of Habsburg (1452) and Francesco Marino Caracciolo Arcella (1663) were in good state of preservation except for some stains and some lacks probably due to rodent action. While the parchment signed by Carolus V of Habsburg (1534) was in a poorest state of preservation. This parchment, differently from the others, has the header written with red ink identified as cinnabar.

### References

- [1] Aceto, M., et al. (2012) *Spectrochimica Acta Part A* 91, 352–359.
- [2] Burgio, L., et al. (2010) *PNAS*, 107, 13, 5726–5731.
- [3] Zannini, P., et al. (2012) *J. Raman Spectrosc.* 43, 1722–1728.
- [4] Chiriu, D., et al. (2017) *Vibrational Spectroscopy* 92, 70–81.

## Emission centers in barite estimated by cathodoluminescence spectrometry

Makiko Tomita (presenting author)  
Okayama University of Science, Japan

Co-author(s): Hirotugu Nishido  
Okayama University of Science, Japan

The CL properties such as color, intensity and spectral-peak features depend on the nature of defect and impurity centers, their concentrations, chemical composition and structure of host crystal. However, the CL of barite, most important Ba-bearing mineral, has not reported so far, whereas its luminescence under UV and laser conditions shows a variety of color involved with an information on the transitions between low energy levels. Recently, the formation age of the barite in sea-floor hydrothermal deposits has been evaluated by an ESR method with a high sensitivity for detection of defects [1]. Therefore, the CL of barite is expected to provide valuable information on defect centers with a deep energy level possibly related to radiation in a natural environment. In this study, we have conducted clarify the emission centers in natural barite by CL spectral analysis.

Twenty-five samples of natural barite were employed for CL measurements. A SEM-CL system combined with a grating monochromator was used to obtain spectra with operating conditions of 15 kV and 2.0 nA in a scanning mode with a temperature-controlled stage from -190 to 50 °C. All CL spectra by a photon-counting method were obtained in the range from 300 to 800 nm in 1 nm steps and were corrected for the total instrumental response. The corrected CL spectra in energy units were deconvoluted into the Gaussian components corresponding to each emission center using the OriginPro9J.

Color CL imaging shows the emissions with deep blue to light blue from five samples, whereas most samples employed here exhibit a various luminescent color of blue, beige, yellow, white and magenta under a UV lamp. Blue CL barite has almost same CL spectral pattern with a broad emission band at 350–400 nm in a UV-blue region, but not any distinct emission in a red region. EPMA (WDS) analysis indicates two types of barite with Pb and without Pb among blue CL samples. The deconvolution analysis of CL spectra reveals that Pb-bearing barite has a singlet emission at 3.26 eV (380 nm), but doublet emissions at 3.32 eV (373 nm) and 3.85 eV (322 nm) for non-Pb barite. The CL intensity of Pb-bearing barite indicates a slight reduction to 90–80% during one-hour electron irradiation, whereas non-Pb barite exhibits a sharp drop of CL intensity immediately after electron irradiation and a decrease in the intensity down to 20% when one-hour electron induced. The temperature-controlled CL measurements result in the peak energy of blue CL in non-Pb barite is independent on the sample temperature, while the intensity varies in accordance with the sample temperature, suggesting the emission as defect center due to the features unaffected by the crystal field. Therefore, the blue CL emissions found in barite might be composed of an impurity center of Pb-ion activator and defect centers with two components.

### References

[1] Fujiwara, T., et al. (2015) Subseafloor Biosphere Linked to Hydrothermal Systems, Springer Verlag, 66, 369–386.

## Zincoberaunite from Krásno, Czech Republic

Jaromír Tvrďý (presenting author)  
Department of Geological Sciences, Faculty of Science, Masaryk University, Kotlářská 2, CZ-61137 Brno, Czech Republic

Co-author(s): Jakub Plášil<sup>1</sup>, Radek Škoda<sup>2</sup>  
<sup>1</sup>Institute of Physics, Academy of Sciences of the Czech Republic, v.v.i., Na Slovance 2, CZ-18221 Prague, Czech Republic  
<sup>2</sup>Department of Geological Sciences, Faculty of Science, Masaryk University, Kotlářská 2, CZ-61137 Brno, Czech Republic

Zincoberaunite, ideally  $ZnFe^{III}_5(PO_4)_5(OH)_5 \cdot 6H_2O$ , the Zn analog of beraunite, has been described as a new mineral from the Hagendorf South granitic pegmatite, Bavaria, Germany a few years ago [1]. Nevertheless, the  $Zn^{2+}$ ,  $Al^{3+}$ -rich variety of beraunite had been described from Krásno nearby Horní Slavkov yet in 2006 [2], but the contents of both elements were not high enough for the definition of the new species. We have undertaken a complex XDR structure and chemical study of the newly obtained specimen from Krásno that has been identified recently as  $Zn^{2+}$  dominant. The results shed light onto peculiar behavior of  $Al^{3+}$  in the beraunite structures and give a better idea on hydrogen bonding scheme in beraunite related minerals.

According to single-crystal X-ray data, zincoberaunite from Krásno is monoclinic, space group C2/c, with  $a = 20.3440(19)$  Å,  $b = 5.1507(3)$  Å,  $c = 19.1361(15)$  Å,  $\beta = 93.568(8)^\circ$ ,  $V = 2001.3(3)$  Å<sup>3</sup>,  $Z = 4$ . Its crystal structure has been refined to an  $R = 0.0356$  based on 1906 unique [ $I > 3\sigma I$ ] reflections with the Jana2006 software [3]. The general structural architecture given in previous studies on beraunite-related structures has been confirmed. Crystal structure of studied zincoberaunite contains three distinct  $H_2O$  groups playing a different role in the structure (following the classification given by [4]): while O11(Wa) and O12(-Wa) are transformer groups with  $^{18}O$  atom, O14(Wa) localized in the channels running parallel to  $b$ , is non-transformer group with  $^{16}O$  atom. Two OH groups help to propagate bond-valence within the framework. Interestingly, based on site-scattering refinement,  $Al^{3+}$  is distributed over the M-sites without preferential ordering. Based on refined occupancies and bond-valence considerations the structural formula of studied zincoberaunite is  $(Zn_{0.81}Al_{0.19})(OH)_2(Fe_{0.61}Al_{0.39})(OH)_2(H_2^{18}O)_2(Fe_{1.52}Al_{0.48})(H_2^{16}O)_2(Fe_{1.72}Al_{0.28})(OH)(PO_4)_4(H_2^{16}O)_2$ ,  $Z = 4$ .

Electron microprobe analyses support the obtained results. However, keeping the same cations occupancy in the M2–M4 sites, the ratio of  $Al^{3+}$  to  $Me^{2+}$  in the M1 position requires the presence of divalent cations as follows:  $(Fe_{0.24}Zn_{0.57}Al_{0.19})_{\Sigma 1.00}(Fe_{3.84}Al_{1.16})_{\Sigma 5.00}[(PO_4)_{4^{3.88}}(AsO_4^{0.10})(SiO_4^{0.01})_{\Sigma 4.00}][O_{0.16}(OH)_{4.60}F_{0.24}\Sigma 5.00] \cdot 6H_2O$ .

Individual zincoberaunite crystals exhibit a zonality manifested by increasing Fe and decreasing Zn and Al contents from cores to margins. Accordingly, there are observed good correlations between Zn–Al ( $r = 0.7$ ), Fe–Zn ( $r = -0.7$ ) and Fe–Al ( $r = -0.9$ ).

In the low-frequency region of the Raman spectra, the strongest peak at  $997\text{ cm}^{-1}$  is attributed to the  $\nu_1(PO_4)^{3-}$  symmetric stretching vibrations. The other main bands observed are assigned to the  $\nu_3(PO_4)^{3-}$  antisymmetric stretching vibrations ( $1038\text{ cm}^{-1}$ ),  $\nu_4(PO_4)^{3-}$  antisymmetric bending modes ( $580, 603$  and  $677\text{ cm}^{-1}$ ),  $\delta M-OH$  bending vibrations ( $843\text{ cm}^{-1}$ ) and metal-oxygen stretching ones ( $206, 247$  and  $316\text{ cm}^{-1}$ ).

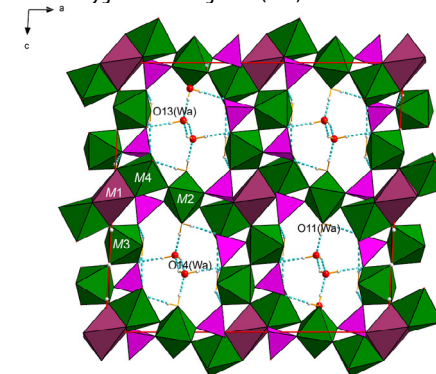


**Figure 1.** The crystal structures of zincoberaunite from Krásno projected along [010]. Metal atoms are labelled; (PO4) tetrahedra in purple colour.

### References

- [1] Chukanov, N.V., et al. (2016) Mineral. Petrol. 111, 351–361.
- [2] Sejkora, J., et al. (2006) J. Czech Geol. Soc. 51, 103–147.
- [3] Petříček, V., et al. (2014) Z. Kristallogr. 229, 345–352.
- [4] Hawthorne, F.C., Schindler, M. (2008) Z. Kristallogr. 223, 41–68.

## Mineralogy of stibnite deposit at Chříč near Rakovník (Czech Republic)

**František Veselovský** (presenting author)

Czech Geological Survey, Prague, Czech Republic

Co-author(s): Petr Pauliš<sup>1,2</sup>, Jan Pašava<sup>3</sup>, Karel Žák<sup>4</sup>, Lukáš Ackerman<sup>4</sup>, Ondřej Pour<sup>3</sup>, Zdeněk Dolníček<sup>3</sup>, Luboš Vrtiška<sup>2</sup>, Tomáš Kadlec<sup>5</sup>, Radana Malíková<sup>2</sup>

<sup>1</sup>Smišková 564, 284 01 Kutná Hora, Czech Republic

<sup>2</sup>National Museum, Cirkusová 1740, 193 00 Prague, Czech Republic

<sup>3</sup>Czech Geological Survey, Prague, Czech Republic

<sup>4</sup>Geologický ústav AV ČR, Rozvojová 269, 165 00 Prague, Czech Republic

<sup>5</sup>Stínadla 1045, 584 01 Ledce nad Sázavou, Czech Republic

Small abandoned Sb-deposit at Chříč near Rakovník (17 km SSW) is formed by hydrothermal veins hosted by metagreywackes and metasiltstones of the Barrandian Neoproterozoic, which were contactly metamorphosed by dyke intrusion of a Paleozoic lamprophyre (spessartite). The deposit was discovered in 1856 by found of stibnite in boulder in a creek.

A rich sulphidic association containing together with stibnite, pyrite and arsenopyrite also 19 subordinate or accessory ore minerals (sphalerite, berthierite, galena, tetrahedrite, freibergite, chalcopyrite, ullmannite, jamesonite, boulangérite, cobaltite, costibite, gersdorffite, bournonite, greenockite, native silver and native antimony) was found during our study of dump and museum ore material. Very interesting is especially the presence of Ag- and Se-rich minerals including Ag-rich tetrahedrite, freibergite, naumannite, clausthalite and Se-rich stefanite. The gangue is formed mainly by quartz but in a lesser amount there occur also either and younger carbonates (dolomite-ankerite), in places together with illite-muscovite and rare barite.

The oldest ore mineral is pyrite but at least part of it could originate by remobilization from pyrite containing black shales because shreds of them are in spessartite. The oldest hydrothermal mineral is arsenopyrite, which is mostly dispersed in carbonatized spessartite. This process was followed by brecciation of altered parts of the host rock. Quartz in veins was followed by stibnite accompanied with berthierite, jamesonite, and antimony and then carbonate veins with other sulphide minerals were the further stages of this deposit origin.

Rare microscopic grains of fluorapatite, rutile, zircon and monazite-(Ce) were also found. The low-temperature hydrothermal or supergene processes gave rise to kermesite and chapmanite. The youngest phases are clearly supergene minerals including jarosite, cerusite, anglesite, valentinite and very abundant limonite.

Three types of gold chips containing 24%, 9%, and 0,1% of Ag were found in creek sediments. The first and the third type are well mostly rounded and most likely come from denudated Carboniferous-Permian sediments. Dendritic aggregates of the second type are very likely of local origin.

This study is a contribution to the Czech Science Foundation project 17-15700S. It was also supported by the Ministry of Culture, Czech Republic (Národní muzeum - DKRVO 2019-2023/1.II.a, 00023272) and GIÚ AV ČR (RVO67985831).

## Temperature effects on cathodoluminescence of Ba- and Sr-feldspar

**Yuto Yamauchi** (presenting author)

Department of Biosphere-Geosphere Science, Okayama University of Science, Japan

Co-author(s): Hirotsugu Nishido

Department of Biosphere-Geosphere Science, Okayama University of Science, Japan

Celsian ( $\text{BaAl}_2\text{Si}_2\text{O}_8$ : Cn) and slawsonite ( $\text{SrAl}_2\text{Si}_2\text{O}_8$ : Sla) are Ba and Sr end members of a solid solution with K-feldspar, respectively. Cathodoluminescence (CL) of feldspar has been extensively investigated in the fields of geoscience and planetary science, and as a result the details of the emission centers in K-feldspar and plagioclase has been reported so far [1, 2]. However, the CL of Ba- and Sr-feldspar have been little studied with respect to the emission mechanism. In this study, we have conducted to assign the emission centers and characterize luminescent features of Ba- and Sr-feldspar upon varied temperatures by CL spectral analysis.

The CL spectra of celsian have three broad-band emissions at around 470 nm in a blue region, at around 560 nm in a yellow region and at around 725 nm in a red region. These emissions are assigned to Al-O-Al defect center,  $\text{Mn}^{2+}$  and  $\text{Fe}^{3+}$  impurity centers, respectively. Such emission centers are closely similar to those of anorthite, whereas the structure of celsian is referred to as an analog of K-feldspar. The CL intensity of blue emission of celsian decreases with an increase in sample temperature above  $-193$  °C. However, the CL intensity of red emission of celsian increases with an increase in sample temperature from  $-193$  °C to  $-150$  °C, and decreases with an increase in sample temperature above  $-150$  °C. On the other hand, the CL spectra of slawsonite have two broad-band emissions at around 400 nm in a blue region at around 730 nm in a red region. These emissions are assigned to Al-O-Al defect center and  $\text{Fe}^{3+}$  impurity center, respectively. The CL intensity of blue emission of slawsonite decreases with an increase in sample temperature above  $-193$  °C. However, the CL intensity of red emission of slawsonite is independent on sample temperature.

The blue CL of both celsian and slawsonite reduces with rising temperature, of which phenomenon has been recognized as a temperature quenching. This process was quantitatively analyzed by a Mott-Seitz model assuming an increase in the probability of a non-radiative transition with a rise in sample temperature. The red CL of celsian has two processes of sensitizing from  $-193$  °C to  $-150$  °C and quenching above  $-150$  °C, of which the former might be due to energy transfer from Al-O and/or Al-O-Si vibrations and the latter should be related to a consumption energy with the heat of lattice vibration [3]. Contrarily, the red CL of slawsonite shows little change in the intensity with response to sample temperature, whereas the peak energy shifts to lower-energy side as the temperature rises, suggesting the alteration of crystal field with changes in temperature. Further investigation should be required on this matter.

### References

- [1] Götze, J., et al. (2000) Cathodoluminescence in Geosciences, Springer Verlag, 245–270.
- [2] Kayama, M., et al. (2010) American Mineralogist 95, 1783–1795.
- [3] Freeman, J.J., et al. (2008) Canadian Mineralogist 46, 1477–1500.

## Bohseite-bavenite from intragranitic NYF pegmatites of the Třebíč pluton

Adam Zachař (presenting author)

Department of Geological Sciences, Masaryk University, Kotlářská 2, 611 37 Brno, Czech Republic

Co-author(s): Radek Škoda

Department of Geological Sciences, Masaryk University, Kotlářská 2, 611 37 Brno, Czech Republic

Bavenite and bohseite are beryllsilicates with a general formula  $\text{Ca}_4\text{Be}_{4-x}\text{Al}_x\text{Si}_{9-24+x}\text{O}_{4-x}\text{(OH)}_{4-x}$ . Although bavenite ( $x=2$ ) is widespread and long-known beryllium mineral in granitic pegmatites [1], often as a hydrothermal product of beryl breakdown [2], bohseite ( $x=0$ ) was defined in last decade [3, 4]. Compositions with  $\text{Be}=2.95\text{--}3.85$  apfu in bavenite-bohseite from NYF pegmatites of the Třebíč Pluton (TP), Moldanubian zone, Czech Republic represents one of the most Al-poor bohseite known to date.

A Variscan, late-orogenic Třebíč Pluton (335 Ma), intruded HP/HT-metamorphosed Moldanubian rocks as a flat, relatively shallow-seated body [5, 6]. TP is built of so-called durbachites, ultrapotassic, porphyritic melagranites to melasyenites:  $\text{Kfs}+\text{Pl}+\text{Phl}+\text{Act}\pm\text{Qz}$  ( $\text{ASI}=0.79\text{--}0.93$ ). These rocks are very high in Mg (up to 10 wt.% MgO) contrasting high LILE (up to 7 wt.%  $\text{K}_2\text{O}$ , Rb-400 ppm, Cs-40 ppm), HFSE (1 wt.%  $\text{TiO}_2$ , Nb-35 ppm), LREE, U and Th. TP is a parental body of numerous intragranitic NYF (Niobium-Yttrium-Fluorine) pegmatites belonging to euxenite subtype [7, 8]. They form vertical, up to 1 m thick, zoned lenticular dykes locally with amazonite and massive quartz core. Accessory minerals include Fe,Mg,Ti-rich tourmaline, allanite-(Ce), aeschynite- and euxenite - group minerals, columbite/ixiolite, Nb-rutile, cassiterite and zircon. Primary Be-minerals, represented by Na,Mg-rich beryl, helvite-group minerals (HGM) and phenakite, were affected by late hydrothermal Ca-metasomatism, which generated minerals of bavenite-bohseite series. Bohseite-bavenite forms white, chalky to flaky aggregates, of microscopic scale to 1 cm across. Their typical mineral association and composition are related to the primary precursor:

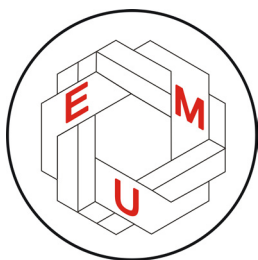
- beryl-hosted bavenite-bohseite forms veinlets and nests (with rare Mg-bazzite) in primary beryl (~1.5 apfu Al), varying between 2.68-3.25 apfu Be and 0.75-1.13 apfu Al.
- rare replacement of milarite (1 apfu Al): 2.94-3.13 Be apfu and 0.82-1.02 apfu Al is present
- HGM-hosted rims, veinlets and pseudomorphoses yield 2.96-3.63 apfu Be and 0.36-1.05 apfu Al
- phenakite-hosted veinlets and pseudomorphoses with 3.12-3.86 apfu Be and 0.15-0.77 apfu Al

The position of Ca is partly substituted by Na (up to 0.11 apfu), Fe and Mn (both ~ 0.1 apfu). Regarding the variability of Al-content, decreasing trend from Al-rich, beryl-hosted to Al-very low, phenakite-hosted environment, could be seen. Hence, the chemical composition of bavenite-bohseite solid solution mirrors the chemical compositions of replaced primary phases in the local environment and shows low Al mobility at such conditions.

### References

- Černý, P. (2002) Reviews in Mineralogy & Geochemistry 50, 405–444.
- Černý, P. (1968) Neues Jahrbuch für Mineralogie Abhandlungen 108, 166–180.
- Friis, H., et al. (2010) Mineralogical Magazine 74, 797–800.
- Szeleg, E., et al. (2017) Min. Mag. 81, 35–46.
- Kusiak, M.A., et al. (2010) Gondwana Research 17, 153–161.
- Leichmann, J., et al. (2017) International Journal of Earth Sciences 106, 59–77.
- Černý, P., et al. (2012) Elements 8, 289–294.
- Škoda, R., et al. (2006) Acta Mus. Moraviae, Sci. Geol. 91, 129–176.

## PARTNERS



## SPONSORS



Phase ID and elemental analysis on a benchtop

### SMART X-RAY COMBINATION



- MiniFlex: Multipurpose benchtop XRD instrument
- Enhanced phase ID using your XRF results
- Enhanced XRF FP results with phase ID data
- Determine % crystallinity
- Phase ID and quantification of crystalline materials



- Supermini200: High-power benchtop sequential WDXRF spectrometer
- Low limits of detection (LLD)
- Elemental analysis of oxygen (O) through uranium (U)
- Analyze solids, liquids, powders, alloys and thin films
- Superior FP and empirical software capabilities





## Stanovení chemického složení v terénu? Nebo v laboratoři?



Umíme!

Prodej a servis ručních a stolních  
EDXRF a OES spektrometrů firmy  
HITACHI a Rigaku

Tel.: +420 296 796 444  
E-mail: [analytika@pcs.cz](mailto:analytika@pcs.cz)  
Web: [www.pcs.cz/analytika](http://www.pcs.cz/analytika)

